UNIVERSITÀ DEGLI STUDI DI MILANO

CORSO DI DOTTORATO

Fisiologia XXVIII ciclo

BIO-09

TESI DI DOTTORATO DI RICERCA

Cardiac pacemaking: pathophysiology and pharmacology of the I_f current

Dott. Manuel Paina

Tutor: Prof. Mirko Baruscotti

Coordinatore: Prof. Michele Mazzanti

Anno Accademico 2014-2015

SUMMARY

1. ABSTRACT **page 5**

2. GENERAL INTRODUCTION **page 7**

2.1 The heart page 7

Heart anatomy page 7

Cardiac innervation page 10

Cardiac conduction system page 12

2.2. Action potentials page 13

Fast response action potentials page 13

Slow response action potentials page 14

2.3. I_f current page 16

Kinetics page 19

Tissue distribution of I_f in the heart page 19

2.4. HCN channels page 20

HCN channels isoforms page 22

2.5. The electrocardiogram page 24

Bipolar leads page 25

Unipolar leads page 25

Normal ECG page 25

Monitoring page 27

Normal cardiac rate page 27

2.6. Radiotelemetry in freely-moving mice page 28

2.7. Heart-rate reducing agents page 29

Alinidine page 29

Zatebradine page 30

Cilobradine page 30

ZD7288 page 30

Ivabradine page 31

3**. TRADITIONAL CHINESE MEDICINE** **page 33**

3.1. Introduction page 33

Tong Mai Yan Xin page 35

3.2. Materials and methods page 36
Animals page 36
In-vitro experiments page 36
Cell isolation page 36
Patch-clamp solutions page 37
Equipment page 38
Protocols and data analysis page 38
Treatments page 41
In-vivo experiments page 42
Telemetric setup page 42
Implantation protocol page 43
Telemetric protocols page 43
3.3. Results page 45
In-vitro experiments page 45
Action potential parameters page 45
Autonomic modulators interactions page 49
I_f current page 52
In-vivo experiments page 54
4. INAPPROPRIATE SINUS TACHYCARDIA page 59
4.1. Introduction page 59
4.2. Materials and methods page 61
Including criteria page 61
Genomic DNA analysis and mutagenesis page 61
Functional studies in HEK 293 cells page 61
Whole-cell studies page 62
Inside-out macropatch studies page 62
Functional studies in neonatal rat cardiac myocytes cultures page 63
Action potential studies page 63
Current density and kinetics properties page 63
Video detection of cell rate page 64
4.3. Results page 65
R524Q mutation in a family with IST page 65
Functional analysis by heterologous expression in HEK293 cells page 69

R524Q mutant proteins increase automaticity in neonatal cardiac myocytes page 72
5. DYNAMIC CLAMP page 74
5.1. Introduction page 74
5.2. Materials and methods page 76
Experimental setup page 76
Dynamic clamp protocols page 77
Ivabradine page 77
Isoprenaline/Acetylcholine page 78
Data processing and statistical analysis page 79
5.3. Results page 80
Preliminary results on IVA protocol page 80
Rate-adaption of Dynamic Clam for cell-specific experiments page 81
Ivabradine results page 82
Isoprenaline results page 84
Acetylcholine results page 86
6. DISCUSSION page 88
7. BIBLIOGRAPHY page 94

1. ABSTRACT

During my Ph.D. I focussed my experiments on the investigation of physiopathological and pharmacological role of the cardiac sinoatrial I_f since it has a key role in the generation and modulation of cardiac pacemaker activity.

The identification of pharmacological agents able to reduce sinus heart rate has a strong interest in the clinic since they could be useful in the treatment of ischemic heart disease. Despite longstanding and intense investigation at present there is only one such agent (ivabradine) that has reached therapeutic application since all other compounds tested have shown undesired side-effects. I therefore investigated the effect of Tong Mai Yan Xin (TMYX), a drug currently used in China as a cardiac regulator of both brady- and tachy-cardic condition. Electrophysiological experiments performed on rabbit SA node cells have shown a dose-dependent slowing effect of TMYX on pacemaking rate, associated with a reduction of the early part of the pacemaker depolarization and with a moderate prolongation of APD50. The investigation of the effects of TMYX on the I_f current, the major contributor of diastolic depolarization phase, has revealed a dual effect: TMYX causes a leftward-shift of the activation current curve and an increase of the channel conductance. At physiological potential the bradycardic action (leftward shift) strongly prevails, thus confirming the effect on the spontaneous automaticity observed in SA node cells.
The effect of TMYX was also evaluated in freely moving mice implanted with ECG transmitters. Preliminary experiments surprisingly show an increment of heart rate after the i.p. injection of the drug, while when TMYX was delivered during pharmacological blockade of only sympathetic or both sympathetic and parasympathetic autonomic system, a deep bradycardia was observed.

Given the importance of the I_f current in the pacemaking process, it is important characterize the functional role of mutations in the HCN4 channels, the molecular constituent of I_f current, that are associated with clinically relevant modification of heart rate. So far all mutations reported in the literature are associated with tachycardic conditions. During my study I had the opportunity to investigate the properties of the R524Q mutation which is located in the first

portion of C-linker, a region connecting the S6 transmembrane domain to the CNBD; this mutation cosegregates in familial members affected by inappropriate sinus tachycardia. Electrophysiological analysis carried out on HEK 293 cells showed an increment of cAMP sensitivity in the R524Q channels resulting in a rightward shift of the activation curve that mimic the effect of β-adrenergic stimulation. When transfected with mutant rather than wild-type HCN channels newborn ventricular myocytes, an excitable cellular model used to test the effect of mutations on spontaneous rate, showed a faster pacemaking rate.

Finally I carried out some experiments to test the quantitative relevance of the I_f current during pacemaking. The study was carried out by means of an indirect approach based on mathematical models of SA node action potentials combined with the dynamic-clamp technique. I compared the models developed by Maltsev-Lakatta and Severi-DiFrancesco. Both these formulations describe the SA node automaticity, but they have differences in quantitative contribution of I_f current. My experiments allowed to validate the Severi-DiFrancesco model, that is associate with a higher contribution of I_f current during the diastolic depolarization than Maltsev-Lakatta formulation.

In conclusion, using independent and separate approaches, my experiments confirm that alterations of the amount of the I_f current flowing during the diastolic depolarization leads to robust effect on automaticity of the SA node.

2. GENERAL INTRODUCTION

2.1. THE HEART

Heart anatomy

The heart is a muscular organ located under the ribcage in the center of the chest between the right and left lungs. The inferior tip of the heart, known as the apex, rests just superior to the diaphragm. Because the heart points to the left, about 2/3 of the heart's mass is found on the left side of the body and the rest is on the right. The superior end, termed base of the heart, is located along the body's midline with the apex pointing toward the left side. A normal heart has the size of a closed fist and it weighs between 200 and 425 grams. By the end of a long life, a human heart may have beaten (expanded and contracted) more than 3.5 billion times. In fact, each day, the average heart beats 100.000 times, pumping about 7.500 liters of blood.

The heart contains 4 chambers: the upper chambers (atria), and the lower chambers (ventricles); the septum, a wall of muscular tissue, separates the left and the right atria and ventricles (**fig. 1**).

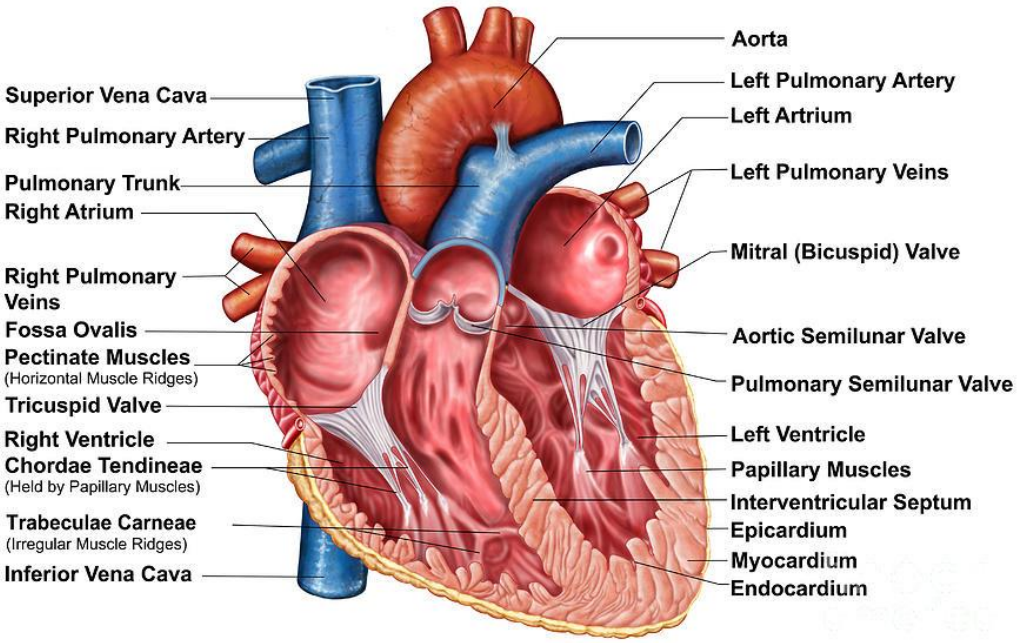

Fig. 1. **Anatomy of the heart.**

The atria are smaller than the ventricles and have thinner muscular walls than the ventricles, because they have to pump blood only to the nearby ventricles. The ventricles, on the other hand, have a very thick myocardium which is necessary to pump blood to or throughout the entire body. The atria are connected to the veins that carry blood to the heart (superior and inferior *vena cava* on the right, and pulmonary veins on the left atrium), while the ventricles, connected to the arteries (pulmonary artery on the right, and aorta on the left), send blood out of the heart.

The heart wall of the right chamber is smaller and has less myocardium then the left side of the heart; this difference in size depends on the specific function. In fact, the right side of the heart maintains the pulmonary circulation to the nearby lungs, while the left side pumps the blood all the way to the extremities of the body throughout the systemic circulatory loop (**fig. 2**).

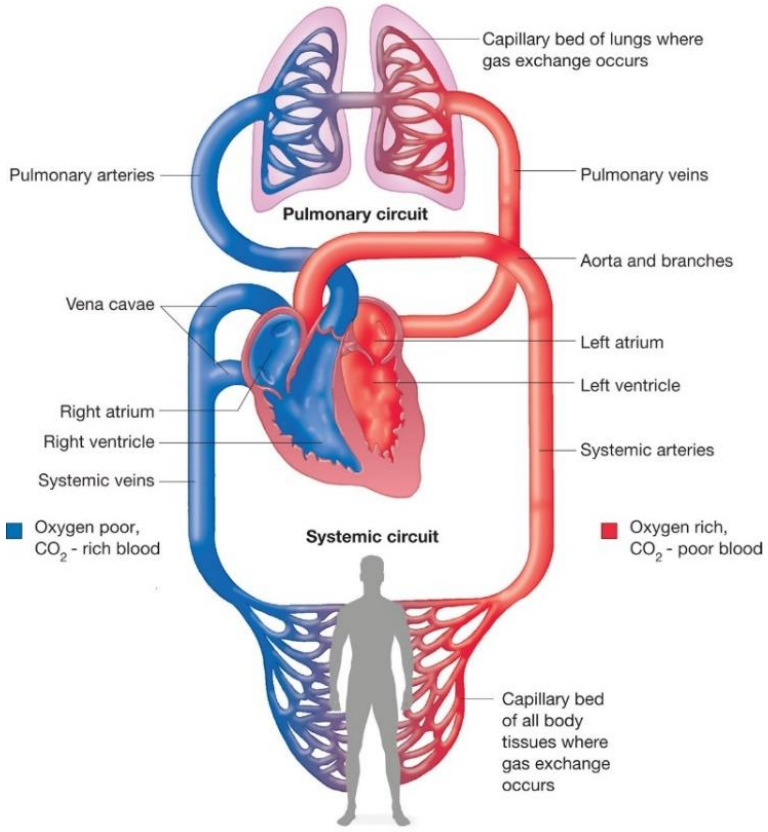

Fig. 2. **Circulatory loop**. In the pulmonary circuit the blood poor of oxygen and rich of CO_2 moves from right ventricle to the lungs; after the oxygenation process the blood returns on the left side of the heart, where starts the systemic circuit. Oxygen rich and CO_2 poor blood reaches the entire body and comes back in the right atrium.

The heart functions are pumping blood both to the lungs and to the organs of the body; in order to prevent the return of blood flow into the heart a system of one-way valves is present: the heart valves can be divided into two types: atrioventricular and semilunar (**fig. 3**).

- Atrioventricular valves. They are located between the atria and the ventricles and they only allow the blood flow from the atria to the ventricles. The AV valve on the right side of the heart is called tricuspid, while the valve on the left side is termed mitral or bicuspid. The AV valves are attached to the ventricular tissue by means of tough strings called *chordae tendineae*. The *chordae tendineae* keep the AV valves from folding backwards during the systole.
- Semilunar valves. They are located between the ventricles and the arteries. The semilunar valve on the right side of the heart is the pulmonary valve, and it prevents the backflow of blood from the pulmonary trunk into the right ventricle. The semilunar valve on the left side is the aortic valve that prevents the aorta from regurgitating blood back into the left ventricle. The semilunar valves are smaller than the AV valves and don't have *chordae tendineae* to hold them in place. Instead, the cusps of the semilunar valves are cup shaped to catch regurgitating blood and use the blood's pressure to snap shut.

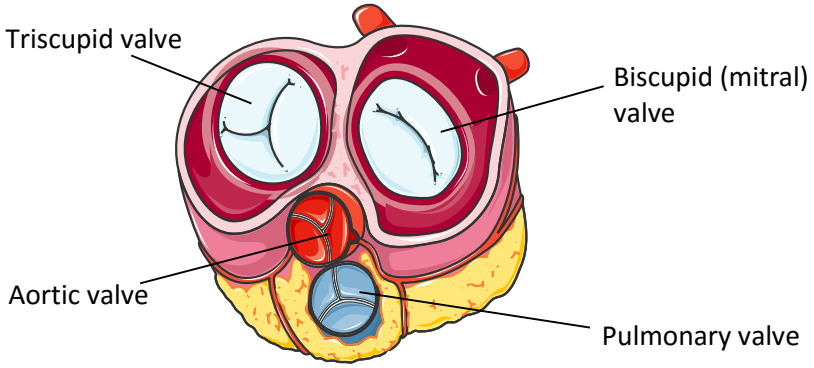

Fig. 3. **Cardiac valves.** Atrioventricular valves allow the blood flow only from atria to ventricles; semilunar valves carry blood away from the heart in the pulmonary and systemic trunk.

The heart is located within a fluid-filled cavity (pericardial cavity), covered with a special membrane termed pericardium. The pericardium is a type of serous membrane that produces serous fluid to lubricate the heart and prevents friction between the heart and its surrounding organs. In addition the pericardium helps keeping the heart in position and it maintains a hollow space for the heart to expand when it is full. The pericardium has two layers: a visceral layer

that covers the outside of the heart and a parietal layer that forms a sac around the outside of the pericardial cavity.

The heart wall is made of three layers: epicardium, myocardium, and endocardium **(fig. 4)**.

- Epicardium. The epicardium, the outer layer of the heart wall, is a thin layer of serous membrane that lubricates and protects the outside of the heart.
- Myocardium. It is the muscular middle layer of the heart wall that contains the cardiac muscle tissue. Myocardium makes up the majority of the thickness and mass of the heart wall and is the part of the heart responsible for pumping blood.
- Endocardium. It is a simple squamous endothelium layer that covers the interior surface of the heart. The endocardium is very smooth and is responsible for keeping blood from sticking to the inside of the heart and forming blood clots.

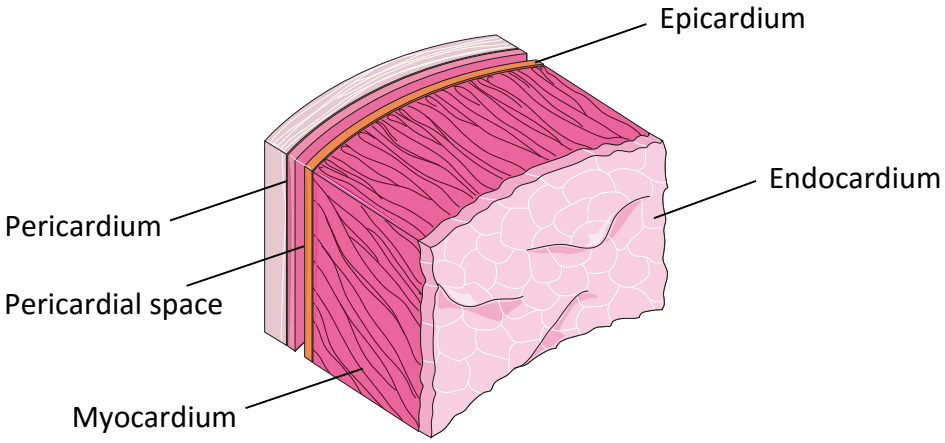

Fig. 4. Layers of the heart

Cardiac innervation

The heart is innervated by the autonomic nervous system (**fig. 5**). The primary site of the brain that host the source of autonomic outputs to the heart and blood vessels is the medulla, whose activity is modified by the hypothalamus and higher centers that are particularly important in regulating cardiovascular responses to emotion and stress.

Autonomic outflow from the medulla is divided principally into sympathetic and parasympathetic branches.

Sympathetic efferent nerves are present throughout the atria, especially in the sinoatrial (SA) node, and ventricles, including the conduction system of the heart. Sympathetic stimulation of the heart induces an increment of heart rate (positive chronotropy), force of muscular contraction (positive chronotropy), and conduction velocity (positive dromotropy).

Parasympathetic branch is represented by the vagus nerve that innervates the SA node and the atrioventricular (AV) node; parasympathetic innervation is absent in the ventricles.

Parasympathetic stimulation has an opposite effect with respect to sympathetic output, and it induces negative chronotropy, inotropy and dromotropy.

Sympathetic and parasympathetic effects on heart function are mediated by β-adrenoceptors and muscarinic receptors, respectively.

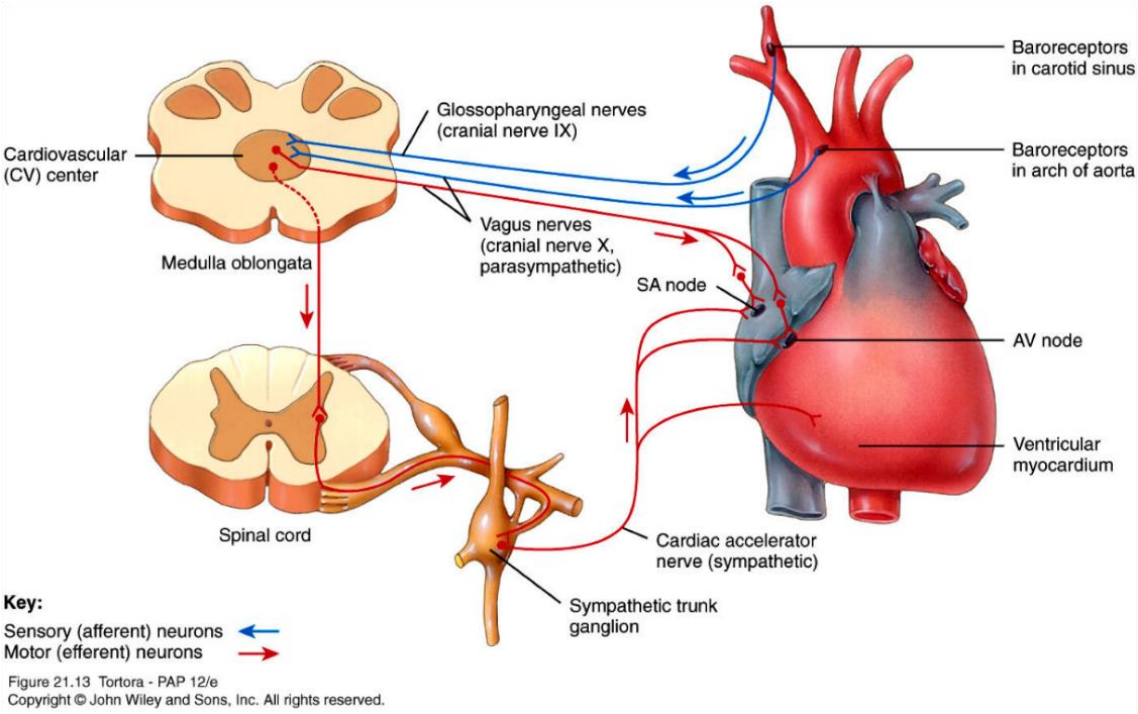

Fig. 5. Autonomic innervation of the heart. SA and AV node are innervated by both sympathetic and parasympathetic fibers, whereas the ventricular myocardium is only innervated by vagal efferents.

Cardiac conduction system

The conduction system of the heart consists in a group of specialized cardiac cells responsible for initiating and coordinating the electric signal that causes the rhythmic and synchronized contractions of the atria and ventricles.

The main components of the conduction system are the SA node, the AV node, the bundle of His, divided in left and right bundle branch, and the Purkinje fibers **(fig. 6)**.

The SA node is located at the junction of the superior *vena cava* with the right atrium. It represents the natural pacemaker of the heart and it releases electrical stimuli at regular rate, based on the needs of the body.

From there, the signal reaches the AV node, located in the right posterior portion of the interatrial septum; there are three bundles of atrial fibers containing Purkinje-type fibers that connect the SA node to the AV node: the anterior intermodal tract of Bachman, the middle intermodal tract of Wenckebach, and the posterior intermodal tract of Thorel. In the AV node the conduction is slow and a delay of about 0.1 s (AV nodal delay) occurs before excitation spreads to the ventricles.

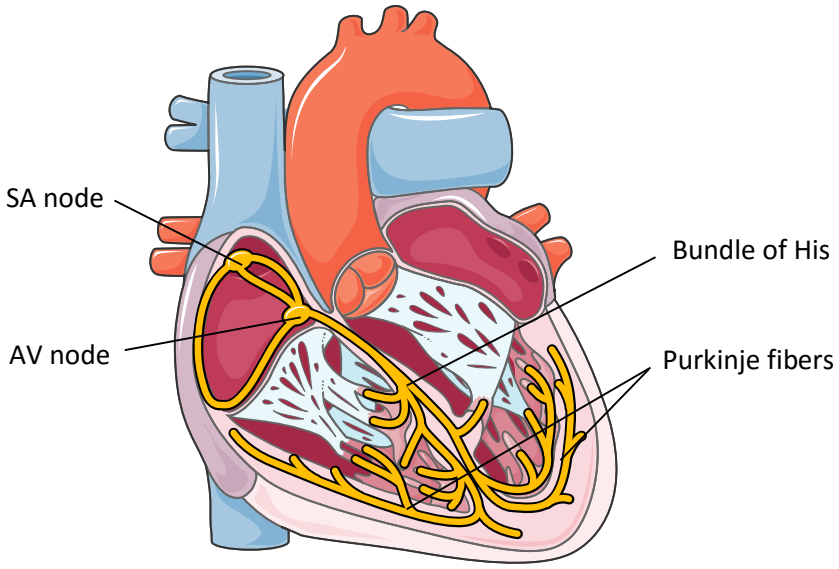

Fig. 6. Conducting system of the heart. The SA node generates impulses; the AV node slows down the excitation spread (0.1 s); the bundle of His connects the AV node to the ventricles; the left and right branches conduct the impulses through the interventricular septum; the Purkinje fibers stimulate the contractile cells of both ventricles.

The AV node is in conjunction with the bundle of His, which gives off a left bundle branch and a right bundle branch. The bundle branches divide into an anterior fascicle and a posterior fascicle. The branches and fascicles run in the sub-endocardium down to either side of the septum and come into contact with the Purkinje system, whose fibers spread to all parts of the ventricular myocardium.

Failure in the function of the nodes or bundles leads to arrhythmias. On the other side, ectopic pacemaker or conductive activity may cause arrhythmias requiring intervention.

2.2. ACTION POTENTIALS

The action potential represents the changes in voltage of a single cardiac cell. Different action potentials are recorded in different regions of the heart.

- Atrial and ventricular myocardium have fast response action potentials, characterized by a rapid depolarization (phase 0).
- SA node and AV node cells show slow response action potentials, characterized by a slower initial depolarization phase.

Fast response action potentials

Atrial and ventricular myocytes are examples of non-pacemaker cells in the heart. Because these action potentials undergo very rapid depolarization, they are sometimes referred to as "fast response" action potentials (**fig. 7**). They can be divided into 5 phases:

- Phase 0 (depolarization). When these cells are depolarized from -90 mV to a threshold voltage of about -70 mV (i.e. by an action potential in an adjacent cell), a rapid depolarization caused by a transient increase in the fast Na^+ channel conductance through the opening of cardiac fast sodium channels (hNav1.5) occurs. This increases the inward, depolarizing Na^+ current (I_{Na}) responsible for the generation of the "fast-response" action potentials.
- Phase 1. It represents an initial repolarization caused by the opening of a special type of transient outward K^+ channel (K_{to}).
- Phase 2. It is the plateau phase in the action potential. This inward calcium movement is through long-lasting (L-type) calcium channels that open when the membrane potential depolarizes to about -40 mV. This plateau phase prolongs the action potential duration and

permits the excitation-contraction coupling. The balance of inward calcium current generated by L-type calcium channels and outward potassium current (I_{Krs}, I_{Ks}) allows the maintenance of the membrane potential near 0 mV for about 200 ms. The influx of calcium ions during the plateau phase is necessary for the activation of ryanodine receptors (RyR) located on the endoplasmic reticulum. The activation of RyR induces the outflow of the calcium from the *cisternae* of endoplasmic reticulum.

- Phase 3. During this phase the membrane potential repolarizes to the resting value. The processes involved in the repolarization are: the inactivation of L-type calcium channels and the active presence of potassium channels; the potassium current described in this phase are rapid (I_{Kr}) and slow (I_{Ks}), resulting in an outward, repolarizing current.
- Phase 4. The membrane potential is maintained at the resting value of about -90 mV by the inward rectifier current (I_{K1}) until it reaches a new depolarizing stimulus.

Slow response action potentials

The main characteristics of SA node cells are the absence of both a true resting potential and a plateau phase, but they are able to generate regular and spontaneous action potentials. These pacemaker action potentials are referred to as "slow response" action potentials (**fig. 7**). They are divided into the phases described below:

- Phase 4. At the end of repolarization, the membrane potential reaches its more negative value (maximum diastolic potential, MDP) of about -60 mV. In the SA node the MDP is determined by the potassium currents (I_{Kr}, I_{Ks}) (Ono & Ito, 1995) and by the activation of the I_f current. When the membrane potential reaches the value of about -60 mV, a class of ion channels conducting a slow, inward (depolarizing) Na^+/K^+ current gets activated. This current is called "funny" and abbreviated as "I_f" (DiFrancesco et al., 1986). This depolarizing current causes the depolarization of the membrane potential, thereby initiating phase 4. Besides, a spontaneous calcium release from endothelial reticulum contributes to the late phase of diastolic depolarization by activating the Na^+/Ca^{++} exchanger (Lakatta & DiFrancesco, 2009). During the early part of phase 4 there is also a slow decline in the outward movement of K^+ induced by delayed rectifier potassium channels (I_{Kr}).
- Phase 0. As the membrane potential reaches about -50 mV, another type of channel opens. This channel is called transient or T-type Ca^{++} channel. As Ca^{++} enters the cell through these channels down its electrochemical gradient, the inward directed Ca^{++} currents further depolarize the cell. However this current appears to be present only in some mammalian

species. When the membrane depolarizes to about -40 mV, a second type of Ca^{++} channel opens. These are the so-called long-lasting, or L-type Ca^{++} channels. Opening of these channels causes more Ca^{++} to enter the cell and to further depolarize the cell causing an action potential. It should be noted that a hyperpolarized state is necessary for pacemaker channels to become activated. Without the membrane voltage becoming negative at the end of phase 3 pacemaker channels cannot be activated and no pacemaker activity can take place. This is the reason why cellular hypoxia, which depolarizes the cell and alters phase 3 hyperpolarization, leads to a reduction in pacemaker rate (i.e. bradycardia).

- Phase 3. Repolarization occurs as K^+ channels open, thereby increasing the outward directed, hyperpolarizing K^+ currents. At the same time, the L-type Ca^{++} channels become inactivated and close, which decreases Ca^{++} conductance and the inward depolarizing Ca^{++} currents.

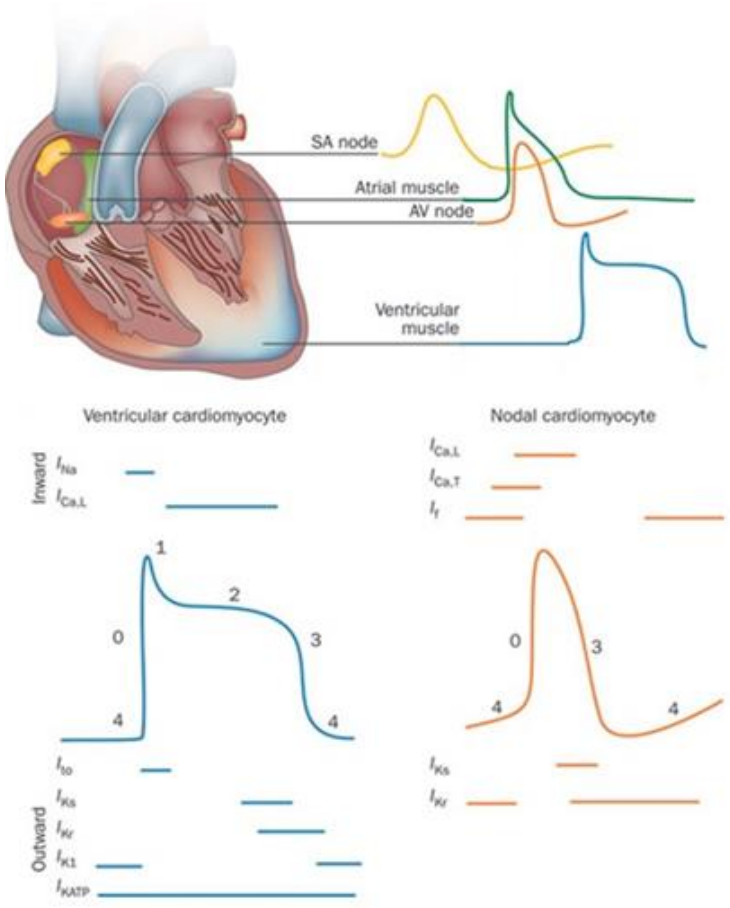

Fig. 7. **Cardiac action potentials.** Different regions of the heart generate different type of action potentials. Working myocardium (atria and ventricles) expresses fast response action potential (left), whereas conduction system cells are characterized by slow response action potential (right).

It is important to note that action potentials described for SA node cells are very similar to those found in the AV node. Therefore, action potentials in the AV node, like the SA node, are determined primarily by changes in slow inward Ca^{++} and K^+ currents, and do not involve fast Na^+ currents. AV nodal action potentials also have intrinsic pacemaker activity produced by the same ionic currents as described above for SA nodal cells.

Once an action potential is initiated in both SA node, atrium, and ventricle, there is a period of time during which a new action potential cannot be initiated. This is termed the effective refractory period (ERP) or the absolute refractory period (ARP) of the cell. During the ERP, stimulation of the cell by an adjacent cell undergoing depolarization does not produce new action potentials. The ERP acts as a protective mechanism in the heart by preventing multiple action potentials (i.e. limiting the frequency of depolarization and therefore heart rate). This is important because at very high heart rates, the heart would be unable to adequately fill with blood and therefore ventricular ejection would be reduced.

2.3. I_f CURRENT

The funny (I_f) current was first described in the SA node (Brown et al., 1979) and was extensively characterized originally in this tissue and in Purkinje fibers (DiFrancesco et al., 1986 a; Brown et al., 1980; DiFrancesco et al., 1980; DiFrancesco, 1981 a; DiFrancesco, 1981 b; DiFrancesco, 1986 b). The current was defined "funny" because it is characterized by several unusual features (DiFrancesco, 1993):

- Voltage-dependence. I_f is activated by hyperpolarization with a threshold of approximately -30/-40 mV in the SA node.
- Ion permeability. Values of the reversal potential measured in the early experiments in Purkinje fibers and in isolated rabbit SA node myocytes were in the range of -10 to -20 mV (DiFrancesco, 1981 a; DiFrancesco et al., 1986 a), indicating a mixed ionic permeability. Ionic substitution experiments indeed identified Na^+ and K^+ ions as the physiological carriers of the current, with a Na^+/K^+ permeability ratio of about 0.27 (DiFrancesco, 1981; Frace et al., 1992). The conductance of f-channels was also shown to increase with external K^+ concentration (DiFrancesco, 1981 a) in a way similar to that of other potassium permeable channels (Hille, 2000).

- Autonomic control. A major contribution to the autonomic control of rate is provided by the cAMP dependence of f-channels. cAMP is an intracellular second messenger activating several cellular processes, and its concentration is strictly controlled by cellular compartmentation of the biochemical factors responsible for cAMP synthesis and degradation (i.e. adenylyl cyclase and phosphodiesterase) in order to prevent unwanted spreading of cAMP signaling (Jurevicius et al., 1996; Rich et al., 2000; Rich et al., 2001; Zaccolo et al., 2002; Jurevicius et al., 2003).

Direct binding of cAMP molecules to the C-terminus of pacemaker channels increases the probability of f-channel opening via a positively-directed shift of the voltage dependence of the activation curve, (DiFrancesco & Tortora, 1991), whereas a reduced intracellular cAMP concentration gives rise to the opposite action (i.e. a negative shift of the activation curve and a reduction of open probability at any given voltage), **fig. 8**.

By activating β-adrenergic (β1 and β2) and muscarinic M2 receptors, respectively, the sympathetic and parasympathetic neurotransmitters control the cytosolic concentration of the second messenger cAMP. This induces an increase/decrease of the net inward current during diastolic depolarization and a consequent increase/decrease of firing rate, respectively.

The adaptive function of sympathetic and parasympathetic innervation relies on the ability of the autonomic nervous system to respond effectively to rapidly changing physiological demands. Pacemaker channels, and specifically HCN4 subunits (**see point 1.4**), are confined, together with the β2-adrenergic receptors (β2-ARs), to membrane *caveolae*, cellular microdomains whose function is to keep in close proximity proteins involved in a specific signal transduction pathway (Anderson, 1998; Rybin et al., 2000; Steinberg et al., 2001; Parton et al., 2003; Deurs et al., 2003).

In cardiac cells, the physiological response to sympathetic stimulation is mediated by both β1 and β2 subtypes of β-ARs. In their expression patterns in cardiac cells, these two subtypes differ in density and localization. β1-ARs are generally more abundant and widely distributed than β2-ARs in the whole heart; in the SAN, however, β2-ARs are expressed at a much higher level than in the rest of the heart (Brodde et al., 1982; Del Monte et al., 1993; Levy et al., 1993; Rodefeld et al., 1996; Brodde et al., 2001).

Furthermore, whereas β2-ARs are specifically localized in *caveolae*, β1-ARs are for the most part excluded from these structures (Rybin et al., 2000; Li et al., 1995; Steinberg et al., 2004) and in rabbit SAN myocytes, β2-ARs co-localize with the HCN4 isoform of pacemaker channels in membrane *caveolae* (Barbuti et al., 2007).

Adrenergic agonists increase I_f at diastolic potentials by shifting the activation curve to more positive voltages. This shift provides more inward current thus increasing the slope of the

diastolic depolarization and accelerating heart rate. Muscarinic agonists have opposite effects on I_f and shift the activation curve to more negative voltages. Thus less inward current is available at diastolic potentials, causing a decreased slope of this phase and decelerating heart rate.

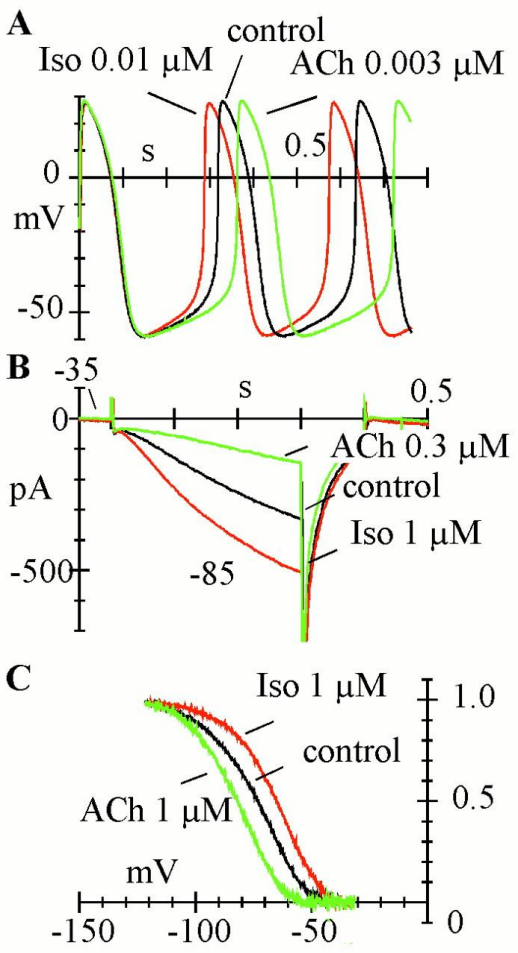

Fig. 8. Effects of autonomic modulators on action potentials and I_f current recorded in rabbit SA node myocytes. (A) The administration of the autonomic modulators (Isoprenaline, Iso, and AcetylCholine, ACh) induces changing in spontaneous rate of action potentials: the frequency is accelerated by Iso and slowed by ACh. (B) The I_f current amplitude increases with Iso and decreases with Ach. (C) The activation curves, reflecting the steady-state fraction of open channels, is shifted to more positive (Iso) or negative (ACh) voltages.

Kinetics

I_f current activation and deactivation processes were described using several types of mechanisms, including single- (DiFrancesco & Noble, 1985; McCormick & Pape, 1990) and double-exponential Hodgkin–Huxley kinetics (Noble et al., 1989; van Ginneken & Giles, 1991; Demir et al., 1994), and more complex, non-Hodgkin–Huxley kinetics (DiFrancesco, 1984). Detailed investigation reveals that I_f kinetics cannot be described using simple Hodgkin–Huxley type of gating, but require complex multistate kinetic modelling based on the existence of distinct delaying and proper gating processes (DiFrancesco, 1984). A similar approach has been used to describe the kinetics of HCN channels. These are reproduced using an allosteric dual voltage- and cAMP-dependent kinetic model. In this model, the HCN are represented as tetramers carrying voltage sensors that can be gated individually by voltage and undergo concerted open/closed allosteric transitions **(fig. 9)** (DiFrancesco, 1999; Altomare et al., 2001).

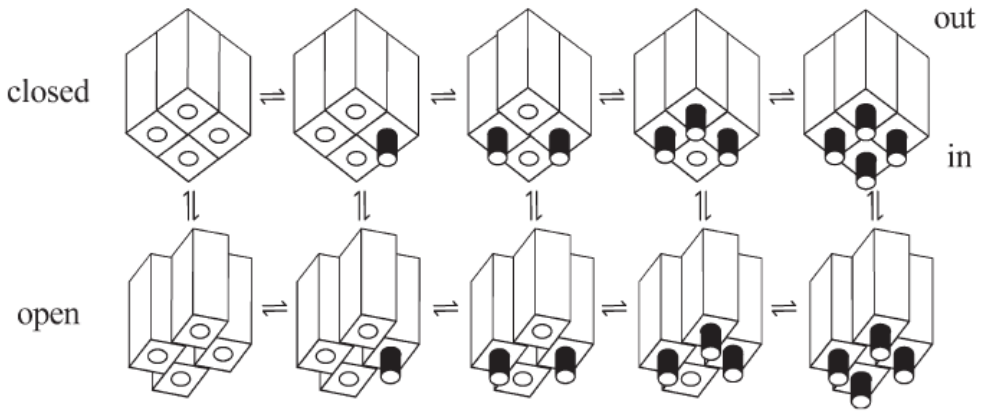

Fig. 9. The f channel kinetics are described using an allosteric voltage-dependent gating model. The HCN channel is represented as a homotetramer; each subunits as a voltage sensor (cylindrical shape) that can occupy a reluctant (hidden) or a willing state (protruding from the subunit). Voltage sensors are independently gated by voltage, whereas subunits switch from the closed to the open configuration all at once. The probability of the opening increases every time 1 voltage sensor enters the willing state (Accili et al.,2002).

Tissue distribution of I_f in the heart

In the adult heart f-channels are densely expressed throughout the cardiac conduction system (SA node, AV node, Purkinje fibers), while their presence is at a much lower level if not absent in the rest of the myocardium. During embryonic and neonatal development, HCN channels are

functionally expressed also in myocytes programmed to develop into working myocardial cells (atrial and ventricular myocytes). In adult ventricular and atrial myocytes, a clear-cut physiological role of I_f is not apparent: this is because either the channel density is very low, or the voltage range of channel activation is too negative, or both (Robinson et al., 1997; Cerbai et al., 1999).

Nevertheless, expression of f-channels in working myocardium may become important under several pathological conditions. For example, I_f is upregulated in ventricular myocytes of hypertrophic hearts as a consequence of remodeling, leading to the hypothesis that it may contribute to arrhythmias in chronic hypertension and cardiac failure, a condition associated with increased risk for sudden cardiac death (Cerbai et al., 2006).

It is well known that cardiac fibers surrounding atrioventricular valves may display rhythmic activity (Wit et al., 1973; Wit et al., 1979). Beating cells from the region surrounding the mitral valve in the rabbit express a large I_f, indicating a correlation between spontaneous activity and the pacemaker current (Anumonwo et al., 1990). More recently, it's observed that the tissue surrounding canine and human pulmonary veins contains pacing cells expressing I_f (Chen et al., 2000; Chen et al., 2001 a; Greenwood & Prestwich, 2002; Perez-Lugones et al., 2003).

2.4. HCN CHANNELS

The Hyperpolarization-activated Cyclic Nucleotide-gated (HCN) is a family of channels cloned in the late 1990s (Zagotta et al., 2003), composed by 4 isoforms (from HCN1 to HCN4) with different biophysical properties and pattern of expression.

HCN channels are classified on the basis of their sequence as members of the superfamily of voltage-gated K^+ (Kv) and CNG channels; they have a tetrameric composition (Ulens & Siegelbaum, 2003; Zagotta et al., 2003), and each subunit is composed of 6 transmembrane domains (S1–6), **fig. 10**. Similarly to Kv channels, they have a positive charged S4 domain, with the function of voltage sensor that in HCN channels includes 10 basic residues whose mutation strongly affects the channel voltage dependence (Chen et al., 2000; Vaca et al., 2000). However, while Kv channels open on depolarization, HCN channels open on hyperpolarization. This difference could be due to an inverted movement of the voltage sensor of HCN compared to Kv channels in response to the same voltage change, or to an inverted coupling between S4 movement and channel gating. The second possibility appears more likely since cysteine

accessibility experiments have shown that, like in Kv channels, hyperpolarization induces an inward movement of the S4 segment in HCN channels (Mannikko et al., 2002).

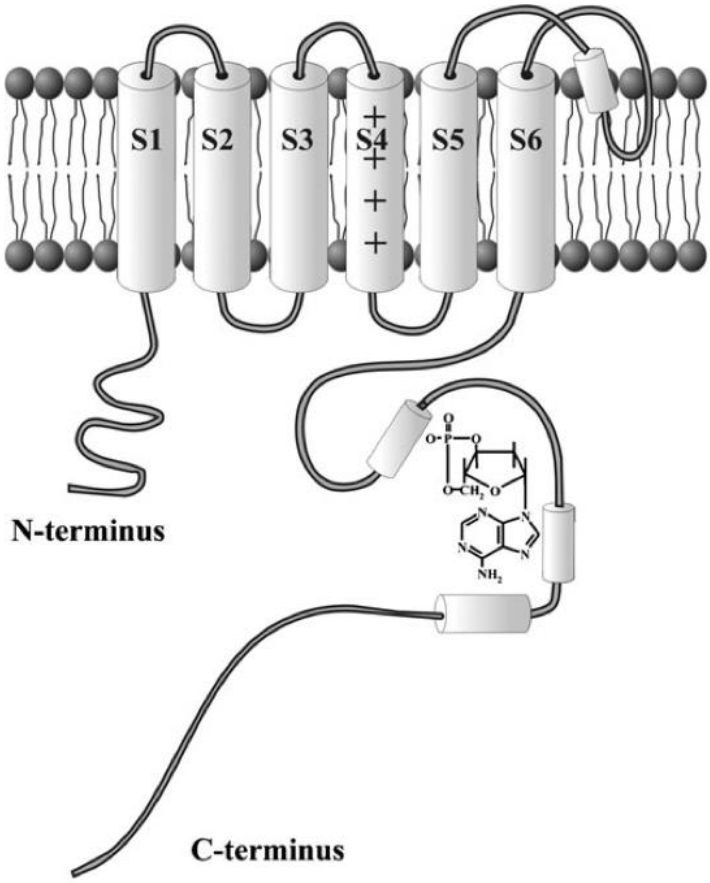

Fig. 10. **HCN channels structure**. Each subunits is composed of 6 transmembrane segments, from S1 to S6. S4 is positively charged and acts as voltage sensor; GYG pore sequence is located between S5 and S6; C-terminus includes the C-linker and the CNBD interacting with cAMP

The segments S4 and S5 are connected by a linker that contains important residues for the gating machinery and they act as coupling elements between the S4 voltage sensor and the channel gate. The region at the border between S4 and the S4–S5 linker contains a histidine residue and it is important for the pH sensitivity of HCN channels (Zong et al., 2000). The pore of the HCN channels has the GYG sequence, typical of K^+-permeable channels. The C-terminus can be subdivided into different regions, including a central cyclic nucleotide-binding domain (CNBD), and a C-linker (about 80 aa long) that connects the C-terminal part of S6 to the CNBD, homologous to that of CNG channels (Viscomi et al., 2001; Wang et al., 2001). A more detailed

identification of functionally relevant sub-domains of the C-terminus and of the CNBD has been established based on the homology with the CNBD structure of both the bacterial catabolite-activating protein and the regulatory subunit of cAMP-dependent protein kinase, and recent data obtained from X-ray crystallography of the C-terminus of HCN2 (Weber & Steitz, 1987; Wainger et al., 2001; Zagotta et al., 2003). The CNBD structure includes an h-roll sub-domain, acting as a constitutive inhibitor of the channel, and a helix located at the C-terminal end (termed C-helix), which contributes to the interaction with the purine ring of cAMP. cAMP binds with a greater affinity to the open, rather than the closed state of the channel (Varnum et al., 1995; Matulef et al., 1999; Wainger et al., 2001; Zagotta et al., 2003).

HCN channel isoforms

The HCN core region, including the transmembrane domain and the CNBD, is highly conserved among the different isoforms (80% identity), from sequence alignment studies. Whereas the sequences diverge at the N- and C-termini, suggesting a relevant role of the terminal region for some of the differences in the biophysical properties among isoforms (Viscomi et al., 2001). Indeed, there are quantitative differences between the different isoforms. For example (**fig. 11**), the activation/deactivation kinetics of HCN2 are faster than those of HCN4 and slower than those of HCN1; typical values of activation time constant at -95 mV are 0.11, 1.13, and 2.52 s at room temperature (24-25°C) for HCN1, HCN2, and HCN4, respectively (Altomare et al., 2001). HCN2 has a more negative activation threshold than both HCN1 or HCN4; when channels are over-expressed in HEK293 cells, typical values of the half-maximal activation voltage are -73, -81, and -92 mV for HCN1, HCN4, and HCN2, respectively (Accili et al., 2002), but these values can be significantly altered by several conditions. Finally, the binding with cAMP activates HCN channels by shifting the activation curve to more positive voltages, but maximal shifts vary among isoforms, with HCN1 being much less responsive (range 4.3–5.8 mV) than both HCN2 (range 16.9–19.2 mV) or HCN4 (range 11.1–23 mV) (Ludwig et al., 1999; Seifert et al., 1999; Moroni et al., 2000; Viscomi et al., 2001; Wainger et al., 2001; Wang et al., 2001; Altomare et al., 2003; Zagotta et al., 2003). These differences appear to be determined by differential inhibitory interactions of the C-terminus with the transmembrane domains in the various isoforms, more than by a variable cAMP binding affinity to the CNBD (Wang et al., 2001). The properties of the HCN3 isoform have been only partially investigated; HCN3 kinetics are intermediate between those of HCN2 and HCN4 (Moosmang et al., 2001).

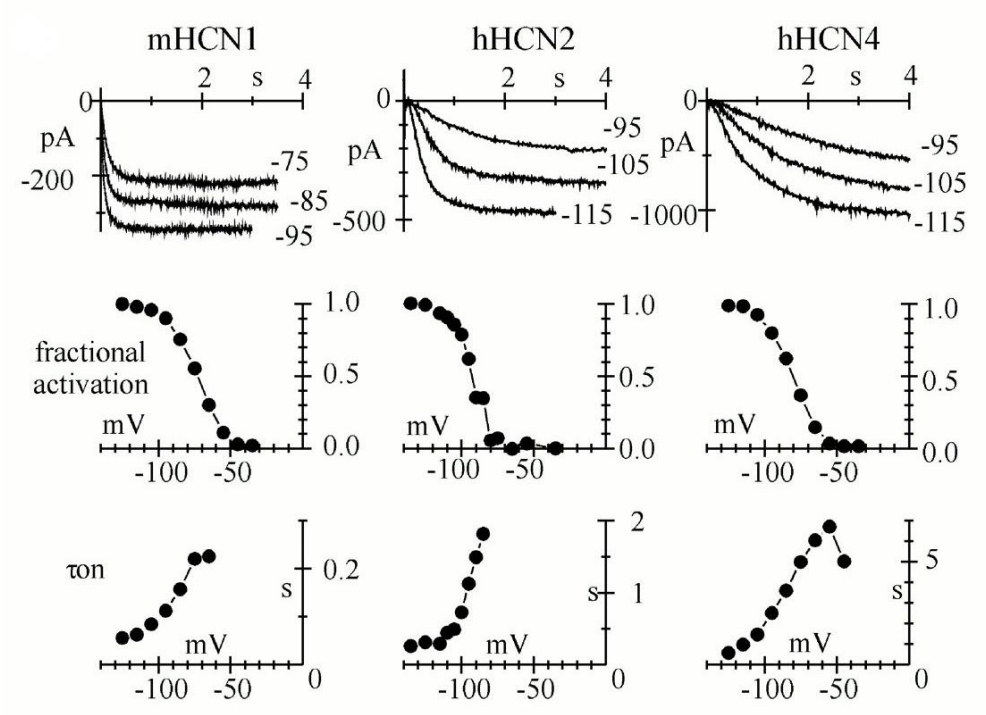

Fig. 11. Kinetic properties of HCN1, HCN2, and HCN4 isoforms. (Top) activation traces recorded on hyperpolarizing steps from a holding potential of -35 mV in HEK293 cells. (Middle) mean activation curves of HCN1, HCN2, HCN4, respectively. (Bottom) mean time constants of activation obtained by single exponential fitting of activation traces.

The various regions of the heart and the brain are characterized by different kinetics and modulatory properties of native currents that partly reflect a different tissue distribution of HCN isoforms (DiFrancesco, 1993; Pape, 1996). However, the channel properties can be modified by several factors, and simple electrophysiological analysis is not sufficient to reveal the isoform composition of native channels. For example, native channels can be formed by heteromultimers of different isoforms, with properties intermediate between those of individual components (Chen et al., 2001 b; Ishii et al., 2001; Ulens & Tytgat, 2001; Xue et al., 2002; Altomare et al., 2003); also, HCN activity can be modified by interaction with auxiliary subunits such as MiRP1 (Qu et al., 2004) or with scaffold proteins such as filamin-A for HCN1 (Gravante et al., 2004), or by specific subcellular compartmentation such as the caveolar compartmentation of HCN4 in SA node cells (Barbuti et al., 2004). The kinetic properties and expression levels of HCN channels are also regulated by auxiliary proteins (TRP8), and lipids (phosphatidylinositol 4,5-bisphosphate); finally, the expression of a given isoform may yield quantitatively different biophysical properties according to whether the isoform is expressed in

heterologous or in homologous expression systems, suggesting that a contextdependent modulation occurs (Qu et al., 2002).

In the heart, HCN1, HCN2, and HCN4 are all expressed with HCN4 being the major component in the pacemaker region, although low expressions of HCN1 and HCN2 have also been reported (Santoro et al., 1999; Shi et al., 1999; Moroni et al., 2001).

2.5. THE ELECTROCARDIOGRAM

The electrocardiogram (ECG) allows to record on the body surface the potential fluctuations which originate during the cardiac cycle. The ECG may be recorded using two different methods: unipolar recording that consists of an electrode connected to an indifferent electrode at zero potential, and bipolar recording that uses two active electrodes. In a volume conductor, the sum of the potentials at the points of an equilateral triangle with a current source in the centre is zero at all times. A triangle with the heart located in the centre (Einthoven's triangle, **fig. 12**) can be approximated by placing electrodes on both arms and on the left leg. These are the three standard limb leads used in electrocardiography. If these electrodes are connected to a common terminal, an indifferent electrode that stays near zero potential is obtained.

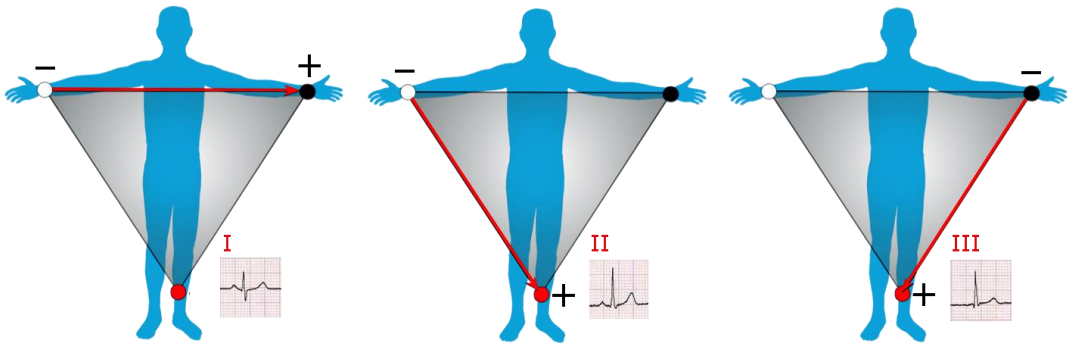

Fig. 12. Graphical representation of Einthoven's triangle. (Lead I) the axis moves from right arm (negative electrode) to left arm (positive electrode). (Lead II) The axis goes from the right arm (negative electrode) to left leg (positive electrode). (Lead III) the axis moves from the left leg (positive electrode) to the left arm (negative electrode).

Depolarization moving toward an active electrode in a volume conductor produces a positive deflection, whereas depolarization moving in the opposite direction produces a negative deflection. By convention, an upward deflection is written when the active electrode becomes positive relative to the indifferent electrode, and a downward deflection is written when the active electrode becomes negative. The P wave is produced by atrial depolarization, the QRS complex by ventricular depolarization, and the T wave by ventricular repolarization. The U wave is an inconstant finding, believed to be due to slow repolarization of the papillary muscles.

Bipolar leads

Bipolar leads were used before unipolar leads were developed. The standard limb leads (leads I, II, and III, **fig.13**) record the differences in potential between two limbs. Because current flows only in the body fluids, the records obtained are those that would be obtained if the electrodes were at the points of attachment of the limbs, no matter where on the limbs the electrodes are placed. In lead I, the electrodes are connected so that an upward deflection is inscribed when the left arm becomes positive relative to the right (left arm positive). In lead II, the electrodes are on the right arm and left leg, with the leg positive; and in lead III, the electrodes are on the left arm and left leg, with the leg positive.

Unipolar leads

Nine additional unipolar leads (**fig. 13**) are commonly used in clinical electrocardiography to record the potential differences between an exploring electrode and an indifferent electrode. There are six unipolar chest leads (precordial leads) designated V1–V6 and three unipolar limb leads: VR (right arm), VL (left arm), and VF (left foot). Augmented limb leads, designated by the letter a (aVR, aVL, aVF) are generally used. The augmented limb leads are recordings between one limb and the other two limbs. This increases the size of the potentials by 50% without any change in configuration from the nonaugmented record.

Normal ECG

The sequence in which the parts of the heart are depolarized and the position of the heart relative to the electrodes are important considerations in interpreting the configurations of the waves in each lead (**fig. 14**). The atria are located posteriorly in the chest. The ventricles form the base and anterior surface of the heart, and the right ventricle is anterolateral to the left. Thus, aVR "looks at" the cavities of the ventricles. Atrial depolarization, ventricular depolarization, and

ventricular repolarization move away from the exploring electrode, and the P wave, QRS complex, and T wave are therefore all negative (downward) deflections; aVL and aVF look at the ventricles, and the deflections are therefore predominantly positive or biphasic. There is no Q wave in V1 and V2, and the initial portion of the QRS complex is a small upward deflection because ventricular depolarization first moves across the midportion of the septum from left to right toward the exploring electrode. The wave of excitation then moves down the septum and into the left ventricle away from the electrode, producing a large S wave. Finally, it moves back along the ventricular wall toward the electrode, producing the return to the isoelectric line.

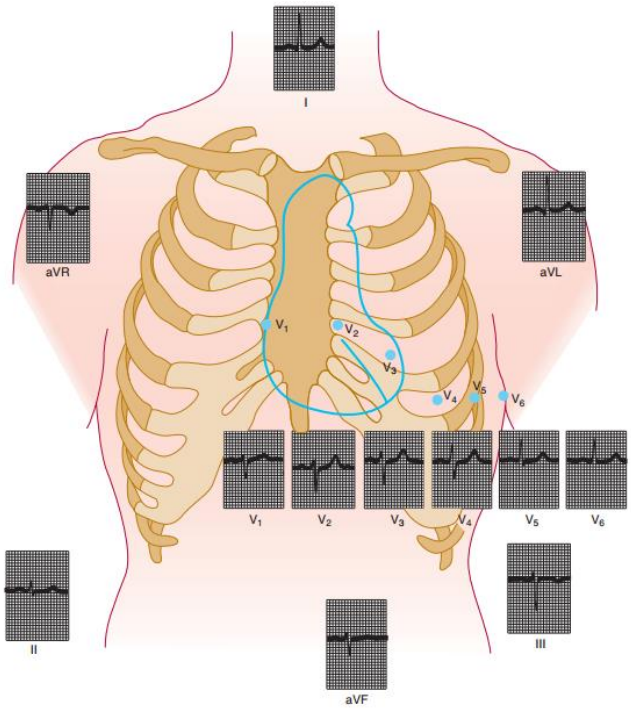

Fig. 13. Bipolar and unipolar leads positioning. Normal ECG is composed of three bipolar leads (I, II, III), and nine additional unipolar leads (V1-V6, aVR, aVL, aVF). (Reproduced with permission from Goldman MJ: Principles of Clinical Electrocardiography, 12th ed. originally published by Appleton & Lange. Copyright © 1986 by McGraw-Hill.)

Conversely, in the left ventricular leads (V4–V6) there may be an initial small Q wave (left to right septal depolarization), and there is a large R wave (septal and left ventricular depolarization) followed in V4 and V5 by a moderate S wave (late depolarization of the ventricular walls moving back toward the AV junction). There is considerable variation in the

position of the normal heart, and the position affects the configuration of the electrocardiographic complexes in the various leads.

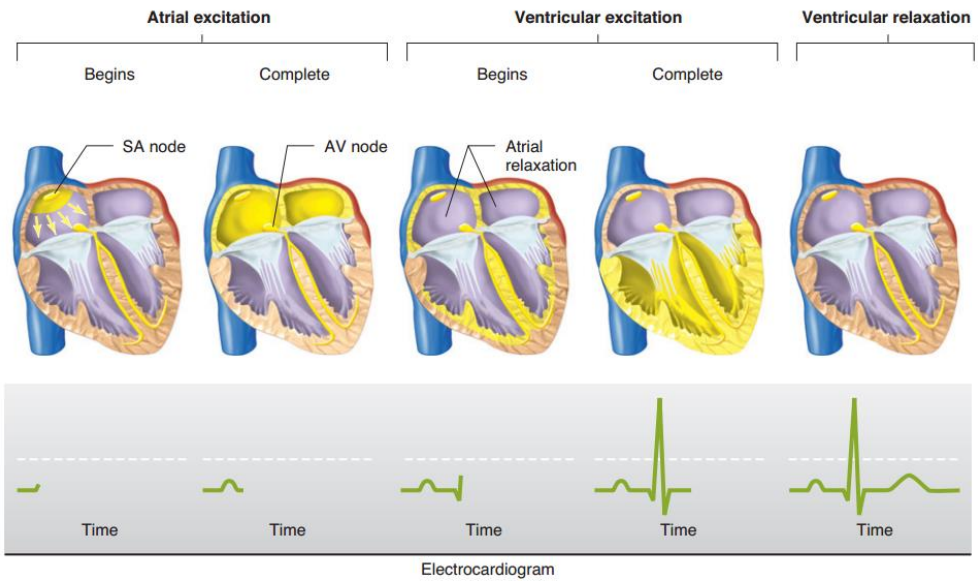

Fig. 14. Sequence of cardiac excitation. Top: Anatomical position of electrical activity. Bottom: corresponding electrocardiogram. The yellow colour denotes areas that are depolarized. (Reproduced with permission from Goldman MJ: Principles of Clinical Electrocardiography, 12th ed. originally published by Appleton & Lange. Copyright © 1986 by McGraw-Hill.)

Monitoring

Using a small portable tape recorder (Holter monitor), it is also possible to record the ECG in patients during their normal activities. The recording is later played back at high speed and analysed. Long-term continuous records can be obtained. Recordings obtained with monitors have proved valuable in the diagnosis of arrhythmias and in planning the treatment of patients recovering from myocardial infarctions.

Normal cardiac rate

In the normal human heart, each beat originates in the SA node. The heart beats about 70 times per minute at rest. The rate is slowed (bradycardia) during sleep and accelerated (tachycardia) by several stimuli (i.e. emotion, exercise, fever, and many other). In healthy young individuals the heart rate varies with the phases of respiration: it accelerates during inspiration and

decelerates during expiration, especially if the depth of breathing is increased. This normal phenomenon, termed “sinus arrhythmia”, is due primarily to fluctuations in parasympathetic output to the heart. During inspiration, impulses in the *vagi* from the stretch receptors in the lungs inhibit the cardio-inhibitory area in the *medulla oblongata*. The tonic vagal discharge that keeps the heart rate slow decreases, and the heart rate rises. Disease processes affecting the sinus node lead to marked bradycardia accompanied by dizziness and syncope (sick sinus syndrome), sinus pause/arrest, chronotropic incompetence, and sinoatrial exit block. Sinus node dysfunction are also associated with alteration in conduction system and different supraventricular tachyarrhythmias (i.e. atrial fibrillation and atrial flutter).

2.6. RADIOTELEMETRY IN FREELY-MOVING MICE

Cardiovascular research requires an accurate measurement of parameters relating to the circulatory system of laboratory animals. Determination of heart rate and heart rate variability are based on electrocardiogram (ECG) recordings.

Radiotelemetry combines miniature sensors and transmitters to detect and record biological signal in animals to remote receiver. The receiver converts the analog frequency signal into a digital signal to be imputed into a computerized data acquisition system.

Radiotelemetry enables recording of data from conscious and freely-moving animals without requiring the presence of investigators in the proximity of the animal.

This methodology also reduces the number of animals used, rendering this technology the favourite method of monitoring physiological parameters in laboratory animals (Kramer & Kinter, 2003; Kramer et al., 1993). The constant innovations in radiotelemetry technology (i.e. implant miniaturization) make possible the recording of physiological parameters and locomotors activity continuously and in real time over longer periods such as hours, days or even weeks (Kramer & Kinter, 2003; Arras et al., 2007).

Telemetry setup consists of an implantable hermetically sealed transmitter, coated with a biocompatible material, and an external receiver system. Using sterile procedures, the transmitter is implanted directly within the peritoneal cavity (Sgoifo et al., 1996). The mice implanted with a transmitter is located in plastic cage placed on top of the receiver that provides reliable reception of data transmitted via digital telemetry. Several receivers are connected to a

matrix that detects changes in signal strength to indicate movement in the animal, and provides one or more digital pulses to the computer upon each movement.

Miniaturized cardiovascular telemetry technology can be used to study the effects of several drugs with cardiovascular action. Measurements of ECG and HR using telemetry in mouse treated with pharmacological compounds have resulted in qualitative and quantitative changes in definitions of ECG waveforms, in baseline values of HR, and in responses to autonomic agents, compared with placebo control mice (Anderson et al., 1993; Mattes & Lemmer, 1991; Wood et al., 2005; Parisella et al., 2012)

2.7. HEART-RATE REDUCING AGENTS

The relevance of the I_f current to cardiac pacemaking makes it the obvious target for the search of drugs able to modify this ionic current, and acquires a large interest for the pharmacological research. In the past few years, substances able to act as specific blockers of the pacemaker current have been developed. These molecules, originally known as "pure bradycardic" agents and termed today "heart rate-lowering" agents, are potentially important therapeutic agents able to induce rate slowing without the inotropic side effects typical of drugs currently used to slow heart rate, such as Ca^{2+} antagonists or β-blockers (Yusuf & Camm, 2003; DiFrancesco & Camm, 2004).

Specific heart rate-lowering agents include, ST567 (alinidine), UL-FS49 (zatebradine), DK-AH269 (cilobradine), ZD-7288, and S16257 (ivabradine).

The main action of these substances is to induce a reduction of the diastolic depolarization slope by blocking I_f (Baruscotti et al., 2005); however some of these drugs, particularly at high concentrations, might affect other channels and lead to arrhythmias (Bois et al., 1996).

Alinidine

One of the first compounds developed as a bradycardic agent was alinidine. It is able to reduce heart rate by prolonging the diastolic depolarization phase, an effect caused by a dual inhibitory action on the pacemaker current. First, it induces a reduction of the maximal channel conductance, and second, it shifts the activation curve of the current to more negative voltages; furthermore, the action of alinidine is not use- or frequency-dependent (Snyders & Van Bogaert, 1987). Despite its efficacy in reducing heart rate, alinidine also blocks calcium and potassium

currents and prolongs the action potential repolarization process (Satoh & Hashimoto, 1986) and therefore is potentially an arrhythmic compound.

Zatebradine

Zatebradine (UL-FS49) is a bradycardic agent derived from verapamil, a Ca^{++} channel blocker. The effect induced by this drug is mediated by a use-dependent block of the pacemaker current, without modification of the voltage dependence (Van Bogaert & Goethals, 1987; Goethals et al., 1993; Van Bogaert & Pittoors, 2003), but zatebradine has a secondary effect since it can also block the I_h current, the neuronal counterpart of I_f, a current that plays a major functional role in the transduction of light signal in photoreceptors (Satoh & Yamada, 2002; Gargini et al., 1999). These undesired symptoms limited possible clinical application, despite zatebradine resulted more specific than alinidine.

Cilobradine

Cilobradine is a compound similar to zatebradine, but with improved selectivity for I_f. In *in-vitro* experiments performed on cardiac myocytes, cilobradine (1 µM) reduced the I_f current by 80% and, at a concentration of 0.3 µM, slowed the rate of diastolic depolarization without apparent changes in action potential shape and duration (Van Bogaert & Pittoors, 2003), and without substantial inotropic or vascular alterations (Schmitz-Spanke et al., 2004).

ZD7288

ZD7288 is a compound able to reduce the spontaneous rate of intact right atria, without modifying ventricular contractility (Marshall et al., 1993.). Experiments in single SA node myocytes isolated from guinea pig hearts showed that the primary effect of ZD7288 is to block the I_f current, but this drug has a minor effects also on Ca^{++} and K^+ currents, that limited the clinical use of ZD7288 (BoSmith et al., 1993). In fact, when tested in intact SA node, ZD7288 (0.3 µM) induced a slowing of rate (-61%), but also caused a modest prolongation (+10%) of action potential duration (Briggs & Heapy, 1992). The effect of ZD7288 on the I_f current depends on a use independent block associated with a shift of the channel activation curve to more negative potentials (-16.2 mV) and a decrease of maximal channel conductance (-52% at 0.3 mM) (BoSmith et al., 1993). In addition it also affects the neuronal I_h current in several

regions of the central nervous system (Harris & Constanti, 1995; Gasparini & DiFrancesco, 1997).

Ivabradine

Ivabradine (S16257) represents a new compound approved by the European Medicines Evaluation Agency as a new symptomatic treatment for patients with chronic stable *angina pectoris* (**fig. 15**). The efficacy of this drug and its mechanism of action have been extensively investigated both in preliminary *in-vitro* and *in-vivo* studies, as well as in clinical trials.

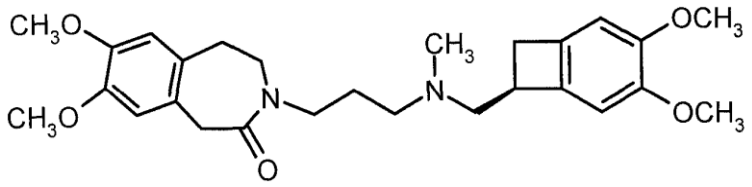

Fig. 15. Chemical structure of the ivabradine

At a concentration of 3 µM, ivabradine reduces by 24% the rate of spontaneous action potential in the isolated rabbit SA node, and its bradycardic action is associated with a decrease in the slope of the early diastolic depolarization, without alteration of action potential amplitude and only a minor increase of its duration (+ 9%), **fig. 16** (Thollon et al., 1994). Experiments performed in rabbit SA node cells show that, at the same concentration, ivabradine also strongly reduces the I_f current (-60%) without affecting T-type Ca^{++}, L-type Ca^{++} and delayed outward K^+ currents (Bois et al., 1996). Investigation of the detailed blocking mechanism of native f-channels (Bucchi et al., 2002) has shown that ivabradine can access the blocking site only when channels are in the open state (state-dependence), and its block is favoured by depolarization; however, block depends on the presence of an outward flow of current through the channel (current-dependence). This latter property is unique and is not found in other f-channel inhibitors (Bucchi et al., 2002). Because channels open on hyperpolarization, and block is favoured by depolarization, block develops quickly and strongly when channels cycle through open/closed states at high rates (use-dependence), and this property results useful for a drug targeted to be more effective during tachycardia. Clinical studies have shown that ivabradine reduces heart rate both at rest and during exercise without modification of parameters unrelated to heart rate, confirming the ability of ivabradine to prevent *angina* symptoms and the

underlying ischemia; in addition ivabradine also displays anti-ischemic properties (Borer et al., 2003; Tardif et al., 2005). These results demonstrated the efficacy of ivabradine for angina prevention and validated the clinical requirements for drug marketing (Vilaine, 2006); the SHIFT study shows that ivabradine is associated with a reduced risk of the cardiovascular death or hospital admission for worsening heart failure (Swedberg et al., 2012). Ivabradine, as happened with zatebradine, may cause visual symptoms which, however, are normally well tolerated.

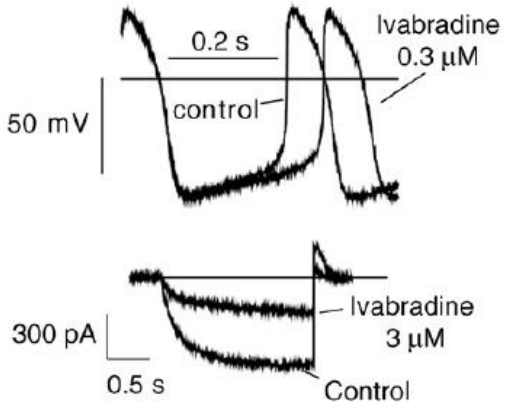

Fig. 16. Heart rate reducing action of the ivabradine. The slowing effect of the spontaneous activity (top) of isolated SA node cells depends on a reducing of the diastolic depolarization. Bottom, block of the I_f current induced by Ivabradine (Bucchi et al., 2007 b).

3. TRADITIONAL CHINESE MEDICINE

3.1. INTRODUCTION

Given the importance of the pharmacological aspects of the pacemaker current, the search for new drugs used in the Traditional Chinese Medicine (TCM) as bradycardic agents has acquired a large interest.

TCM, born more than 2000 years ago in ancient China, is still currently used as a system of medical practice. According to the ancient tradition, TCM is based on the *yin-yang* and the five elements theories; taken together this philosophical system explains all change as well as all natural phenomena in the universe (Lao et al., 2012). The *yin-yang* theory describes the universe as a whole composed of two opposites, *yin* and *yang*, which are interdependent and can transform into each other. Their equilibrium ensures that harmony, including the harmony for the body, is maintained. In this perspective, the *yin-yang* theory reposition the human beings within a rich and deep perspective highlighting the interrelationship of the cosmos and human nature. The five element theory developed from an ancient Chinese philosophical system in which the universe was supposed to consist of five basic elements: wood, fire, earth, metal and water. The five element theory describes the relationship between the human body and the external environment and the physiological and pathological interactions among the internal organs within the body (Lao et al., 2012).

The holistic view of human and nature is also present in medicine; TCM treatments are in contrast to the disease-target approach used by Western medicine, where each disease is treated with a standard protocol. TCM is widely practiced in Asian populations, but in the last decades, many non-Asian countries have recognized the huge therapeutic potential of this traditional practice. Large amount of basic research has been conducted on TCM herbs, mostly in characterizing the multiple-herb constituents and testing their pharmacological activities in the pursuit of new drug discovery; in order for TCM to be rationally used, it is essential to demonstrate its efficacy and safety by high-level evidence using methods accepted in Western medicine (Fung & Linn, 2015).

TCM modalities include Chinese herbal medicine, acupuncture, Chinese massage (*tui na*), mind/body exercise, and dietary therapy. Of these, Chinese herbal medicine and acupuncture are the most commonly used.

Chinese herbal medicine (*zhong yao*) is an integral part of traditional Chinese culture and medical practice. The Chinese *materia medica* includes plants, minerals, and animal parts. These are categorized by nature, flavor, and function. There are four natures (cold, cool, hot, and warm), and five flavors (pungent, sweet, sour, bitter, and salty). Functions include heat-clearing, expectoration and antitussive action, dampness elimination, and interior warming. Typically, an herbal practitioner will prescribe a formula containing ten or more herbs with differing functions, natures, and flavors, which are selected based on the syndrome to be treated. In these constructed formulas, the herbs are believed to act synergistically to harmonize their effects and to neutralize or minimize any toxicity of the individual constituents (Bensky & Barolet, 1990; Bensky & Gamble, 1993).

Recently, several compounds of TCM have acquired importance in Western countries for their therapeutic properties. For example berberine (JKL1073A), an alkaloid found in many medicinal plants of the genera *Berberis* and *Coptis*, has important cardiovascular effects: it induces vasodilatation in smooth muscle (Chiou et al., 1991; Bova et al., 1992) and has been reported to exert both positive inotropic and negative chronotropic actions, exerting a blockade on the ionic currents I_{to} e I_{k1} (Chi et al., 1996).

Another compound characterized by cardiac activity is Wenxin Keli, a Chinese herb extract reported to prevent the induction of persistent atrial fibrillation in isolated canine right atria preparations (Burashnikov et al., 2012)**.**

Wenxin Keli is comprised of 5 components: Nardostachys chinensin batal extract (NcBe), Codonopsis, Notoginseng, Amber, and Rhizoma polygonati (Burashnikov et al., 2012). Very limited data are available in the literature concerning the electrophysiological actions of the individual components of Wenxin keli, but is reported that NcBe, a traditional Tibetan medicinal compound extracted from *Valerinanaceae* plants, significantly blocks I_{Na} and I_{to} in rat ventricular myocytes (Liu et al., 2009). Using rabbit ventricular myocytes, NcBe is able to block I_{Na}, $I_{Ca\text{-}L}$, I_K and I_{to} in a concentration dependent manner using rabbit ventricular myocytes (Tang et al., 2004; Tang et al., 2008).

Tong Mai Yan Xin

Tong Mai Yan Xin (TMYX) drug is currently used in China for the treatment of cardiac disease and acts as a "cardiac regulator" to treat both conditions brady- and tachy-cardia, **fig. 17**. TMYX is a mixture of different compounds (*Colla Corii Asini, Fructus Jujiubae, Radix Codonopsis, Radix Rehmanniae, Rhizoma Glycyrrhizae, Plastrum Testudinis, Ramulus Cinnamomi, Raxid Polygoni Multiflori Praeparata, Caulis Spatholobi, Radix Ophiopogonis, Fructus Schisandrae Chinensis*). Liquorice derives from root extract of *Glycyrrhiza glabra*, a perennial herb cultivated in temperate and subtropical regions. Since ancient times, liquorice roots were used in traditional herbal medicine for treatment of a large many disease (Armanini et al., 2002; Fiore et al., 2005). Only in the last 25 years the effects of Glycyrrhiza compounds have been scientifically investigated, confirming the knowledge acquired during history; for example liquorice constituents exhibit several biological and endocrine properties including anti-inflammatory (cortisol-like), antihepatotoxic, antibacterial, antiviral, and anticancer effects (Aly et al., 2005; Lee et al., 2009; Fiore et al., 2008; Hibasami et al., 2005); in addition they possess cardioprotective properties (Parisella et al., 2012).

Fig. 17. Tong Mai Yan Xin

3.2. MATERIALS AND METHODS

Animals

The in-vitro experiments were performed on sinoatrial myocytes isolated from female New Zealand rabbits of about 0.8-1.2 Kg weight. The in-vivo telemetric recordings were carried out on male wild type mice ≥ 2 months old.

Animal protocols conformed to the guidelines of the care and use of laboratory animals established by Italian (DL. 26/2014) and European (2010/63/UE) directives.

In-vitro experiments

Cell isolation

Young white albino rabbits were deeply anesthetized by intramuscular injection of acepromazine (1 mg/Kg) and euthanized with intravenous injection of sodium thiopental (60 mg/Kg), and exsanguination.

The heart, quickly removed, was placed in prewarmed (37°C) Tyrode solution (mM: NaCl, 140; KCl, 5.4; $CaCl_2$, 1.8; $MgCl_2$, 1; D-glucose, 5.5; Hepes-NaOH, 5; pH 7.4) containing 1000 units of heparin to prevent blood clots formation, and after surgical isolation, the SA node tissue (**fig. 18**) was cut into 5-6 stripes.

In the first phase of cell dissociation protocol, the SA tissue is washed three times with a solution containing NaCl 140 mM, KCl 5.4 mM, $MgCl_2$ 0.5 mM, KH_2PO_4 1.4 mM, taurine 50 mM, Hepes-NaOH 5 mM, D-glucose 5.5 mM (pH 6.9). In the second phase the SA stripes are kept in the enzymatic solution containing NaCl 140 mM, KCl 5,4 mM, MgCl2 0.5 mM, KH2PO4 1.2 mM, Hepes NaOH 5 mM, taurina 50 mM, D-Glucose 5.5 mM, albumine 1 mg/ml, CaCl2 200 mM, collagenase (224 U/ml, Worthington), elastase (1.42 U/ml, Sigma), and protease (0.45 U/ml, Sigma) at the temperature of 37°C for 25/30 minutes, to degrade intercellular matrix and loosen cell-to-cell adhesions in order to facilitate the following mechanical dissociation procedure.

Fig. 18. Isolated rabbit SA node.

The final step consisted in rinsing 3 times the stripes in a solution containing: KCl 20 mM; KOH 80 mM; albumine 1mg/ml, glutamic acid 70 mM; hydroxibutyric acid 10 mM; KH_2PO_4 10 mM; taurine 10 mM; HepesKOH 10 mM; EGTA-KOH 0.1 mM; pH 7.4. Cells were then dissociated with mechanical shacking for 5/10 minutes at 37°C in the same solution (DiFrancesco, et al., 1986 b).

Before starting the electrophysiological experiments, the cells were gradually readapted to proper extracellular calcium concentration by adding increasing volumes of the following solutions: tyrode and albumin 1 mg/ml; NaCl 10 mM, $CaCl_2$ 1,8 mM.

SA node myocytes were stored for the day at 4°C. During patch-clamp experiments, cells were plated in a 30 mm plastic petri dish placed on the stage of an inverted microscope and superfused with Tyrode solution at the temperature of 35 ± 0.5°C.

Patch-clamp solutions

Tong Mai Yan Xin (TMYX), kindly provided by Zhongin Pharma (Tianjin Le Ren Tang Pharmaceutical Factory), was dissolved in water, warmed at 80°C for 15 minutes, filtered and used to prepare Tyrode solution.

To study the effect of TMYX in the presence of autonomic modulators, isoprenaline (Iso) 1 µM (Sigma-Aldrich) and acetylcholine (Ach) 0.01 µM (Sigma Aldrich) were added to the Tyrode solution.

The extracellular solution used to record the I_f current was Tyrode solution plus $BaCl_2$ (1 µM) and $MnCl_2$ (2 µM) to improve I_f dissection over other ionic components.

Electrophysiological experiments were performed using glass pipette with the resistance of about 5-8 mΩ filled with a solution containing (mmol/L): K-Aspartate, 130; NaCl, 10; EGTA-

KOH, 5; $CaCl_2$, 2; $MgCl_2$, 2; ATP (Na-salt), 2; creatine phosphate, 5; GTP (Na-salt), 0.1; pH 7.2.

Equipment

Standard patch-clamp setup which includes:

- Inverted microscope (Axiovert S100) positioned on an anti-vibration table.
- Patch-clamp amplifier (Axopatch 200B, Axon Instruments).
- Digital interface (Digidata 1440, Axon Instruments).
- Micromanipulators.
- Solution temperature control.
- pClamp 10.0 software (Axon Instruments).

All the electrical devices are positioned inside a Faraday cage, to shield from electrical noise.

Protocols and data analysis

Electrophysiological protocols were designed with pClamp software. All data were acquired with pClamp software and an Axopatch 200B amplifier. To record the capacitive current, we used a protocol with a single hyperpolarizing step of 10 mV amplitude (from -35 to -45 mV) for 30 ms of duration.

Action potentials were recorded in current-clamp configuration from single SA node cells or small uniformly-beating aggregates as continuous traces for several hundred seconds at a sampling rate of 2 KHz and filtered at 1 KHz with pClamp software. Raw AP records were digitally smoothed by a 10-point adjacent averaging smoothing procedure and the time derivative calculated according to a second polynomial, 8-point smoothing differentiating routine (Origin 7, Origin Lab, Northampton, MA).

For each AP cycle the following parameters were analysed (**fig. 19**):

1) Rate (Hz), calculated as the reciprocal of the cycle length from peak-to-peak dV/dt traces.

2) Maximum Diastolic Potential (MDP, mV), defined as the most negative potential reached during AP repolarization.

3) Take-Off Potential (TOP, mV), defined as the voltage measured at the time when the voltage derivative (dV/dt) overtakes a given threshold, set to 0.5 mV/ms (dashed horizontal line in the bottom panel of **fig. 19**); this value normally represents a level across which, regardless of rate, the voltage derivative dV/dt changes abruptly during the transition from phase 4 to phase 0 of the AP; since dV/dt is proportional to the whole-cell current density (I_{wc}) according to the

equation $-dV/dt=I_{wc}/C$, with C being the cell capacity, the sudden change of dV/dt (bottom panel) corresponds to the sudden change of current associated with activation of the Ca^{++} current; the TOP value can therefore also be viewed as the voltage at which the $Ca+^{+}$ current responsible for AP depolarization takes off.

4) Slope of Early Diastolic Depolarization (EDD, mV/ms); for each cycle the diastolic depolarization (EDD) is defined as the slope of the AP in the interval immediately following the MDP.

5) Action Potential Duration (APD, s), defined as the time between the Take-Off Potential and the following MDP, measured at 50% of repolarization.

6) Overshoot (OS, mV) defined as the most positive potential reached during the AP depolarization.

All the parameters were analysed using a customized software as previously described (Bucchi et al., 2007 a; Bucchi et al., 2007 b).

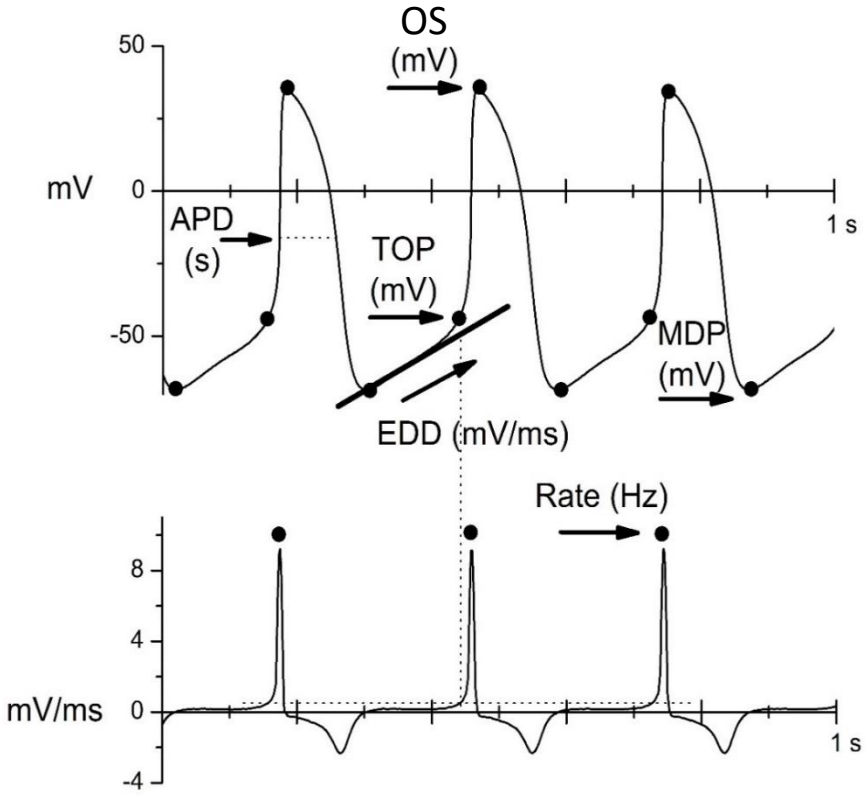

Fig. 19. AP traces (top) and corresponding time derivative dV/dt (bottom). Parameters identified are MDP (mV); TOP (mV); EDD (mV/ms); OS (mV); APD50 (s); rate (Hz). The vertical line identifies the TOP of the AP, which corresponds to the point when the voltage derivative (dV/dt) overtakes the threshold of 0.5 mV/ms (horizontal line).

Dose-response curve of the action potentials frequency reduction was obtained fitting data points using Hill equations:

$$y = V_{max} \frac{x^n}{k^n + x^n}$$

- "V_{max}" parameters is the maximum reaction velocity
- "x" is the drug concentration.
- "n" is the Hill coefficient, that estimates the magnitude of cooperativity in gating transitions of voltage-dependent ion channels.
- "k" is the half –maximal concentration constant and indicates the concentration where the rate is reduced by 50%.

To understand the effect of the TMYX on the I_f current we used a double step protocol consisted of 1.5 s voltage pulses to -125 mV, preceded by 0.75 s pulses to -65 mV, from a holding potential of -35 mV, recorded in control solution and after the addition of the drug.
The activation curve was obtained by hyperpolarizating steps to the range of -35/-140 mV, followed by a fully activating 1.5 s step at -140 mV, from a holding potential of -35 mV. The duration of the first step was decreased (from 12 to 4 s) as the activation of the current became progressively faster. The current amplitudes were divided for the cell capacitance to obtained current densities (pA/pF). After normalization to maximum amplitude, tail current measured at -140 mV were fitted using Boltzmann equation:

$$y = \frac{1}{1 + e^{\frac{V - V_{1/2}}{s}}}$$

- "V" is voltage.
- "y" is fractional activation.
- "$V_{1/2}$" is the half activation voltage.
- "s" is the inverse-slope factor.

The fully-activated current/voltage (I/V) relationship was evaluated in the range of potentials from -120 to 20 mV by measurement of the amplitude of tail current after a hyperpolarizating step to -125 mV, which fully activates I_f. The current amplitudes were divided for the cell capacitances to obtained current densities (pA/pF). Data points were fitted by linear fit:

$$y = a + bx$$

- “a” is the intercept.
- “b” is the slope.

Data are presented as mean ± standard error of the mean (S.E.M.); the statistic test used is the Student t-test; statistical significance: $P < 0.05$.

Treatments

The cell under investigation were exposed to the tyrode solution containing the drug at a given concentration. For each drug dose, we evaluated whether the overall rate in the presence of the drug was statistically different from that obtained in control conditions (**fig. 20**).

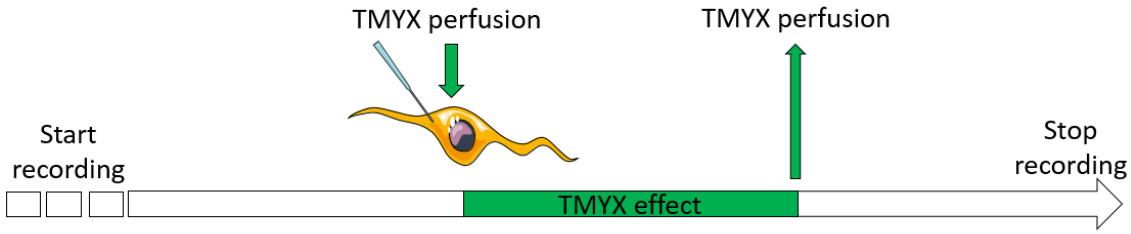

Fig. 20. Experimental protocol to study TMYX effect on action potentials and on I_f current.

To understand the effects produced by TMYX on cell rate in the presence of autonomic modulators, we used the experimental protocol shown in **fig. 21**. The duration of each step was about 1 minute to permit the stabilization of cell rate. The first perfusion of TMYX allows to verify the rate-slowing effect induced by the drug. During the perfusion of the autonomic modulators (Iso/ACh) we added TMYX and recorded the effects on rate.

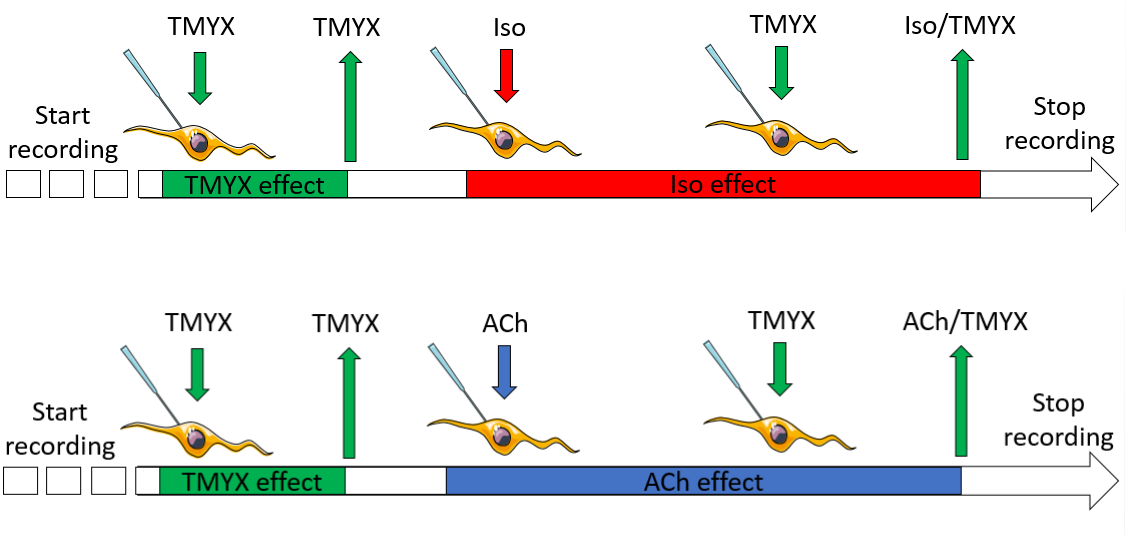

Fig. 21. Experimental protocol of experiments with autonomic modulators: isoprenaline (top), acetylcholine (bottom).

In-vivo experiments

Telemetric setup

The recording system (**fig. 22**) (Data Sciences International) consists of implantable transmitters (TA10ETA-F20), telemetry receivers and a matrix which conveys information from the telemetry receivers to the computer. The transmitter has a weight of 3.9 g and a volume less than 1.9 cc. It contains a pair of flexible leads connected to a preamplifier. The battery could be switched on and off using a magnet. The receivers are able to detect ElectroCardioGram (ECG), body temperature, and the activity of the mouse.

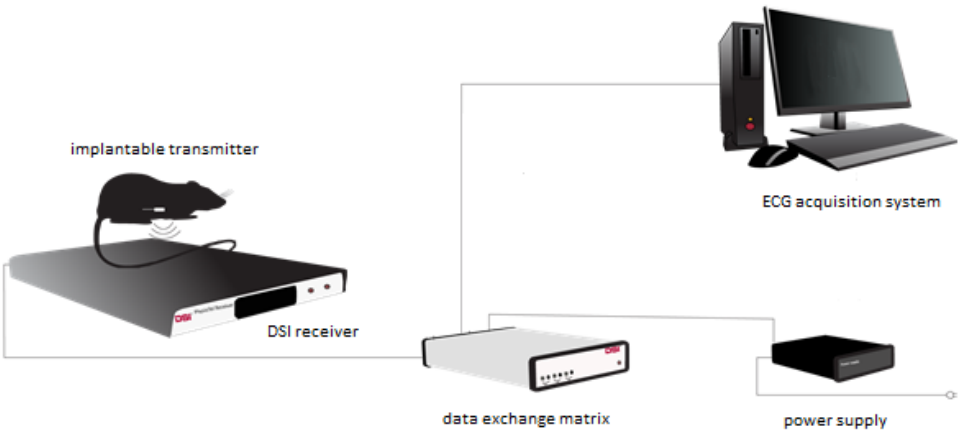

Fig. 22. ElectroCardioGram telemetric setup.

Implantation protocol

Male adult mice (> 60 days old) were anesthetized with 30 mg/kg tiletamine and 30 mg/kg zolazepam. The recording device was inserted into the intraperitoneal cavity as previously described (Sgoifo et al., 1996; Baruscotti et al., 2011). Briefly, after the removal of the hair from the abdominal area, the peritoneal cavity was opened by an incision along the midline under the processus *xiphoideus*. One lead was fixed to the dorsal surface on the xiphoid process. The other electrode was subcutaneously tunnelled on the thorax toward the upper insertion of the sternohyoid muscle and pushed under the muscle into the anterior mediastinum in a location close to the right atrium (**fig. 23**).

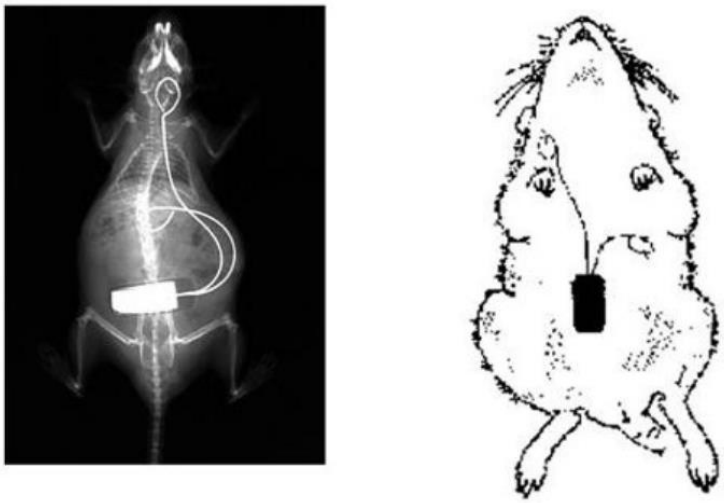

Fig. 23. Positioning of the implantable transmitter

Telemetric protocols

Telemetry experiments started 2 weeks after surgical implantation of the transmitter. After baseline registration for 24 h, the animals were randomly split in four groups (**fig. 24**). The first one received only TMYX 5 mg/g mouse. The drug was dissolved in saline solution, warmed at 80°C for 15-20 minutes and a final volume of 150 µl were i.p. injected. The second group (control group) received saline injection.

In the third group the effect of TMYX on the intrinsic heart rate was evaluated; in this case TMYX was injected 15 minutes after the pharmacological autonomic blockade, induced by i.p. injection of atropine 2 mg/kg (Sigma-Aldrich) and propranolol 1 mg/kg (Sigma-Aldrich). The control group (number four) received saline i.p. after autonomic blockade.

Data were acquired and analysed by Dataquest 4.2 software (Data Sciences International). Heart rate (HR) was calculated from the RR duration (interval between two consecutive R waves of ECG). Each data point of the cardiac rate is the mean value of a 10 seconds interval, and each interval was collected every 40 seconds.

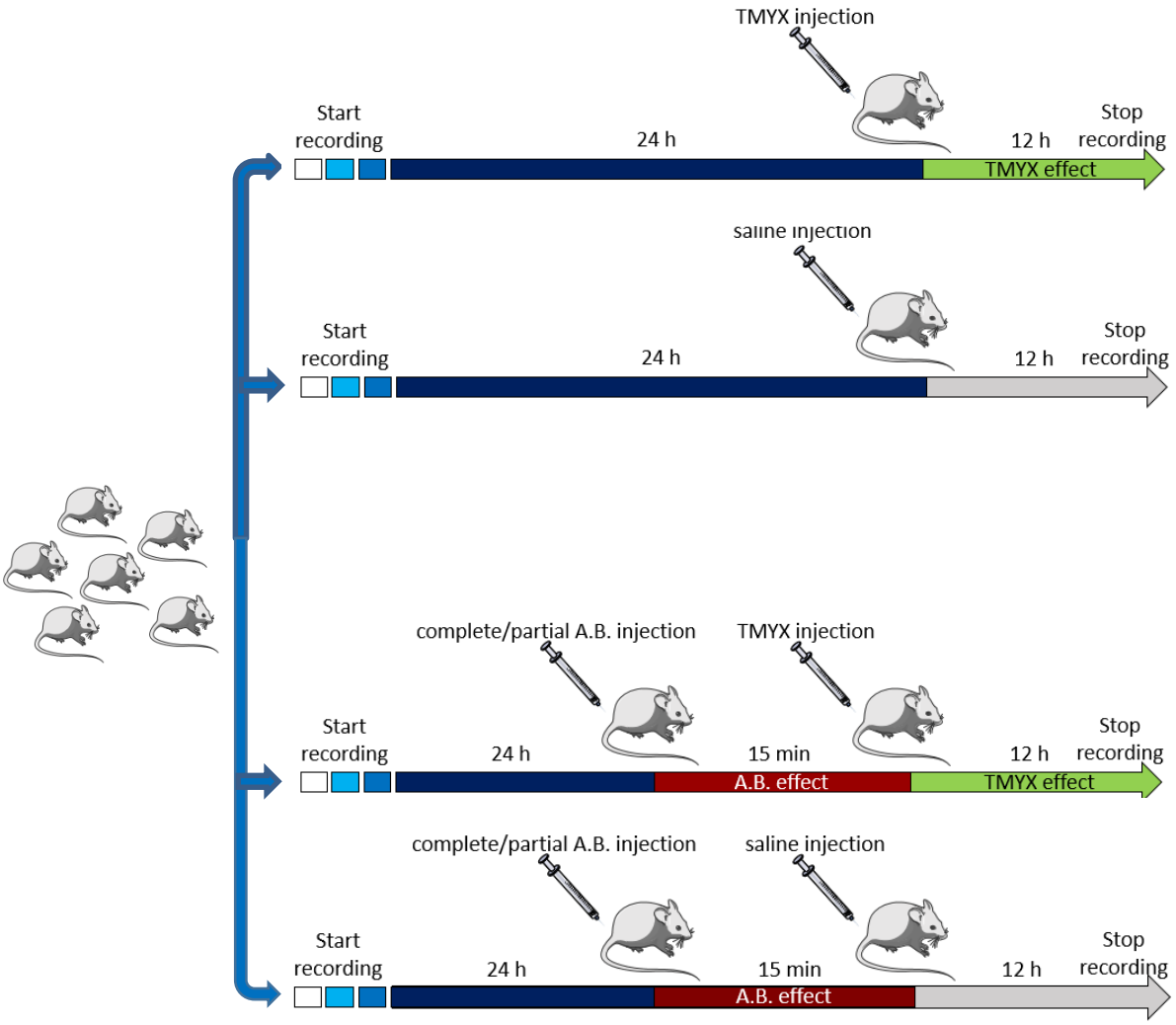

Fig. 24. *In-vivo* experiments protocol.

3.3. RESULTS

In-vitro experiments

Action potential parameters

To identify the effect of TMYX on rate, we carried out patch-clamp experiments where the drug was perfused on small aggregates of SA node myocytes. In **fig. 25** top, the time course of the effect of the drug on rate (100 s recording): a dose-dependent slowing that reaches a steady-state condition within about 20 s is evident. Superfusion on SAN cells with drug concentrations ≥ 20 mg/ml produced a complete block of the spontaneous activity; however event at these high concentrations the rate reduction induced by TMYX was completely reversible after drug wash out.

The superimposition of AP traces recorded in control solution and during perfusion with TMYX 2, 6, and 20 mg/ml is shown in **fig. 25**, bottom.

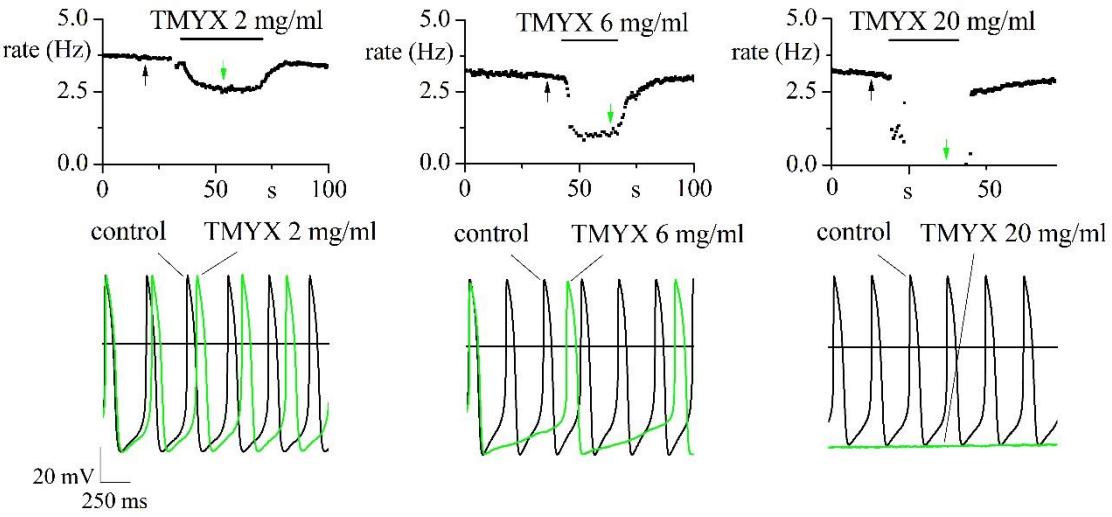

Fig. 25. **Dose-dependent reduction induced by TMYX in rabbit sinoatrial myocytes.** Examples of time course of the rate (top), and AP traces (bottom) in control conditions and after perfusion of different concentrations of TMYX (2, 6, and 20 mg/ml).

Percentage rate reduction obtained after perfusion of different concentrations of TMYX (in the range from 0.2 to 60 mg/ml) are shown in **fig 26**. The dose-response curve of rate is obtained

by fitting the experimental points (reported in **table 1**) with Hill equations, and yields half block concentration (K_d) of 4.8 mg/ml, and Hill coefficient of 1.6.

These data indicate that the superfusion of Traditional Chinese drug TMYX produces a reversible, dose-dependent reduction of the rate at all the concentrations tested.

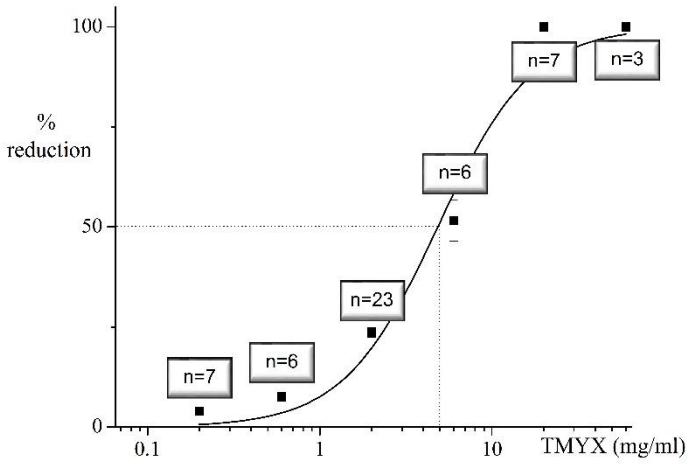

Fig. 26. **Dose-response curve of the rate**; the lines indicate the half block concentration (K_d value = 4.8 mg/ml); Hill coefficient = 1.6; * P < 0.05, Student t-test.

TMYX	n	Rate					
		Ctrl (Hz)		TMYX (Hz)		% Reduction	
		Mean	S.E.M.	Mean	S.E.M.	Mean	S.E.M.
0.2 mg/ml	7	3.34	0.28	3.21	0.27	-3.96 *	0.55
0.6 mg/ml	6	3.59	0.18	3.32	0.18	-7.58 *	1.17
2 mg/ml	23	3.50	0.12	2.67	0.09	-23.55 *	1.20
6 mg/ml	6	3.17	0.19	01.52	0.16	-51.64 *	5.02
20 mg/ml	7	2.94	0.22	0	0	-100 *	0
60 mg/ml	3	2.25	0.25	0	0	-100 *	0

Table 1. AP rate. Data are shown as mean ± S.E.M; n = number of cells. *, P<0.05 vs. control (Student t-test).

Current clamp experiments were carried out to identify which of the AP parameters are affected when small aggregates of SAN myocytes were perfused with different concentrations of TMYX (in the range from 0.2 to 6 mg/ml) (**fig. 27**).

Data analysis shows that at the concentration used slowing of spontaneous rate is associated with EDD % reduction of 12.35 ± 1.90; 22.18 ± 4.17; 53.27 ± 2.63; 80.98 ± 5.00 (n = 6-23, P < 0.05, Student t-test), while the TOP, the MDP and the overshoot did not vary. APD50 was instead slightly increased at all concentrations (+3.60 ± 1.53; +8.46 ± 2.10; +6.50 ± 0.87; +24.68 ± 7.12, n=6-23; P < 0.05, Student t-test). Experimental data are reported in **table 2**.

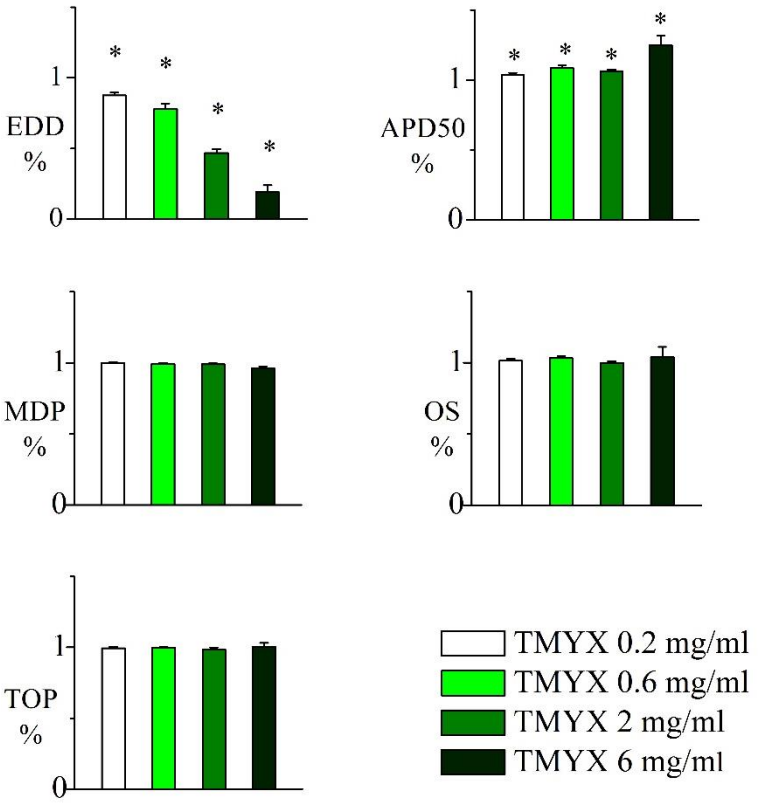

Fig. 27. AP parameters modified by perfusion of different concentration of TMYX drug. Bar graphs show normalized means of EDD, APD50, MDP, OS, TOP in presence of TMYX at the concentrations of 0.2 (n=7), 0.6 (n=6), 2 (n=23), 6 (n=6) mg/ml. * P < 0.05, Student t-test.

TMYX	n	EDD					
		Ctrl (mV/ms)		TMYX (mV/ms)		% Reduction	
		Mean	S.E.M.	Mean	S.E.M.	Mean	S.E.M.
0.2 mg/ml	7	0.079	0.020	0.069	0.018	-12.35 *	1.90
0.6 mg/ml	6	0.120	0.019	0.096	0.017	-22.18 *	4.17
2 mg/ml	23	0.130	0.005	0.061	0.004	-53.27 *	2.63
6 mg/ml	6	0.119	0.009	0.022	0.005	-80.98 *	5.00
TMYX	**n**	**TOP**					
		Ctrl (mV)		**TMYX (mV)**		**% Reduction**	
		Mean	**S.E.M.**	**Mean**	**S.E.M.**	**Mean**	**S.E.M.**
0.2 mg/ml	7	-40.58	1.71	-40.28	1.66	-0.68	0.87
0.6 mg/ml	6	-41.75	0.69	-41.67	0.52	-0.16	0.59
2 mg/ml	23	-40.50	1.22	-39.97	1.37	-1.41	0.37
6 mg/ml	6	-37.57	2.09	-37.54	1.95	+0.23	2.88
TMYX	**n**	**MDP**					
		Ctrl (mV)		**TMYX (mV)**		**% Reduction**	
		Mean	**S.E.M.**	**Mean**	**S.E.M.**	**Mean**	**S.E.M.**
0.2 mg/ml	7	-57.95	3.32	-57.87	3.58	-0.16	0.60
0.6 mg/ml	6	-60.27	0.83	-59.75	1.04	-0.88	0.79
2 mg/ml	23	-60.91	1.04	-60.19	1.04	-1.11	0.84
6 mg/ml	6	-61.36	1.89	-58.83	1.87	-4.07	1.59
TMYX	**n**	**APD50**					
		Ctrl (s)		**TMYX (s)**		**% Reduction**	
		Mean	**S.E.M.**	**Mean**	**S.E.M.**	**Mean**	**S.E.M.**
0.2 mg/ml	7	0.097	0.008	0.100	0.008	+3.60 *	01.53
0.6 mg/ml	6	0.090	0.005	0.098	0.007	+8.46 *	02.10
2 mg/ml	23	0.089	0.003	0.095	0.004	+6.50 *	0.87
6 mg/ml	6	0.083	0.002	0.104	0.007	+24.68 *	07.12
TMYX	**n**	**OS**					
		Ctrl (mV)		**TMYX (mV)**		**% Reduction**	
		Mean	**S.E.M.**	**Mean**	**S.E.M.**	**Mean**	**S.E.M.**
0.2 mg/ml	7	35.39	2.70	35.96	2.91	+1.28	1.47
0.6 mg/ml	6	33.29	2.75	34.47	3.08	+3.12	1.60
2 mg/ml	23	39.70	1.79	39.62	1.79	-0.13	1.01
6 mg/ml	6	37.82	2.20	38.52	1.68	+3.74	7.35

Table 2. AP parameters analyzed in control and in presence of different concentrations of TMYX. Data are shown as mean ± S.E.M; n = number of cells. *, $P < 0.05$ vs. control (Student t-test).

Autonomic modulators interactions

We further proceeded to investigate the presence of interactions when the drug is perfused in the presence of adrenergic β-agonist (isoprenaline, Iso 1 µM) and cholinergic (acetylcholine, ACh, 0.01 µM) autonomic modulators. The concentrations were chosen in order to induce rate changes of approximately 15-25 %, comparable to the range of frequency changes observed with TMYX 2 mg/ml.

Data shown in **fig. 28** demonstrate that TMYX exerts a slowing action regardless it is delivered in the presence (-0.66 Hz ± 0.05, n=8) or absence (control, 0.82 Hz ± 0.08, n = 8) of isoprenaline (**table 3)**.

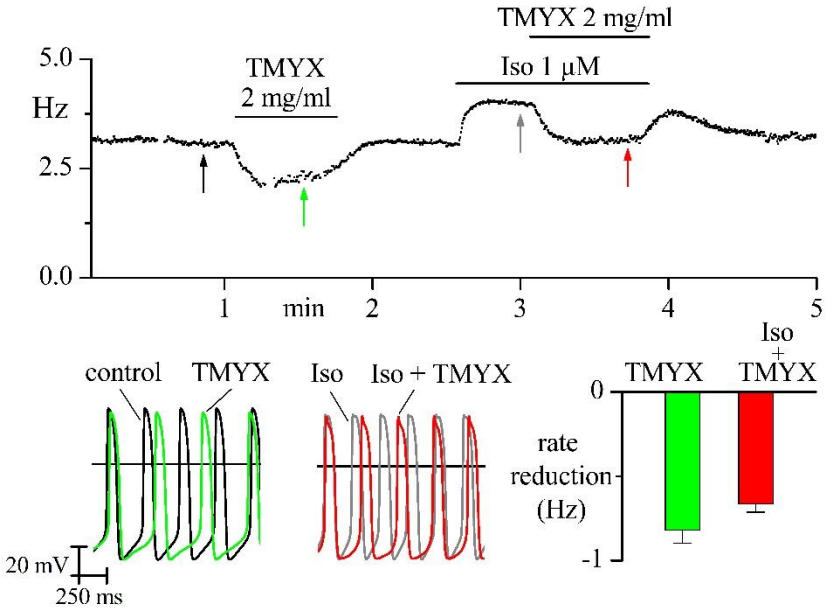

Fig. 28. Effect of TMYX 2 mg/ml in presence of autonomic modulators (isoprenaline 1 µM).. Example time course of the rate (top) suggests the maintenance of slowing action of TMYX during perfusion of Iso. Superimposition of AP traces (bottom, left) and bar graph of the percentage reduction (bottom, right) shows a not different rate reduction induced by TMYX in control (0.82 Hz ± 0.08, n=8) and in presence of Iso (-0.66 Hz ± 0.05, n=8), P > 0.05, Student t-test.

Rate (Hz)	n	Mean	S.E.M.	% Reduction		Δ Reduction (Hz)	
				Mean	S.E.M.	Mean	S.E.M.
Control	8	3.33	0.15	-25.04 *	2.90	-0.82	0.08
TMYX 2 mg/ml	8	2.51	0.17				
Isoprenaline 1 µM	8	3.97	0.08	-16.75 *	1.29	-0.66	0.05
TMYX 2 mg/ml + Iso 1 µM	8	3.31	0.17				

Table 3. Effect of TMYX on rate during isoprenaline experiments. Data are shown as mean ± S.E.M; n = number of cells. *, P < 0.05 vs. control (Student t-test).

The same type of behaviour (maintenance of the effect) can be observed also in the presence of muscarinic stimulation. When TMYX is delivered in the presence of ACh 0.01 µM, its slowing action is preserved (**fig. 29)**. Mean data analysis indicates that the reduction of rate (ΔHz) induced by TMYX perfusion is similar between control condition (-0.68 ± 0.03 Hz, n=6) and in the presence of ACh 0.01 µM (-0.80 ± 0.10 Hz, n=6) (**table 4)**.

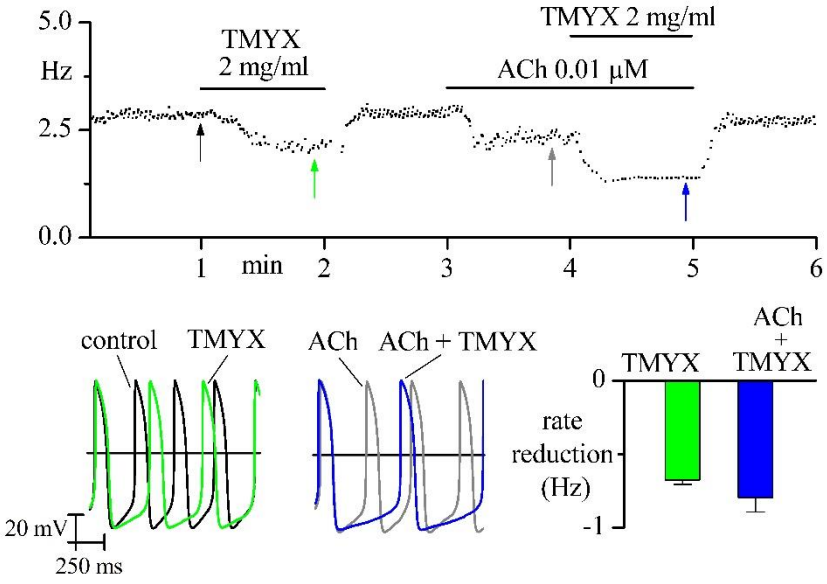

Fig. 29. **Effect of TMYX 2 mg/ml in presence of muscarinic stimulation (acetylcholine 0.01 µM).** Example time course of the rate (top) suggests the maintenance of slowing action of TMYX during perfusion of ACh. Superimposition of AP traces (bottom, left) and bar graph of the percentage reduction (bottom, right) shows a not different rate reduction induced by TMYX in control (-0.68 ± 0.03 Hz, n=6) and in presence of ACh (-0.80 ± 0.10 Hz, n=6), P > 0.05, Student t-test.

Rate (Hz)	n	Mean	S.E.M.	% Reduction		Δ Reduction (Hz)	
				Mean	S.E.M.	Mean	S.E.M.
Control	6	2.99	0.13	-22.89 *	1.76	-0.68	0.03
TMYX 2 mg/ml	6	2.32	0.14				
Acetylcholine 0.01 µM	6	2.09	0.16	-37.66 *	2.92	-0.80	0.10
TMYX 2 mg/ml + ACh 0.01 µM	6	1.29	0.10				

Table 4. Effect of TMYX on rate during acetylcholine experiments. Data are shown as mean ± S.E.M; n = number of cells. *, P < 0.05 vs. control (Student t-test).

To verify whether the slowing action of TMYX depends on basal rate (rate-dependence), we analysed the relationship between the rate decreases vs. basal rate. Sample AP traces in control and after perfusion of TMYX 2 mg/ml are shown in **fig. 30, left**; the dot-plot on the right, describes the correlation between the rate reduction (%) induced by TMYX 2 mg/ml and the spontaneous frequency of APs before drug perfusion (Hz). As shown by the linear regression analysis of the plot (line), TMYX-induced rate slowing is not significantly associated with basal rate (n= 23; correlation coefficient r = 0.03).

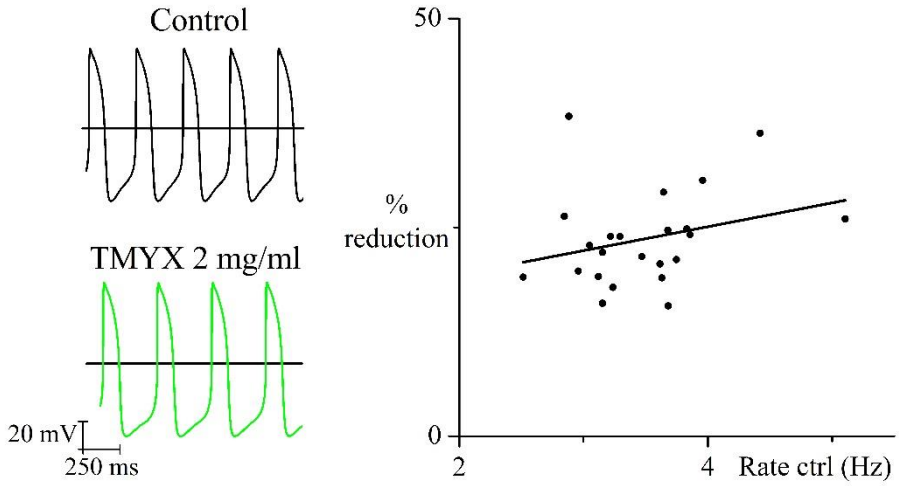

Fig. 30. Rate-dependence. APs in control condition and after TMYX 2 mg/ml administration, left. Linear regression of the rate in control and percentage of reduction, right. The linear regression shows none rate-dependence of TMYX effect.

I_f current

Data shown in **figs 26** and **27** indicate a causative relation between the rate slowing produced by TMYX and the decrease in the slope of the early diastolic depolarization; this observation lead to the involvement of the I_f current, which is the main determinant of the EDD slope. We therefore started to study the effect of TMYX (2 and 6 mg/ml) on the current using a double-step protocol

TMYX induced a significant decrease of the steady-state current at -65 mV both at 2 mg/ml (-20.9% ± 3.2, n= 9; P < 0.05 Student t-test) and at 6 mg/ml (-29.5% ± 4.6, n=5; P < 0.05 Student t-test), but it also induced an increase of the current at -125 mV (2 mg/ml: +37.1% ± 6.2, n=9, P < 0.05 Student t-test; 6 mg/ml: 145.7% ± 17.7, n=5; P < 0.05 Student t-test) as shown in **fig. 31**.

These results suggest a double effect induced by TMYX: a shift of activation curve and an increase of I_f conductance.

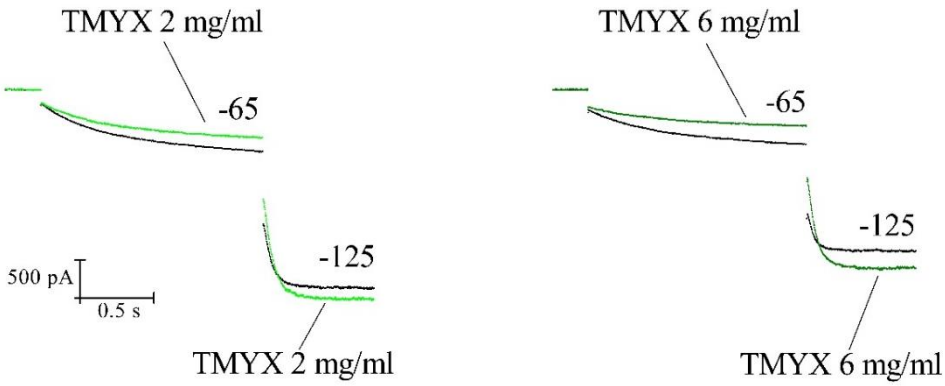

Fig. 31. Effects induced by TMYX 2 and 6 mg/ml on I_f current. The double-step protocol shows a dual action induced by the drug at both the concentrations; the significant reduction of I_f amplitude at -65 mV suggests a shift of activation curve; while the significant increase at -125 mV suggests an enhancement on I_f conductance.

The above observations were confirmed and quantified by analysing the mean activation curves before and after the perfusion of TMYX drug at the concentration of 2 (data not shown) and 6 mg/ml (**fig. 32, top**).

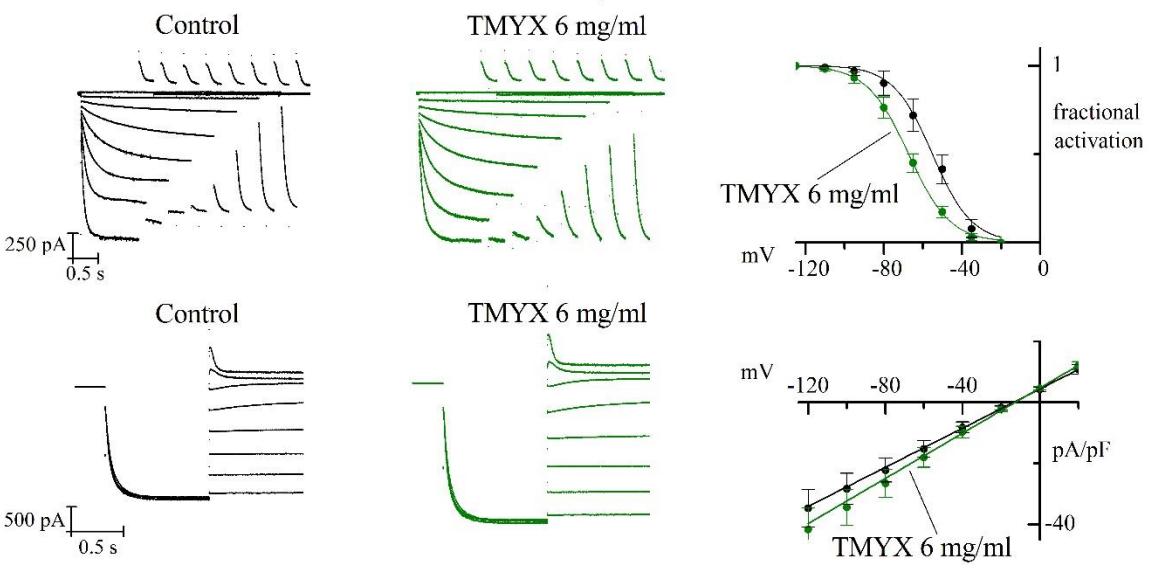

Fig 32. Effects of TMYX on activation curves and current/voltage relationship. Top, mean activation curves in control and after TMYX 6 mg/ml perfusion. The drug induced a significant shift of activation curve from -59.7 ± 4.2 mV to -70.0 ± 3.6 mV, n=6; $P < 0.05$, Student t-test.
Bottom, fully activated current/voltage (I/V) relationship measured before and after TMYX 6 mg/ml perfusion. The drug led to a concentration-dependent increase of the slope conductance from 0.33 ± 0.05 to 0.39 ± 0.06, n=5; $P < 0.05$, Student t-test.

The experimental points were fitted by a Boltzmann function; half activation value (V½) changes from -55.5 ± 2.1 mV in control to -62.3 ± 2.1 mV in presence of TMYX 2 mg/ml (n=4) and from -59.7 ± 4.2 mV to -70.0 ± 3.6 mV in presence of TMYX 6 mg/ml (n=6); $P < 0.05$ Student t-test. TMYX thus induces the activation of the I_f current at more negative potentials than control solution; TMYX 2 mg/ml produces a left shift of activation curve of 6.8 mV, while TMYX 6 mg/ml shifts the curve of 10.3 mV.

We then evaluated the effect of TMYX 2 mg/ml (data not shown) and 6 mg/ml on the open channel I/V relation (**fig. 32, bottom**). As calculated by linear fitting of data points, TMYX caused a significant ($P < 0.05$, Student t-test) concentration-dependent increase of the conductance ($pA*pF^{-1}*mV^{-1}$) from 0.46 ± 0.05 to 0.50 ± 0.04 (n=5), and from 0.33 ± 0.05 to 0.39 ± 0.06 (n=5), significant at both the concentrations.

To obtain the steady-state curve control and in the presence of TMYX 2 (data not shown) and 6 mg/ml, the activation curves were multiplied by the fully activated IV (**fig. 33**). From the curve obtained with TMYX 6 mg/ml it can be appreciated that at potential ≥ -80 mV, and in

particular at pacemaker potential, the net effect of TMYX is to reduce the I_f current due to the quantitative prevalence of the negative shift, while, at voltage < -80 mV the increase of the conductance prevails.

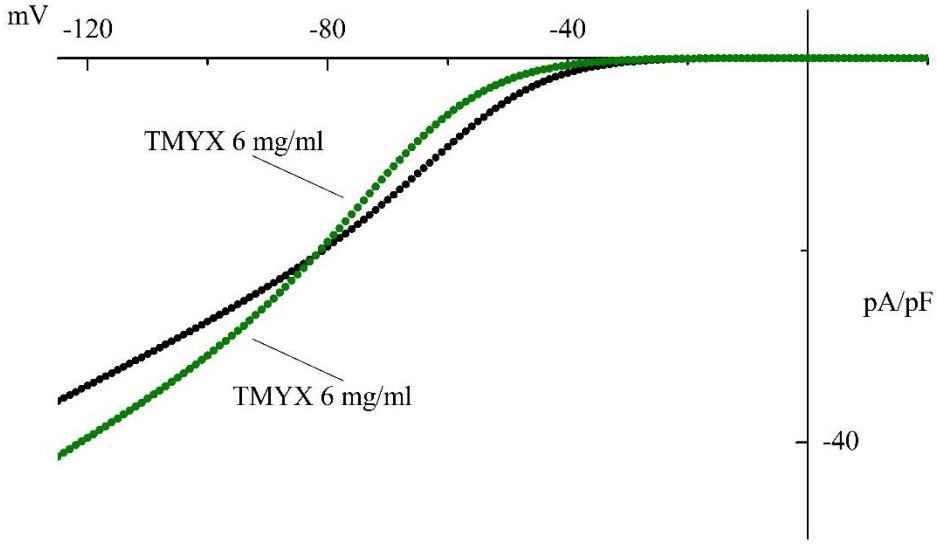

Fig 33. Combined effect of TMYX on I_f current. The curve obtained multiply the activation curve and the I/V functions, shows that at potentials ≤ -80 mV the contribution of the shift induced by TMYX 6 mg/ml is greater than the increment of conductance, and led to a reduction of current amplitude respect to the control condition.

In-vivo experiments

To evaluate the effect of TMYX on heart rate we used an *in-vivo* model based on freely-moving mice implanted with an ECG recording system.

We performed experiments using a concentration of TMYX similar to the half block value (K_d) calculated in *in-vitro* experiments to study the effect of TMYX drug in intact mice.

The time course of HR shows that administration of TMYX induces the increment of heart rate and reduces the heart rate variability for a period of about 4 hours; these effects are not present in control mice treated with saline injection (**fig. 34, top**). Sample ECG recordings are shown in bottom left panel. The bar graph shown in the bottom right part of **fig. 34** reports mean HR values calculated before and during saline or TMYX injection. The i.p. injection of TMYX 5 mg/g produced an increase of rate of 33.2 % (n = 3 mice), whereas control treatment with saline solution (n = 2 mice), did not elicit significant changes in heart rate.

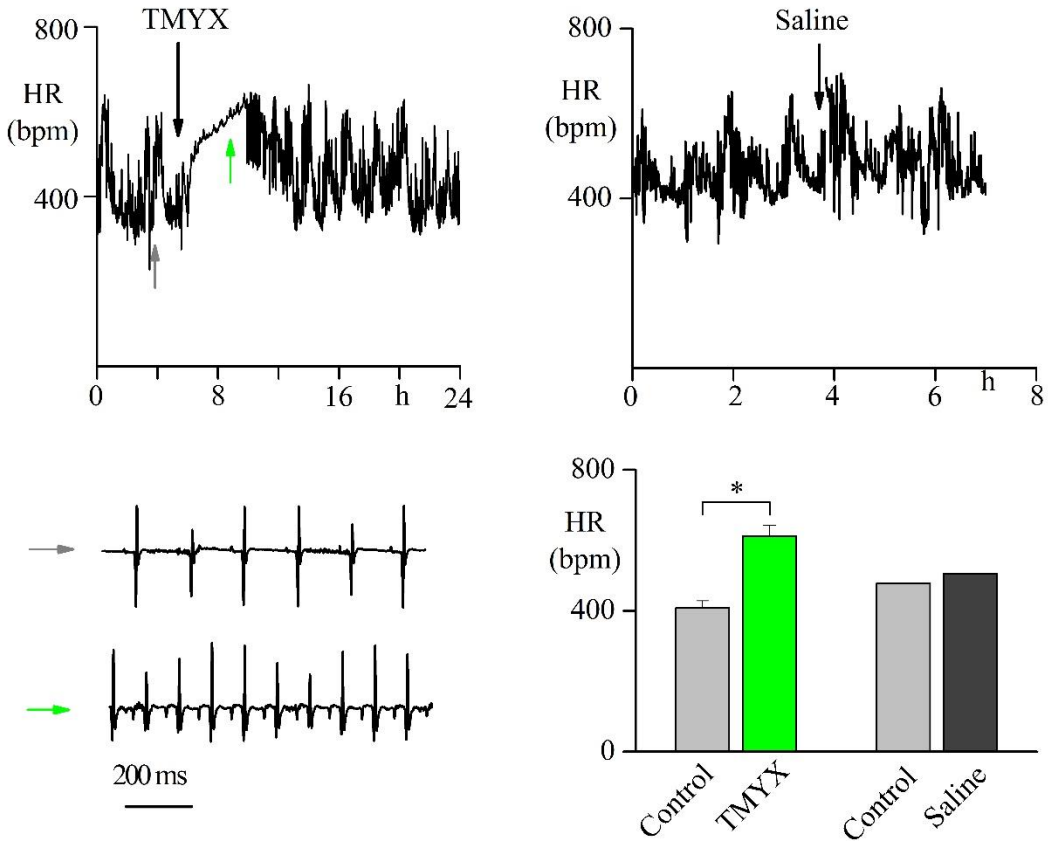

Fig. 34. Effects of i.p. injection of TMYX in freely-moving mice. Top, representative time course of the HR of a mouse treated with TMYX 5 mg/g, left, and saline solution, right. The black arrows indicates the moment of the i.p. injection. The origin of the x-scale has conventionally been set to the 0 and correspond to the 11:00 AM (TMYX) and 01:00 PM (control).

Bottom, left, correspondent ECG traces in control condition (grey arrow) and after drug injection (green arrow).

The bar graph shows the mean values of the HR before (control) and after the injection of both TMYX (n=3) or saline (n=2) solution. *, $p < 0.05$.

We next performed similar experiments except that administration of TMYX was performed after complete autonomic pharmacological blockade; this approach allowed to study the effects of the drug on the intrinsic heart rate in the absence of modulation of the two branches of the nervous system (sympathetic and parasympathetic) so to mimic a condition similar to *in-vitro* experiments.

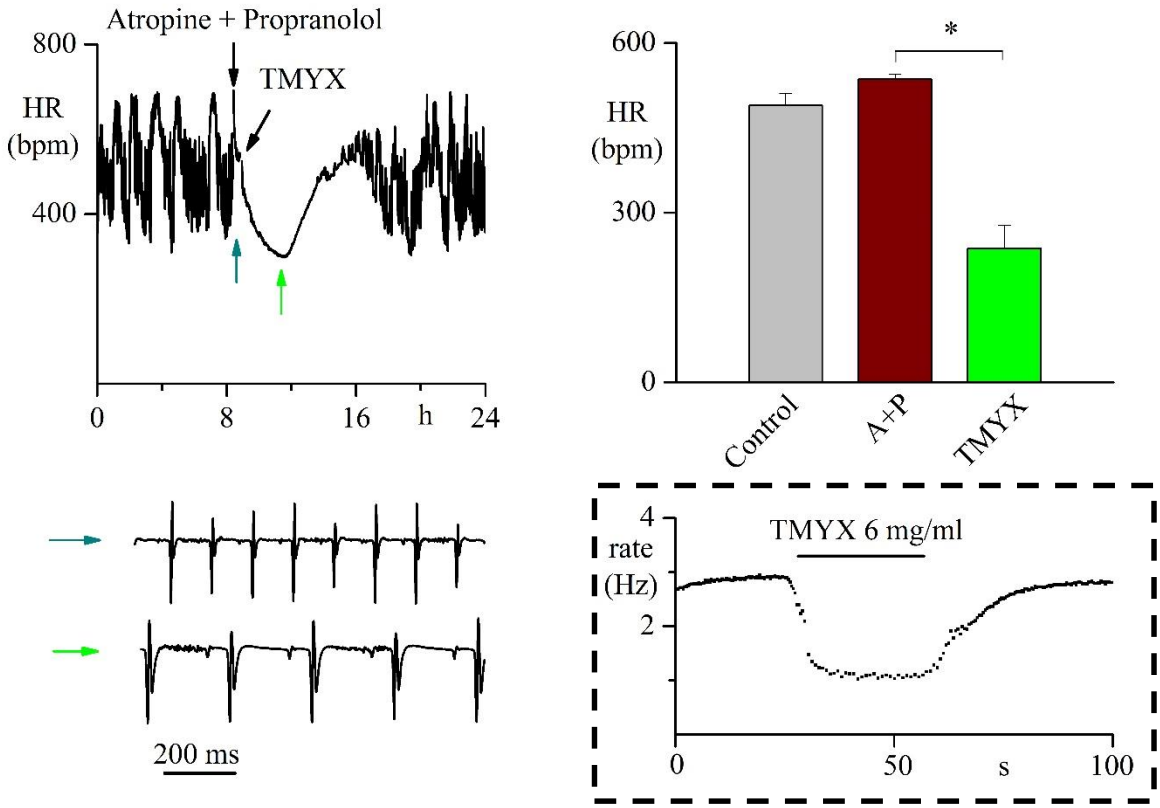

Fig. 35. Effects of TMYX after autonomic blockade in freely-moving mice. Representative tachogram and correspondent sample ECG traces recorded in a mouse treated with TMYX, left; the drug was injected 15 minutes after the complete block of the autonomic system (A+P). The origin of the x-scale has conventionally been set to 0 and corresponds to 08:00 AM. Top, right, mean heart rate values (n=3) obtained in control condition and during autonomic block before (A+P) and after drug injection (A+P+TMYX). The bradycardic action on intrinsic heart rate is in agreement with the effect of the drug observed on spontaneous activity of rabbit SA node cells (insert).

Representative time course of heart rate from one mouse is shown in **fig. 35**. The complete pharmacological blockade, induced by i.p. injection of atropine (2 mg/kg) and propranolol (1 mg/kg), caused a stabilisation of heart rate at the value of about 550 bpm as previously reported (D'Souza et al., 2014). We next administered (i.p. injection) TMYX 5 mg/g and observed the onset of a deep bradycardia, with a reduction of 55.6 % of heart rate (n = 5). This protocol allowed to verify the effect of TMYX on the intrinsic heart rate, and the observed reduction was comparable to that measured in in-vitro experiments (**fig 35, insert**). The duration of this

effect is variable from 5 to 14 hours, and during this period the heart rate variability was completely removed.

No significant changes in heart rate were observed after the injection of saline solution (data not shown).

These data indicate an increment of mean heart rate after complete pharmacological blockade, suggesting a major contribution of parasympathetic system in normal condition; the deep bradycardia induced by TMYX reflects the slowing effect on pacemaking observed during *in-vitro* experiments.

These results suggest a relation between TMYX and autonomic nervous system. To better define this behaviour, we tested the effect of TMYX after blocking either one arm or the other of the sympahovagal balance. When TMYX was delivered after blockade of parasympathetic nervous system, obtained by i.p. injection of atropine (**fig. 36, top**), a competitive antagonist of the muscarinic acetylcholine receptors, the drug produced an effect similar to that observed when TMYX was administered alone, that is an increase of heart rate of 33.6 % (n = 3).We then proceeded by testing the effect of TMYX after blocking the sympathetic nervous system with propranolol, a nonselective β-blocker (**fig. 36, middle**). In this condition the injection of TMYX 5 mg/g induced a deep bradycardia with a rate reduction similar to that observed with complete autonomic blockade (-38.5 %, n = 3). To confirm the relation between TMYX and sympathetic nervous system, we performed the same experiment inverting the order of the drug administration and we observed similar results since the injection of propranolol after TMYX caused a reduction of heart rate of 33.6 %, n = 2 (**fig. 36, bottom**).

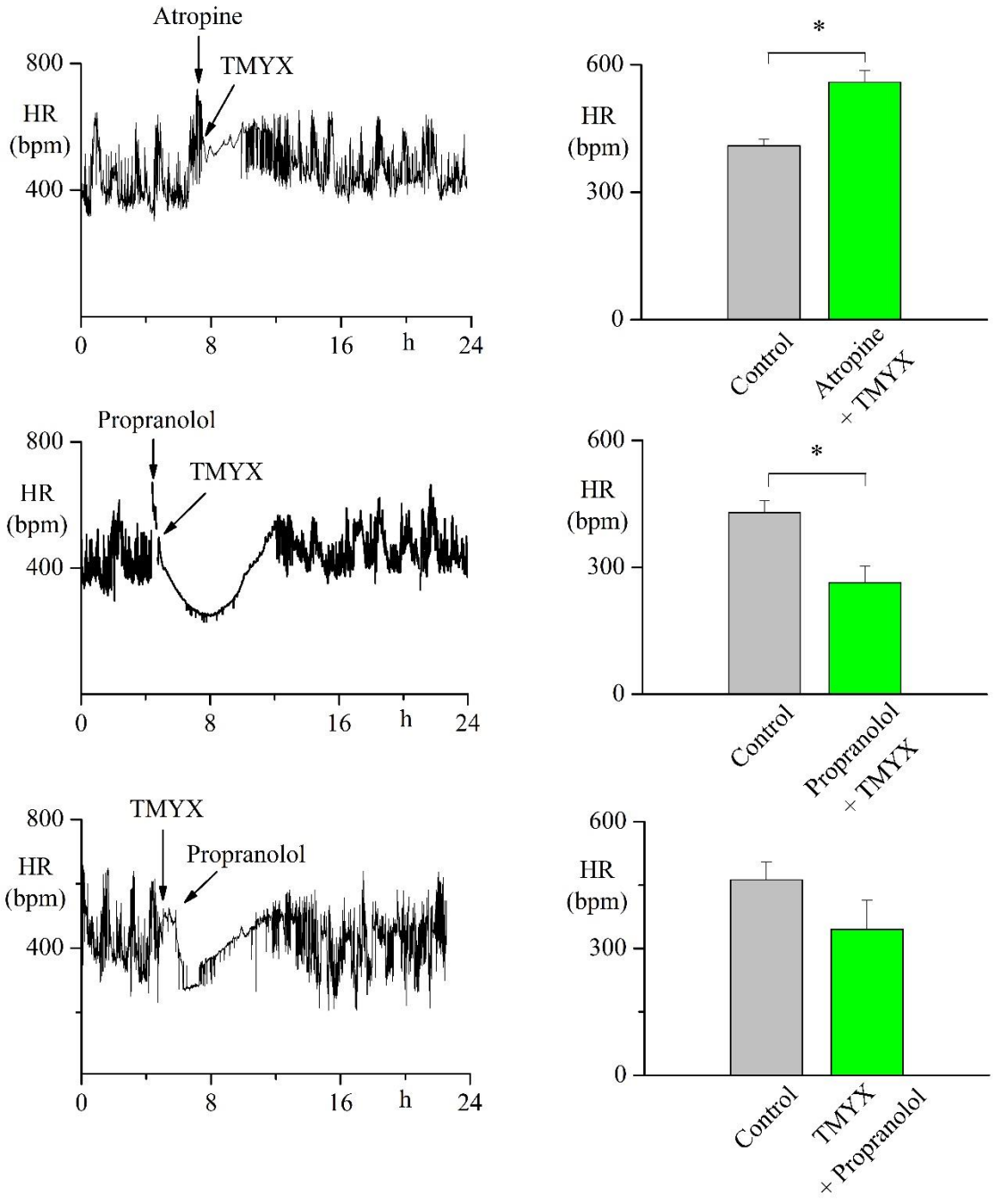

Fig. 36. Representative tachograms recorded in a mouse treated with (top) TMYX 15 minutes after the administration of atropine (2 mg/kg); (middle) TMYX 15 minutes after propranolol injection (1 mg/kg); (bottom) propranolol (1 mg/kg) 15 minutes after TMYX. The origin of the x-scale has conventionally been set to 0 and corresponds to 08:00 AM. Mean heart rate values (n=3) obtained in control condition and during atropine + TMYX injection (A) show an increment of heart rate. The injection of TMYX, before or after propranolol produces a reduction of heart rate.

4. INAPPROPRATE SINUS TACHYCARDIA

4.1. INTRODUCTION

HCN channels are a potential target of several mutations. Functional studies showed that all the mutations investigated are associated with arrhythmic conditions (Milanesi et al., 2015; Verker et al., 2015; DiFrancesco (2015); Verkerk et al., 2014). Most of these mutations are of the type loss-of-function and they are associated with bradycardia (heart rate lower than 60 bpm), usually an asymptomatic condition; however in some cases bradycardia can be symptomatic.

Inappropriate sinus tachycardia (IST) is a syndrome characterized by fast sinus rates at rest, or sudden unjustified increase of rate with minimal physical activity, or both. IST is not defined by a specific heart rate, but patients generally have resting sinus rate of more than 100 bpm and average 24 hours heart rates of more than 90 bmp, that are not explained by physiologic demands.

IST presents with a spectrum of symptoms including palpitations, weakness, fatigue, dizziness or near syncope. As a result of physical exercise, the acceleration in rate is excessive, and heart rate recovery is prolonged (Olshansky et al., 2013).

Whereas sinus tachycardia is a transient and reversible condition with an explainable cause and a rate appropriate for the circumstance (i.e. caffeine ingestion, anxiety, deconditioning), IST is a more long-standing problem that is not easy to explain.

The epidemiologic characteristics of IST are uncertain; generally the prognosis is benign, because although patients have faster heart rates, the sinus frequency slows somewhat during sleep and in various diurnal patterns (Rubenstein et al., 2010).

The diagnosis of IST is a critical point because is necessary to exclude specific physiological and psychological triggers for appropriate sinus tachycardia (i.e. exercise, anxiety, panic attacks, and pain). Also, several medical conditions can explain sinus tachycardia, for example anemia, dehydration, pulmonary embolus, aortic or mitral regurgitation, myocardial infarction, and other (Krahm et al., 1995; Marrouche et al., 2002).

The diagnosis of IST is made for exclusion and is based on persistent or recurrent sinus tachycardia on 12-lead ECG, paying attention to the analysis of P wave morphological features: (1) if the P-wave is the same or similar to that in normal sinus rhythm, IST is possible; (2) if

tachycardia occurs gradually with postural change, a tilt-table test may indicate POTS (Postural Orthostatic Tachycardia Syndrome); (3) if tachycardia is persistent and an underlying cause can be determined, IST is not present; (4) in patients with generally persistent episodes for which no cause can be determined, IST may be diagnosed (Olshansky et al., 2013).

Although the first cases of unexplained sinus tachycardia were described more than 60 years ago, the exact mechanism(s) underlying IST remain poorly understood. Several studies indicate that either excess sensitivity to sympathetic stimuli or blunted response to parasympathetic activity may be involved. Other possible mechanisms include a global decrease in parasympathetic tone, and an ectopic focus in the immediate vicinity of the sinus node (Still et al., 2002). Before the present study no specific channelopathy is implicated in IST.

In this study we performed a genetic screening in patients with inappropriate sinus tachyarrhythmias and found a glutamine-arginine substitution in the HCN4 gene at position 524. This aminoacid is located in the first portion of the A' α-helix of the C-linker, a region connecting the S6 transmembrane domain to the CNBD which functionally couples the binding of the second messenger cAMP to channel activation (**fig. 37**). When the HCN4 channels are assembled as a tetramer, these regions form a ring of positively charged aminoacids which surrounds the internal mouth of the channel. The R524Q mutation acquires large importance since it causes the substitution of a positive charged aminoacid with one uncharged.

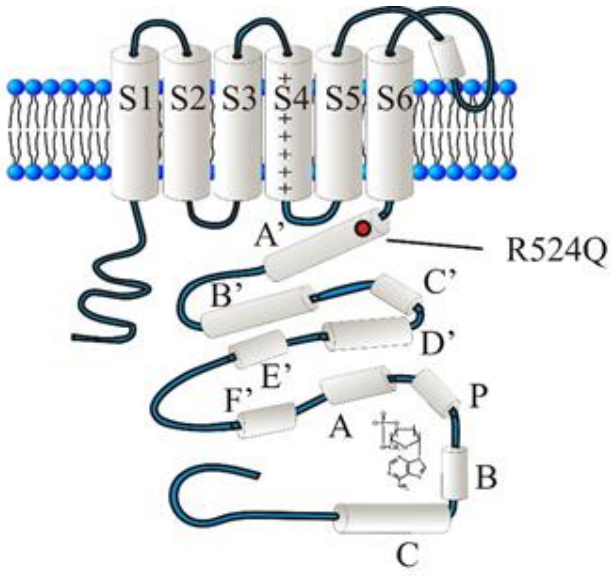

Fig. 37. Spatial localization of the R524Q mutation. The C-linker includes 6 α-helices (A' to F'), and the cyclic nucleotide binding domain (CNBD) includes 4 α-helices (A, P, B, C). The mutation R524Q (indicated by the red dot) is located in the first portion of the A' α-helix of the C-linker

4.2. MATERIAL AND METHODS

Including criteria

The criteria to include patients in our study were (1) symptomatic mean resting heart rate ≥ 95 bpm during the daytime hours of 24 hours Holter monitoring; (2) rapid stable symptomatic increase in resting HR > 25 bpm when moving from a supine to a standing position or in response to biological stress (Cappato et al., 2012).

Genomic DNA analysis and mutagenesis

All the genetic analysis were performed after obtaining the written informed consent. The coding sequence of the hHCN4 gene was amplified by PCR starting from genomic DNA extracted from whole blood or saliva (Puragene Blood Kit, Qiagen). The primers were designed to amplify DNA fragments of 149 to 395 bp in order to screen all the coding portion of the *hHcn4* gene. The PCR reaction mixture included 100 ng of genomic DNA, 1 µM primers and the FastStart Taq DNA Polymerase (Roche Diagnostics). The PCR cycling reaction consisted of initial denaturation for 5 minutes at 95° C, and 30 cycles with denaturation of 30 s at 95° C, annealing for 30 s at different temperature and extension for 30 s at 72° C.

The primers 5'TTCCCTCTCATCCACTGTCCC3' (F), 5'GACCAATGTGCGGGTGCTCC3' (R) were used to amplify exon 4 where the pathological mutation 1571g→a (R524Q) is located. Analysis of the amplicons was carried out by Single-Strand Conformation Polymorphism (SSCP). The presence of mutations was confirmed by DNA sequencing (Bio-Fab Research). The mutation of interest was not identified in a group of 200 healthy subjects, and it allowed to exclude the possibility of a DNA polymorphism.

For functional studies in both HEK293 cells and neonatal rat myocyte cultures the mutation was incorporated into the pcDNA 1.1 vector (Clontech Laboratories) containing the hHCN4 cDNA sequence by means of a commercial kit (QuikChange® Site Directed Mutagenesis, Agilent Technologies). The primers used were:

- 5'CTGGACTCCTCCCAGCGCCAGTACCAG3' (F);
- 5'CTGGTACTGGCGCTGGGAGGAGTCCAG3' (R).

Functional studies in HEK 293 cells

HEK293 cells were transiently transfected (FuGENE® HD Promega) with:

- hHCN4 wild-type 0.8 µg (wt).
- hHCN4 R524Q 0.8 µg (homo).
- hHCN4 wild-type 0.4 µg and R524Q 0.4 µg (hetero).

For each condition we used 0.3 µg of GFP-containing plasmid (pmaxGFP, AmaxaBiosystems). Only GFP-expressing cells were selected for patch-clamp analysis at room temperature. Patch clamp analysis were performed 48-72 hours after transfection.

Whole-cell studies

Electrophysiological studies were carried out using an extracellular solution containing (mM): 110 NaCl, 30 KCl, 1.8 $CaCl_2$, 0.5 $MgCl_2$, and 5 HEPES-NaOH buffer (pH 7.4); 1 mM $BaCl_2$, 2 mM $MnCl_2$ were added to improve I_f dissection over other ionic components. Intracellular solution contained (mM): 10 NaCl, 130 KCl, 1 egtazic acid (EGTA), 0.5 $MgCl_2$, 2 ATP (Na salt), 0.1 GTP (Na salt), 5 phosphocreatine, and 5 HEPES-KOH buffer (pH 7.2).

To understand differences between wt and mutant channels (homomeric and heteromeric configurations) we analysed (1) I_f current densities, measured at the steady-state current amplitude of each test potential and normalized to cell capacitance; (2) activation curves for HCN4 currents obtained by activation and deactivation protocols and analysed by the Boltzmann equation.

Inside-out macropatch studies

Solution used to perfuse the intracellular sides of the patches contained (mM): 130 mM K-aspartate, 10 NaCl, 2 $CaCl_2$, 5 EGTA-KOH, and 10 HEPES-KOH buffer (pH 7.2; pCa, 7). Solution used in patch pipettes contained (mM): 70 NaCl, 70 KCl, 1.8 $CaCl_2$, 1 $MgCl_2$, 1 $BaCl_2$, 2 $MnCl_2$, and 5 HEPES-NaOH buffer (pH 7.4). The activation curves and the shifts induced by cAMP were calculated as previously reported (DiFrancesco & Mangoni, 1994).

Briefly to investigate the action of cAMP on single I_f channel, patches were exposed in sequence to a control solution, a solution containing cAMP 0.1 µM, and back to the control solution, while single channel activity was recorded. The dose-response curves of cAMP-induced shifts were analysed by the Hill equation. Each patch was exposed to cAMP only once. The holding potential was -35 mV in all experiments.

Functional studies in neonatal rat cardiac myocytes cultures

Neonatal ventricular myocytes were isolated from 2 days-old neonatal rats. The hearts were quickly removed and placed in phosphate buffer solution (mM): (137 NaCl, 2.6 KCl,10 Na_2HPO_4, 2 KH_2PO_4, pH 7.4); the ventricles were isolated, cut into 2 mm x 2 mm pieces, and placed in enzymatic solution (mM): 116.4 NaCl, 5.4 KCl; 1 NaH_2PO_4, 0.8 $MgSO_4$, 5.5 Glucose, 20 Hepes, 0,4 mg/ml Pancreatin (Sigma), 136 U/ml Collagenase type 1 (Worthington), and dissociated by mechanical agitation for 15 minutes at 37°C. At the end, the solution containing the cells was centrifuged and kept on ice. The enzymatic dissociation procedure was repeated 5 times. Finally, the cells obtained were centrifuged, resuspended in the medium and plated in a Petri dish containing DMEM/M199, 10% Horse serum, 5% Fetal Bovine Serum (FBS), 2 mM L-Glutamine, 100 units/ml Penicillin, 0.10 mg/ml Streptomycin. Cardiomyocytes were incubated 1 hour at 37°C in 5% CO_2 for two times to remove contaminating fibroblast in the cells culture.

Cardiomyocytes (~$2*10^6$) were transfected by electroporation with Rat Cardiomyocytes-Neonatal Nucleofector® Kit (Lonza) as follows:

- hHCN4 wild-type 1.3 µg (wt);
- hHCN4 R524Q 1.3 µg (homo);
- hHCN4 wild-type 0.65 µg and R524Q 0.65 µg (hetero).

Cells were then plated at the density of $1*10^5$ cells/ml onto gelatin-coated dishes filled with the medium previously described and incubated at 37°C in 5% CO_2. Only GFP-expressing cells were selected for patch-clamp analysis at 35°C. Electrophysiological experiments were carried out 36-60 hours after transfection.

Action potential studies

Action potentials were recorded from spontaneously myocytes superfused with normal Tyrode's solution. Patch pipette solution was the same used in HEK cells electrophysiological experiments. For each AP cycle we analyzed the rate to find differences between wild-type and homo/heteromeric HCN4 expression.

Current density and kinetics properties

The I_f current was recorded from single cells superfused with Tyrode's solution to which $BaCl_2$ (1 mM) and $MnCl_2$ (2 mM) were added to improve I_f dissection over other ionic components.

As in HEK cells we analyzed (1) I_f current densities, measured at the steady-state current

amplitude of each test potential and normalized to cell capacitance; (2) activation curves for HCN4 currents obtained by activation and deactivation protocols and analyzed by the Boltzmann equation cells, to understand differences between wt and mutant channels (homomeric and heteromeric configurations).

Video detection of cell rate

During the video recording experiments, cells were kept in Tyrode's solution at 35°C. The experimental setup consisted of inversion microscope Nikon Eclipse TS100, camera Cohu DSP 3600, VirtualDub software. Only green myocytes expressing the GFP protein were selected for the experiment. For each cells a 30 seconds-long video acquisition (acquisition rate 40 Hz) was recorded and the offline analysis of rate (bpm) was calculated by measuring the time necessary to have 10 complete beats (except for some wt myocytes transfected only with GFP since rate was too slow and highly arrhythmic).

4.3. RESULTS

R524Q mutation in a family with IST

The coding region of the cardiac pacemaker channel gene HCN4 was tested for the presence of mutations in 48 patients affected by Inappropriate Sinus Tachycardia (four of whom with familial history of IST). This screening identified the mutation 1571g→a in an adult female (proband). The mutation generates the missense aminoacidic substitution R524Q in exon 4 of one allele. Genetic analysis was then extended to 8 other members of the family and the mutation was identified in three more adults and in one child (**fig. 38 A**).

The adults were affected by palpitations at baseline and anxiety, while the young girl was asymptomatic.

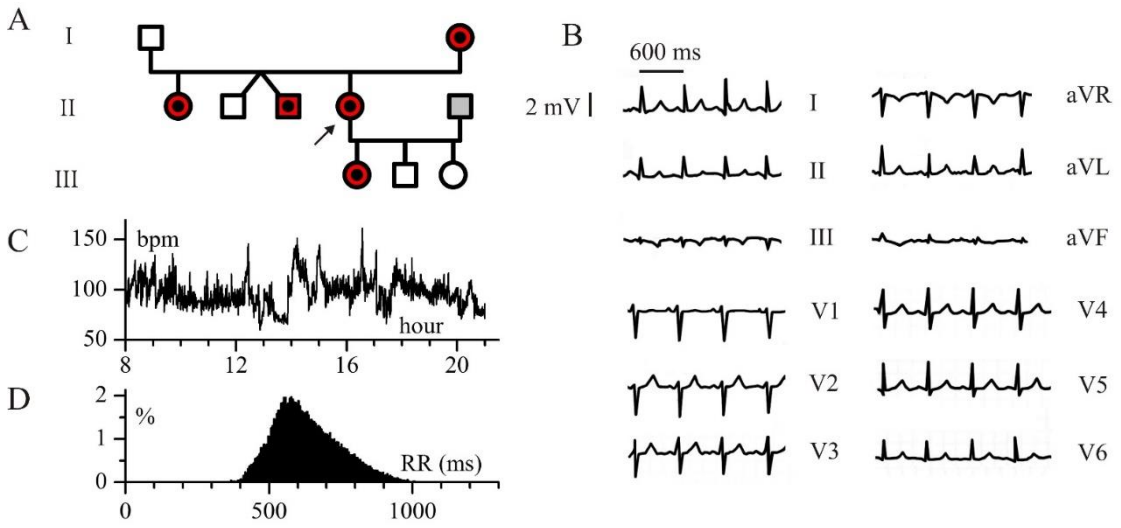

Figure 38. HCN4 mutation associated with IST. (A) Pedigree of a family with IST (the arrow indicates the proband). Red symbols indicate individuals with IST symptoms and/or unjustified sinus tachycardia; dots indicate members of the family carrying the heterozygous mutation R524Q (empty symbols are wild-type, grey symbol indicates a genetically unrelated individual). The twins II-2 and II-3 are heterozygous. (B) 12-lead ECG recorded at baseline in the proband; the heart rate is 103 bpm and the P wave is indicative of sinus node origin. (C) Time course of daytime heart rate (from 8 AM to 9 PM) recorded in the proband during Holter monitoring; the mean rate was 98.5±14.2 bpm (mean ± SD). (D) Histogram of daytime R-R intervals recorded during Holter monitoring.

The clinical profile of the proband (II-4) was characterized by prolonged periods of symptomatic sinus tachycardia (**fig. 38 B**), frequent palpitation at rest and/or during effort and anxiety, orthostatic intolerance with syncope, reproducible dyspnea on effort limiting or causing early termination of any physical activity, and lightheadedness. The patient had a mean value of heart rate of 98.5±14.2 bpm, calculated with an ECG Holter-monitoring (from 8 am to 9 pm), **fig. 38 C**. The diagnosis of IST was performed after excluding other mechanisms potentially causing compensatory tachycardia such as: structural heart disease, neuroendocrine disorder, postural hypotension, fever, anaemia, pregnancy and medications.

In the proband's mother (I-2) the presence of sinus tachycardia with resting heart rates in the range of 100 bpm was confirmed by multiple ECG recordings carried out in 5 years period (103.3 bpm in the ECG of **fig. 39 A**).

In the proband's sister (II-1) the Holter monitoring revealed multiple phases of sudden unexplained sinus tachycardia unrelated to physical activity during both day and night. She also presented with orthostatic intolerance and lightheadedness; Holter monitoring revealed multiple phases of sudden unexplained sinus tachycardia unrelated to physical activity during both day and night (**fig. 39 B**).

The individual II-3 is an adult male with a history of recurrent syncope associated with binodal dysfunction characterized by sinus bradycardia and phases of 1st and 2nd degree AV block (**fig. 40 A,C**). This individual presented several unexpected bursts of increasing heart rate at rest (manifested with "warm-up" phases, characteristic of IST), suddenly interrupted by phases of bradycardia (**40 B,C**), likely induced by a robust vagal discharge. These events were observed during the day, but they were particularly frequent at night-time (**fig. 40 C**).

The proband's daughter (III-1) is a healthy young girl who did not report specific cardiac symptoms, but Holter monitoring revealed phases of anomalous tachycardia unrelated to any physical activity or emotional stress.
The mutation R524Q was not identified in a group of 200 healthy subjects and we therefore excluded the possibility of a DNA polymorphism.

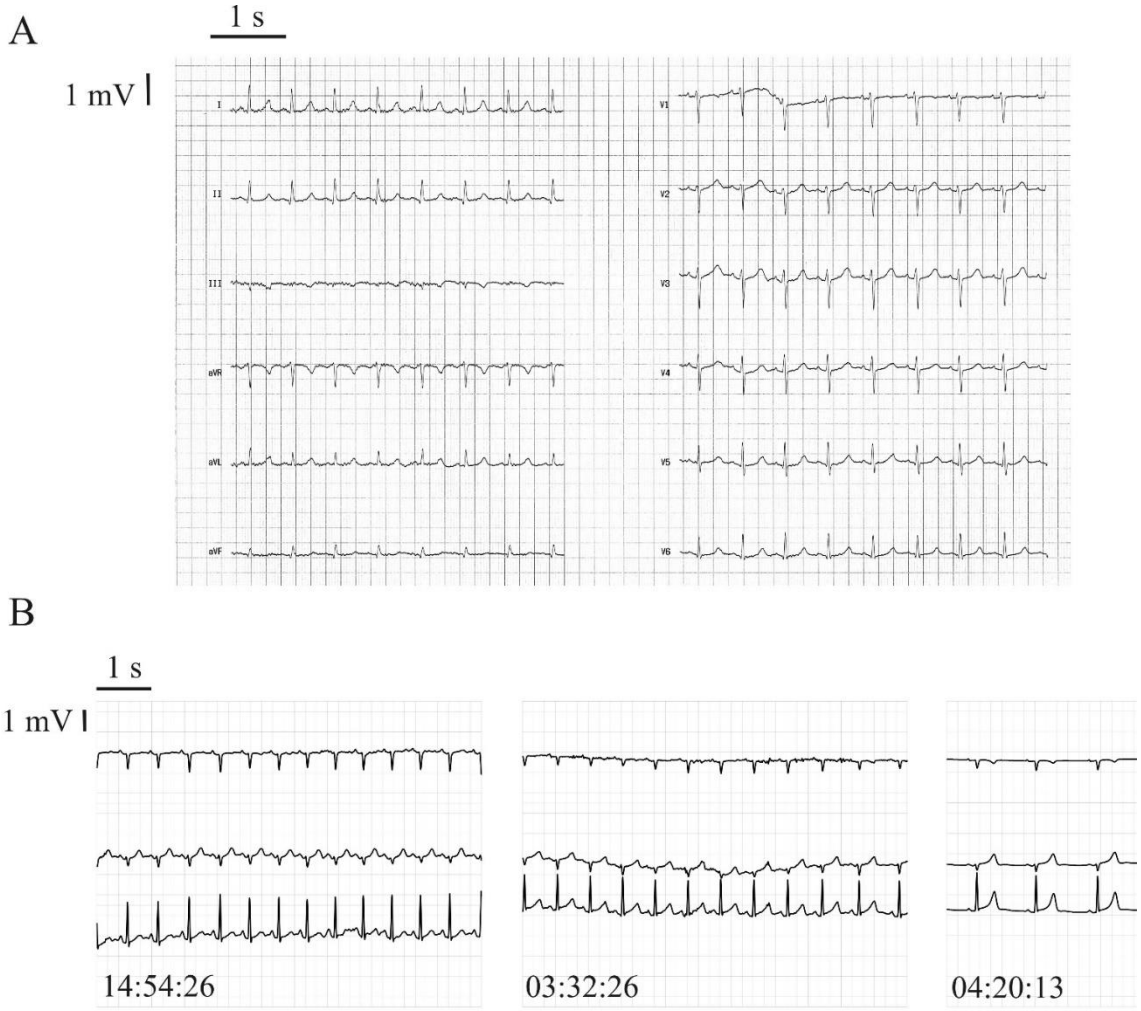

Figure 39. Episodes of unjustified sinus tachycardia recorded at rest from the proband's mother (I-2) and sister (II-1). (A) 12-lead ECG recordings at rest from the proband's mother; the mean heart rate was 103.3 bpm. (B) Stretches of Holter recording showing the occurrence in the proband's sister (II-1) of episodes of sinus tachycardia at rest during daytime (left, 111.5 bpm) and night (middle, 94.3 bpm).

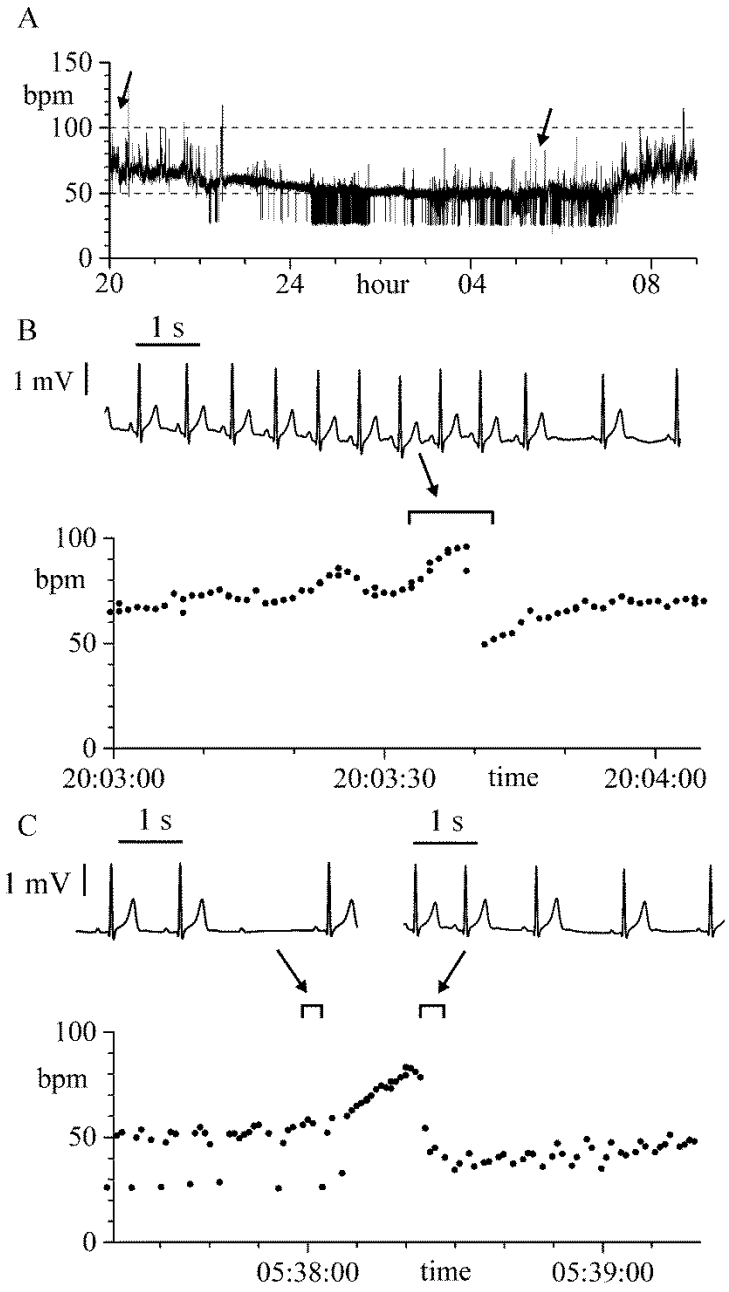

Figure 40. ECG-Holter recordings from the proband's brother (II-3). (A) Plot of heart rate (from 8 PM to 9 AM) during Holter monitoring indicates that sinus rhythm was prevalently bradycardic with several episodes of 2:1 AV block particularly during sleep. Arrows indicate correspondence with enlargements in panels B and C. (B) Time course of heart rate (bottom) and corresponding ECG recording (top) associated with symptomatic palpitation and anxiety at rest during the day, as reported by the patient. (C) Time course of heart rate (bottom) and corresponding ECG recordings (top) showing an episode of asymptomatic sinus tachycardia recorded at night during sleeping (top, right). "Warm-up" events characterized by inappropriate sinus tachycardia followed by sudden rate slowing are apparent in both panels.

Functional analysis by heterologous expression in HEK293 cells

The initial part of the HCN4 C-linker, is an important region that connects the S6 transmembrane domain to the CNBD, responsible of the cAMP binding. In the tetrameric channel assembly they form a ring of aminoacids positively charged which surrounds the internal mouth of the channel (**fig. 41**). The R524 residue is located in the firs portion of the A' α-helix of the C-linker, in proximity to the S6 domain.

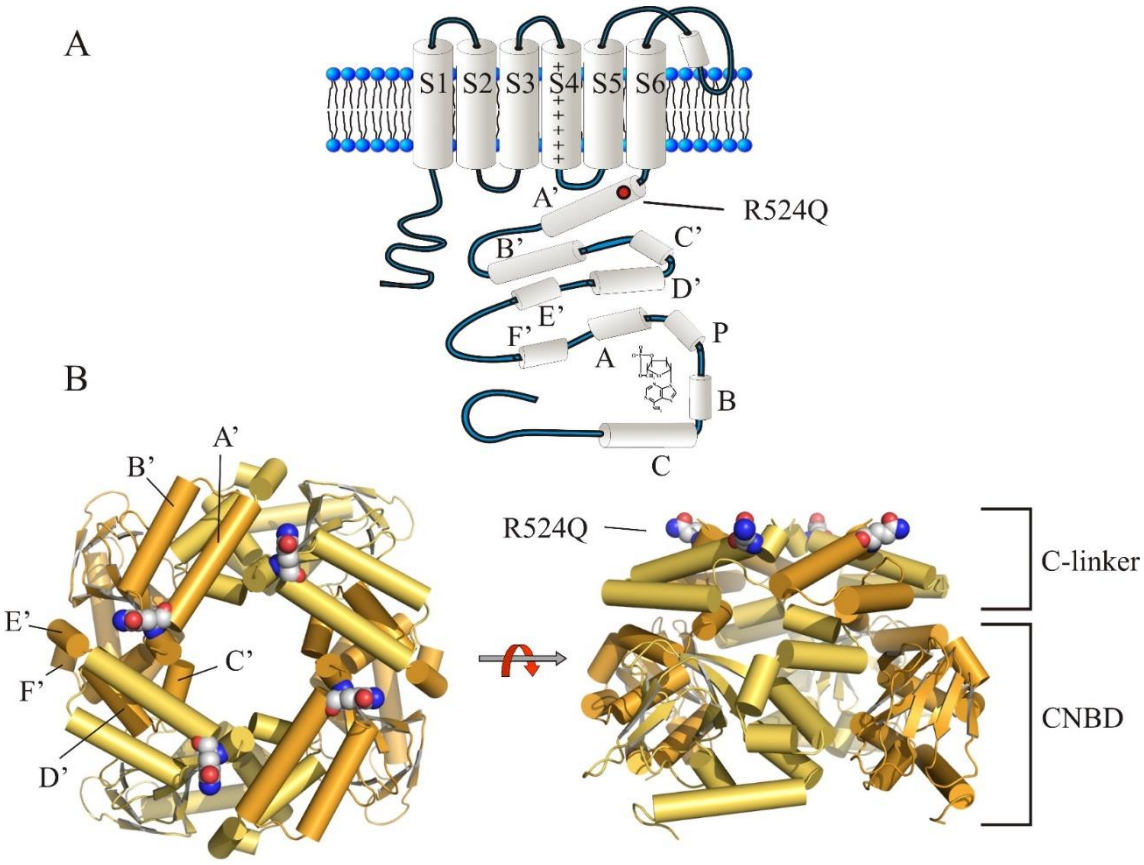

Figure 41. Spatial localization of the R524Q mutation. (A) Schematic representation of the topology of one HCN4 channel subunit. The C-linker includes 6 α-helices (A' to F'), and the cyclic nucleotide binding domain (CNBD) includes 4 α-helices (A, P, B, C). The red dot indicates the approximate position of the mutation R524Q. (B) 3D model reconstruction of the human HCN4 channel C-terminal domain viewed from the membrane (left) and from the side (right). All 4 subunits are shown as cartoon plots, two in dark and two in light orange. R524 residues in the C-linkers, mutated to Q, are drawn as spheres. C-linker α helices of one subunit are labelled in the left panel. The reconstruction is based on a previously published crystal structure of the HCN4 C-terminus (PDB code 3OTF).

HEK293 cells were transfected with wt and mutated hHCN4 channel cDNA to investigate by patch-clamp analysis the kinetic properties of the respective channels.

Both channel types were expressed with similar efficiency; mean current densities measured at -145 mV were: -50.7 ± 11.5 (n = 16), -56.5 ± 11.7 (n = 14), and -48.2 ± 6.9 pA/pF (n = 21) for wt, heteromeric wt-R524Q and homomeric mutant R524Q channels, respectively (not significantly different, $P > 0.05$).

However, we observed an increment in the availability curve of the I_f current caused by a depolarizing shift of 4.2 mV in heteromeric wt-R524Q channels and of 7.6 mV in homomeric mutant R524Q channels (**fig. 42 A, top**).

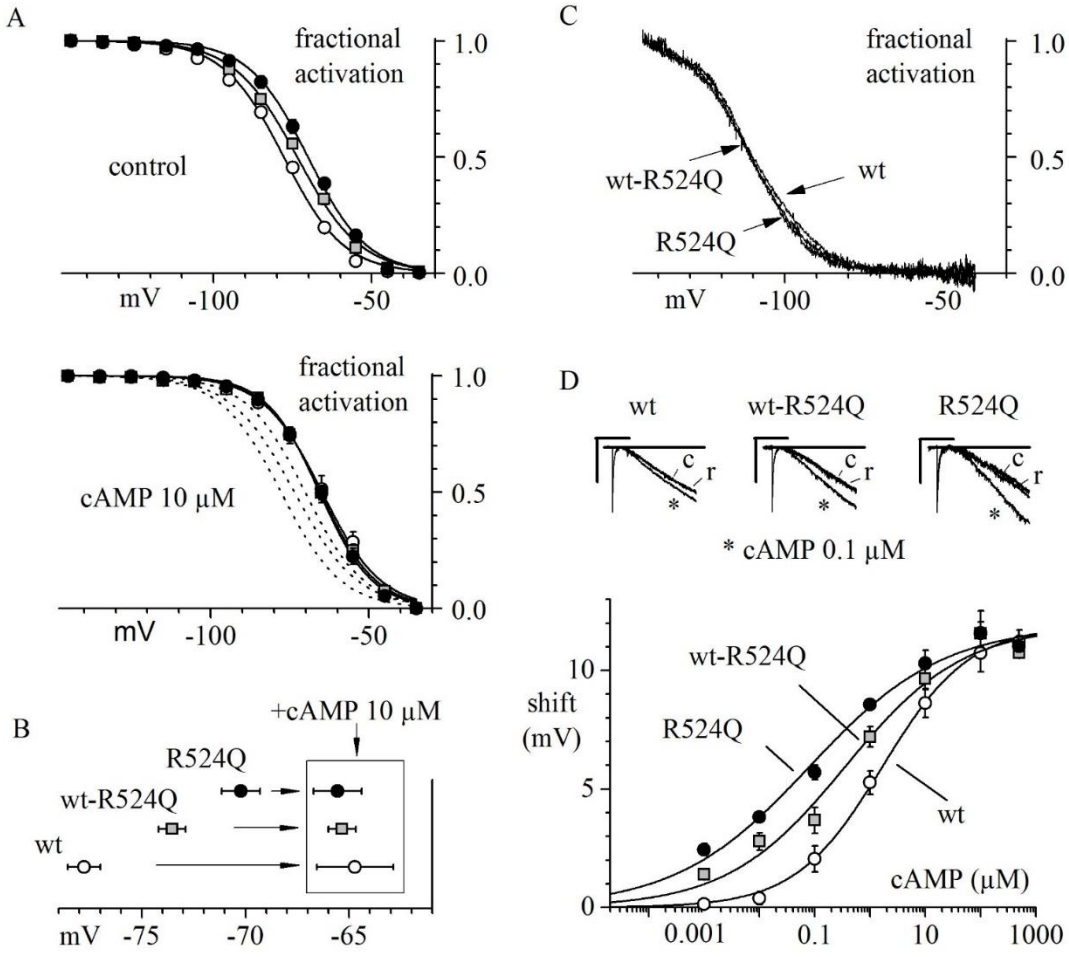

Figure 42. Wild type and mutated channel expression in HEK293 cells. (A) Mean activation curves of HCN4 current measured in HEK293 cells in control (top) and in the presence of 10 µM cAMP in the whole-cell pipette (bottom). Datapoints are means from n = 6-10 cells. $V_{1/2}$ values from Boltzmann fitting (full lines) are: -77.8, -73.6 and -70.2 mV (top) and -64.8, -65.3 and -65.6 mV (bottom) for wild type (open circles), heteromeric wt-R524Q mutant (grey squares) and homomeric

R524Q mutant channels (filled circles), respectively. All curves were significantly different in control, but not in the presence of cAMP. Curves in the upper panel are replotted as broken lines in the lower panel. (B) Mean $V_{1/2}$ calculated from Boltzmann fitting of single-cell activation curves (n = 6-10 cells). Values in the presence of cAMP are boxed. (C) Mean activation curves measured in inside-out macropatches in absence of cAMP of wt, hetero- and homomeric channels (n = 7-9). (D) Dose-response relationships of cAMP dependence of activation curve shift measured in inside-out macropatches expressing wt, wt-R524Q and R524Q channels. Each datapoint is the average of 3-10 exposures. Parameters of Hill fitting of these curves are: K_d=1.67, 0.35 and 0.080 µM and h=0.55, 0.41, and 0.36 for wt, wt-R524Q and R524Q channels, respectively. Maximal shift was fixed to Smax=11.9 mV for all curves. Top panels: sample inside-out traces in control (c), during perfusion with cAMP (*) and upon return (r). Horizontal bar: 1 s; vertical bar: 20 pA.

The differences in the half-activation ($V_{1/2}$) values of activation curves suggest the acquisition of intrinsic new properties of mutant channels or differences in the sensitivity to basal cytoplasmic cAMP. The cells exposition to a saturating cAMP concentration (10 µM) in the whole-cell pipette solution, showed an overlapping of the activation curves of wild-type, heteromeric wt-R524Q, and homomeric mutant R524Q channels. In this condition their $V_{1/2}$ were not significantly different (**42 A, bottom**).

The cAMP-induced shift of $V_{1/2}$ in wt channels (13.0 mV) had the expected size (Altomare et al., 2003; Milanesi et al., 2006), while it was significantly reduced in wt-R524Q (8.3 mV) and in R524Q channels (4.6 mV) ($P<0.05$; **fig. 42 B**).

Results obtained suggest a modified (increased) cAMP sensitivity of mutant channels; to confirm this hypothesis we investigated the action of cAMP in inside-out macro patches. Mean activation curves of wt, wt-R524Q and R524Q channels measured with a voltage ramp protocol in a cAMP-free intracellular solution, indicated that the mutation did not modify the intrinsic voltage dependence of channels in the absence of cAMP (**fig. 42 C**).

A cAMP concentration of 0.1 µM, on the other hand, was more effective on mutant than on wt channels (**fig. 42 D, top**). The dose-response relationships of the $V_{1/2}$ shift against cAMP concentration for the three channel types (**fig. 42 D, bottom**) confirmed the higher cAMP sensitivity of the mutant channels.

R524Q mutant proteins increase automaticity in neonatal cardiac myocytes

The data in **fig. 42** show that R524Q channels respond more strongly to cAMP, and provide a basis to predict an abnormally fast, β-adrenergic sensitive cardiac rhythm of patients carrying the mutation. For a direct evaluation of the effects of the mutation on beating rate, we performed functional analysis using an excitable cellular model. We transfected wt and/or mutant channels into rat neonatal cardiac myocytes (Qu et al., 2001), **fig. 43**. Cardiomyocytes were co-electroporated with wt and/or mutant channel cDNA and with GFPmax-containing plasmids to allow for the identification of green cells. HCN4 channels were equally expressed in all groups and mean current densities measured at -125 mV values were not significantly different: -39.4 ± 8.2 (n = 6), -34.6 ± 6.6 (n = 6), and -37.6 ± 6.1 (n = 7) pA/pF for wt, wt-R524Q and R524Q channels, respectively ($P > 0.05$); for comparison, cells expressing only the GFPmax had a current density of -3.6 ± 0.8 pA/pF (n = 9; $P < 0.05$ vs. control).

Transfected cells acquired a constant, regular rate as previously shown (Qu et al., 2001), and we compared their activity. Relative to wt (65.6 ± 3.7 bpm, n = 9), the mean spontaneous rate was 34.7% (88.4 ± 9.0 bpm, n = 9) and 72.2% faster (113.0 ± 5.8 bpm, n = 10) in cells expressing wt-R524Q and R524Q channels, respectively ($P < 0.05$; **fig. 43 D**). Video detection measurements of rate contraction were also performed, and mean rates of 65.2 ± 5.4 bpm (n = 10) and 96.6 ± 9.3 bpm (n = 10, 48.2% acceleration) were measured from wt and R524Q-channel expressing cells, respectively.

The faster spontaneous rate suggested the presence of a larger pacemaker current; the analysis of the fractional current activation confirmed, as observed in HEK293 cells, the shift of the mean activation curves to more positive voltages by 3.9 and 7.3 mV in wt-R524Q and R524Q channels, respectively (**fig. 43 C**)

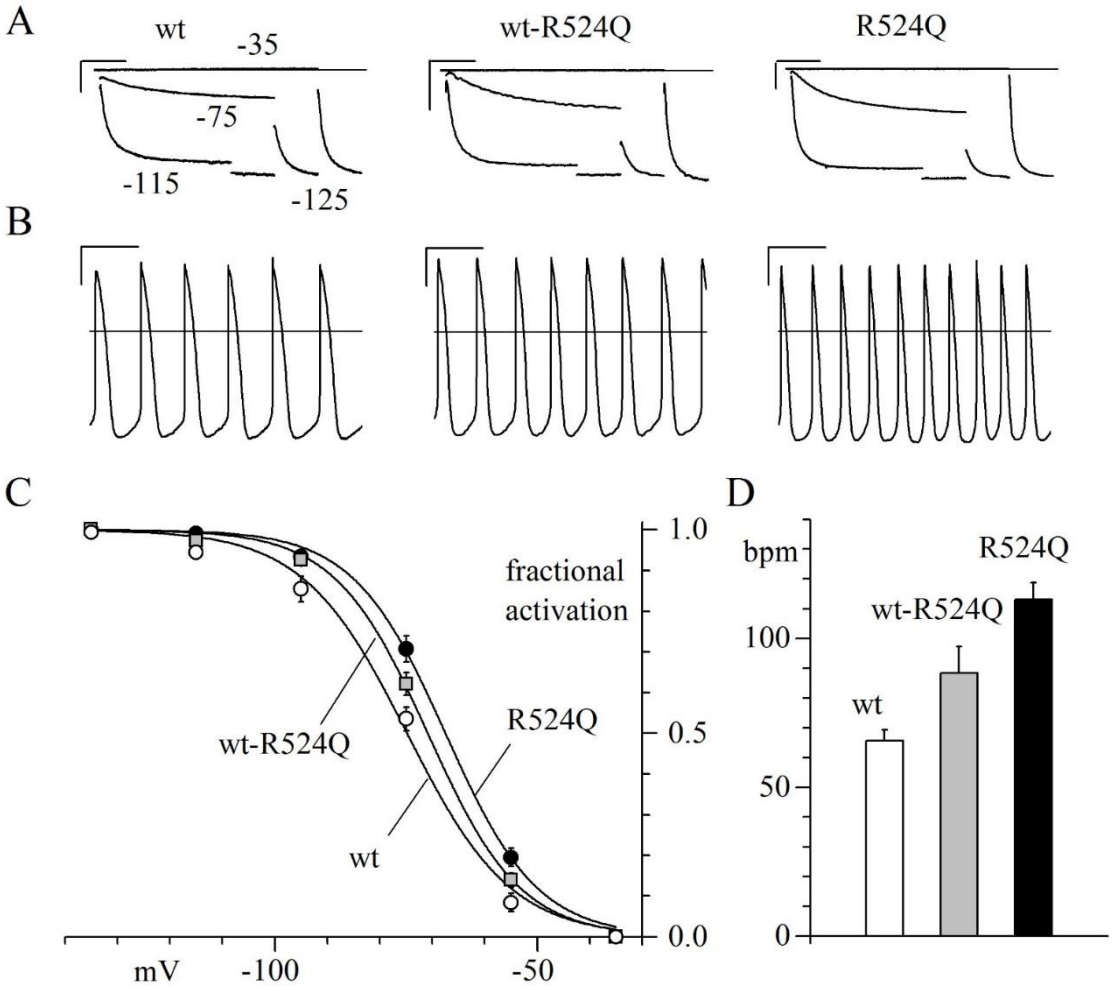

Figure 43. Wild type and mutated channel expression in rat neonatal myocytes. (A) Sample current and (B) free-running voltage traces recorded in cells expressing wt (left), wt-R524Q (middle) and R524Q channels (right). Currents in (A) were measured during two-step protocols to the voltages indicated. In (A) and (B): horizontal bar: 2 s and 1 s; vertical bar: 500 pA and 20 mV, respectively. (C) Mean activation curves (n = 4-10 cells). $V_{1/2}$ values from Boltzmann fitting were: -74.8 (wt), -70.9 (wt-R524Q), and -67.5 mV (R524Q). (D) Mean spontaneous rates were 65.6 ± 3.7 (n = 9), 88.4 ± 9.0 (n = 9), and 113.0 ± 5.8 bpm (n = 10) in cells expressing wt, wt-R524Q and R524Q channels, respectively. All values are significantly different from each other ($P < 0.05$).

5. DYNAMIC CLAMP

5.1. INTRODUCTION

The dynamic clamp (DC) technique consists of a variety of hardware and software implementations used to create artificial conductances in excitable cells. It was introduced in cardiac electrophysiology more than 30 years ago, when an analog circuit was used to electrically connect two independent groups of cardiomyocytes, free of direct physical contact (Scott et al., 1979). At the beginning of the '90s, DC was implemented by a coupling clamp circuit, able to simulate intercellular electrical coupling through the gap junctions (Joyner et al., 1991). Today it represents a standard tool of electrophysiology, used in a large variety of experimental preparations to address different issues; in particular this is a common technique in neurophysiology, but in the last years DC has acquired also interest in the cardiac cell physiology research (Prinz et al., 2004; Goaillard and Marder, 2006; Wilders, 2006).

DC technique uses several basic configurations in cardiac cellular electrophysiology: coupling-clamp, model-clamp, dynamic AP-camp, and cell-type transforming clamp.

The coupling-clamp configuration, for example, simulates intercellular electrical coupling between myocytes through gap junctions. The current-clamp mode is used to record the membrane potentials of both cells. Based on the difference between V_{m1} and V_{m2}, and on a virtual conductance G, the PC computes the coupling current I_C, flowing from cell 1 to 2 in the real-time (**fig. 44**).

The model-clamp configuration instead is used to simulate the presence of an additional conductance on the cell membrane. In this case, a single isolated myocyte is involved in the DC measurement and the V_m-dependent current I_x is injected into the cell (**fig. 44**). Generally, the DC allows to alter the cellular conductance using the measured membrane potential to control the amount of current injected into an excitable cell. (Sharp et al., 1993 a; Sharp et al., 1993 b).

An application of DC is the possibility to introduce into a cell any time- or voltage-dependent conductance that has been described mathematically and can be simulated on a computer. For a voltage-dependent conductance, the injected current is determined by a set of differential equations that describe the voltage and the time dependence of the conductance.

In the DC setup used in the present study, a closed-loop control drives a current-clamp experiment. In this configuration, a myocyte is injected with a current whose amplitude and

dynamics are constantly recalculated by an electronic system based on a specific mathematic model.

Even if the DC technique represents a standard tool of electrophysiology, several limitations are present. For example DC duplicates the electrical but not the signal conduction consequences elicited by specific ion currents. In particular with conventional electrode solutions, the DC can simulate the electrical current from a set of ion channels, but it does not reproduce the changes in intracellular ion concentration that normally are associated with the gating of such channels.

The injected current enters the cell through the glass microelectrode rather than through the real ionic channels, which makes the flow of current concentrated on a very specific spot of the cellular membrane and not distributed on the population of the ion channels.

Errors may be introduced in the experiment by the limitations of the technical setup (i.e. time lag between measuring voltage and applying the current based on that voltage), and by inappropriate DC technique chosen for a specific experiment (i.e. non accurate mathematical description of ionic current).

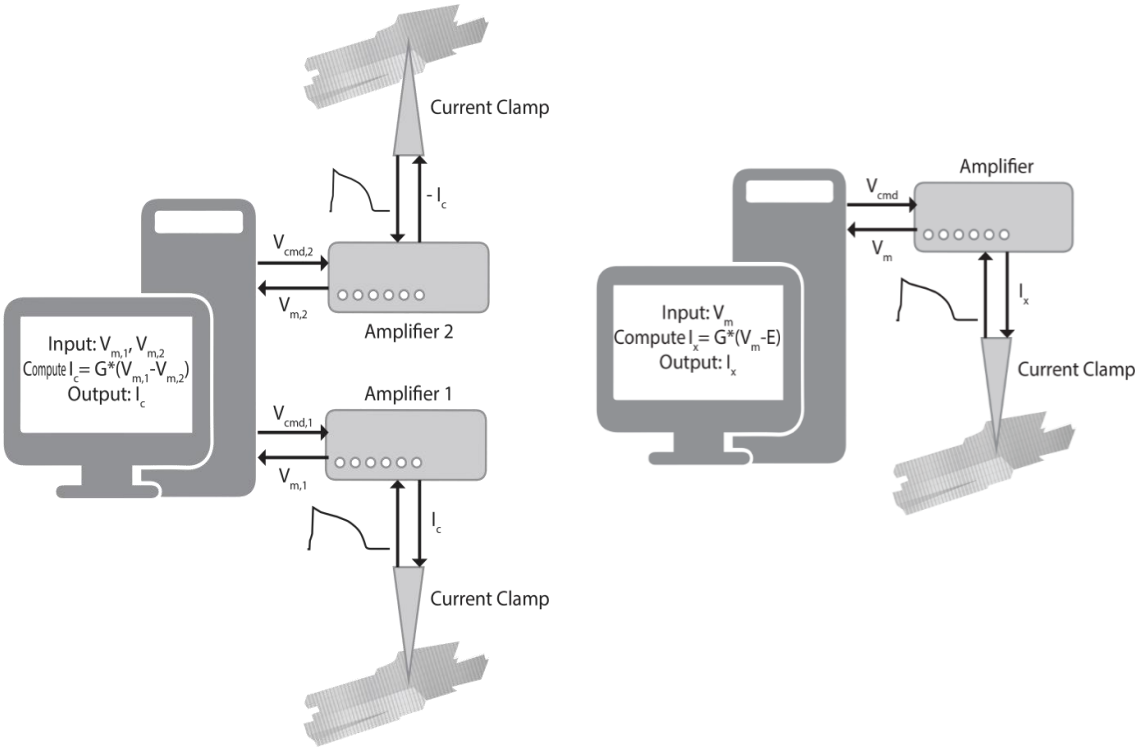

Fig. 44. Dynamic clamp configurations. Representation of the connection between cells, amplifier and PC in coupling clamp (left) and model clamp (right) configuration.

5.2. MATERIALS AND METHODS

Experimental setup

In this study we used a combination of traditional electrophysiological setup and an additional hardware and software for the dynamic clamp.

This instrumentation consists of an amplifier (Axopatch 200B, Molecular Devices), set in current clamp mode, that injects a stimulation current (I_{stim}) and records cellular activity in the form of membrane potential (V_m), **fig. 45**. The shape and intensity of I_{stim} may be modified in real-time through an input voltage signal (V_{Cmd}), using the external command. The amplifier's V_m and V_{Cmd} channels were connected to a data acquisition board, outfitted with a 16-bit resolution analog I/O channels. The board was mounted in a PCI slot of a PC running the RT-Linux Opertive System. The RTXI (Real-Time eXperiment Interface) software platform was used to implement and run the dynamic clamp protocols.

The membrane potential V_m is acquired by the DAQ board input channel, then the specific model for the stimulus current is updated and a new V_{Cmd} value is returned to pilot the amplifier's headstage current injection (I_{stim}).

The updating process of the model-based current includes simple arithmetical operations and the integration of an ordinary differential equation, formulated as a gating variable. The forward-Eulero method was used for this task: between each V_m sampling step, 100 integration steps are performed. The system update frequency was set to 1 KHz, performing these operations every millisecond, much faster than the simulated process.

Since I_f a small current, the computed V_{cmd} was multiplied by a factor of 100 before analog output. After digital/analog conversion, the signal was processed by a passive first-order circuit to restore the correct level (100-factor attenuation) and for low-pass filtering. The cut-off frequency of the smoothing filter was 40 Hz.

Either V_m and V_{Cmd} signals were also recorded by a PC running PCLAMP software. The APs were analyzed with a customized software.

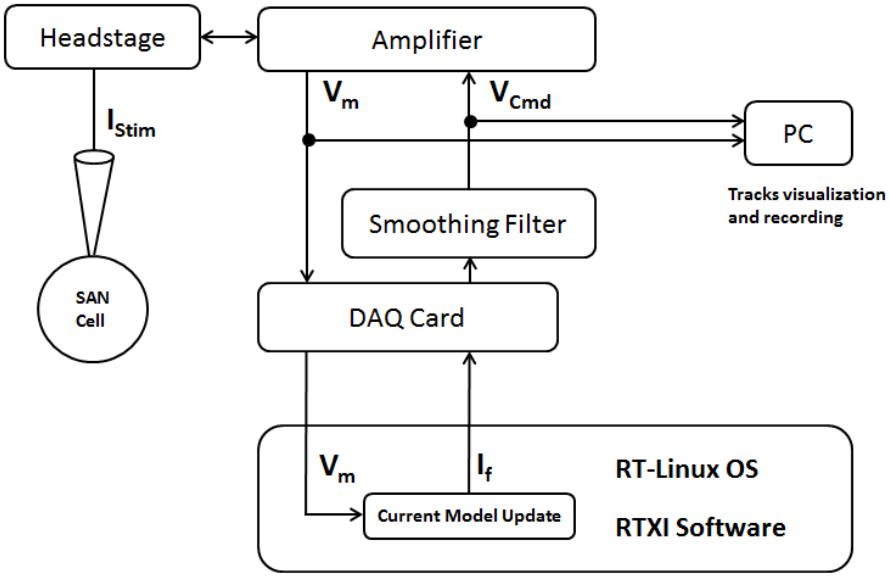

Fig. 45. Experimental setup of dynamic clamp. It consists of a typical electrophysiological tools combined with hardware and software for the dynamic clamp. I_{stim}: stimulation current; V_m: membrane potential; V_{Cmd}: command voltage.

Dynamic clamp protocols

Before starting the dynamic clamp protocols, it was necessary to evaluate the membrane capacitance of each cell under examination. The estimated value was used to scale the injected current amplitude and maintain the same current density regardless of the cell size.

Ivabradine

Two different mathematical models of I_f were tested: (1) Severi/DiFrancesco model (SDiF, Severi et al., 2012), (2) Maltsev/Lakatta model (ML, Maltsev & Lakatta, 2009). These models greatly differ for the intensity of I_f current reached during the slow diastolic depolarization phase.

The IVA protocol consisted of 6 experimental steps: (1) it started with the acquisition of control APs to evaluate basal pacemaking rate; when the AP frequency was stable, (2) 3 µM Ivabradine was perfused. At this concentration, the drug reduced the rate of 65.9 ± 2.4 % (Bucchi et al., 2002). The following step (3) was the injection of the synthetic current using the DC software interface. The current value was computed in real time using one of the two models, and it was scaled to 66% to reproduce the non-total channel block induced by Ivabradine. APs were

recorded in this condition until pacemaking rate changes were detected, and then the current injection was disabled. (4) Still in presence of Ivabradine perfusion, the current injection with the second model was carried out. (5) Than the stimulation current was interrupted and finally (6) ivabradine perfusion was stopped (**fig. 46**).

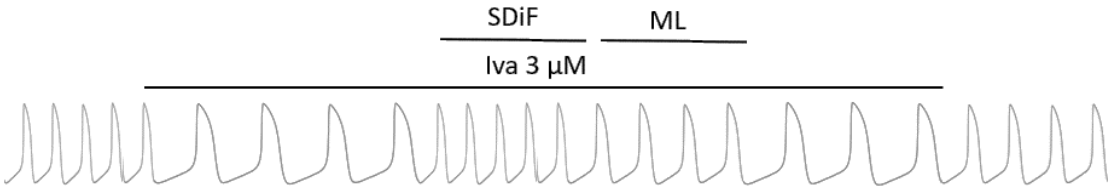

Fig. 46. Ivabradine protocol. (1) control conditions; (2) IVA 3 µM perfusion; (3) SDiF model current injection; (4) ML model current injection; (5) IVA 3 µM perfusion; (6) control conditions.

Isoprenaline/Acetilcholine

Differently from the previous protocol, synthetic current effect and drug effect were evaluated separately, with no direct superimposition in time. Based on the results obtained during ivabradine experiments, only SDiF model was applied.

In this protocol (**fig. 47**), five experimental blocks were present; (1) after recording in control condition, (2) a synthetic current was injected to mimic the autonomic modulation of I_f as reproduced in experiments with isoprenaline and acetylcholine. The effect of isoprenaline on I_f was modeled as positive shift of 7.5 mV (Zaza et al., 1996) and ACh as a negative shift of 4.95 mV (Zaza et al., 1996). Our custom software modules update in real-time the current and gating kinetics equations of both a standard and a voltage-shifted I_f current, resulting in a differential ΔI_f value:

$$\Delta I_f = I_{f,Shifted} - I_{f,Control}$$

After recording a sufficient number of APs, synthetic current injection was disabled, control APs were acquired (3), and then real drug (isoprenaline/acetylcholine) was applied to compare its effect on pacemaking rate with our simulated drug effect on I_f (4). Finally, we returned in control condition (5).

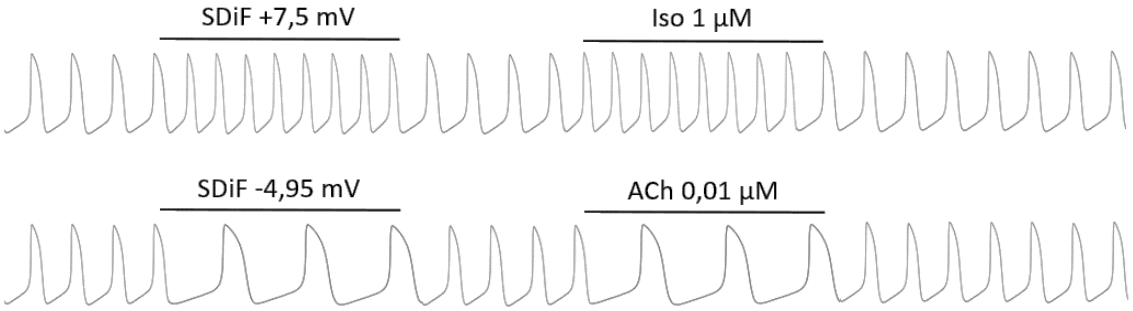

Fig. 47. Isoprenaline/Acetilcholine protocols. (1) Control conditions; (2) SDiF model current injection (isoprenaline: +7.5 mV shift; acetylcholine: -4.95 mV shift); (3) control condition; (4) drug perfusion (Iso 1 µM; ACh 0.01 µM); (5) control conditions.

Data processing and statistical analysis

Recorded traces for voltage and injected current were subject to 10-Points digital smoothing to remove residual noise effects.

AP recordings were undersampled from 2 KHz to 500 Hz and exported in ASCII format for use on custom software used to calculate pacemaking rate, MDP and the EDD slope.

For each protocol the average values of the described parameters were calculated in different experimental conditions (control, current injection, drug application, etc.) and analyzed with the ANOVA test for repeated measures (Geisser-Greenhouse adjustment) and Tukey-Kramer test for multiple comparisons (NCSS 2007, Kaysville, Utah).

All data results are reported as Mean ± Standard Deviation (SD).

5.3. RESULTS

Preliminary results on IVA Protocol

Preliminary dynamic-clamp experiments were carried out in order to understand which between the Severi/DiFrancesco (SDiF) and Maltsev/Lakatta (ML) mathematic models is more accurate to describe the electrical activity of SAN cells. Spontaneous activity of rabbit sinoatrial myocytes was recorded in control condition and then ivabradine 3 µM was perfused; ivabradine caused a significant rate reduction of 20.6% ($P < 0.05$) from 2.77 ± 0.38 Hz (control condition) to 2.20 ± 0.17 Hz (Iva), in agreement with values reported in the literature (-23.8 ± 3.9, Thollon et al 1994, -16.2 ± 1.5, Bucchi et al. 2007 a).

The I_f conductance was scaled up by 66% of the nominal value and injected into the cell so to compensate for the non-total channel block caused by ivabradine (-65.9 ± 2.4%, Bucchi et al., 2002). The injection of this SDiF66 synthetic current increased the average pacemaking rate from the ivabradine level to almost the control value (2.70 ± 0.27, not significantly different form control), whereas the injection of ML66 current only induced a smaller recovery (2.39 ± 0.30, $P < 0.05$ significantly different from control), **fig. 48**.

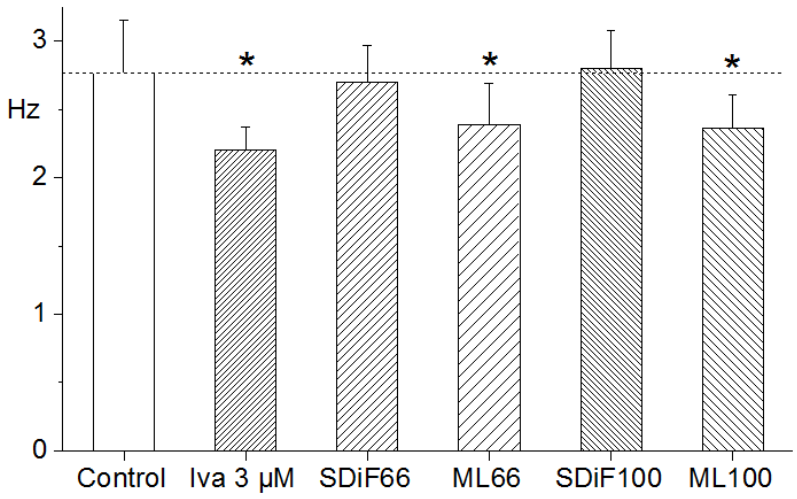

Figure 48. Mean pacemaking rate in control condition, during Iva 3 µM perfusion, and after injection of SDiF66, ML66, SDiF100, ML100 synthetic current (n=9). Mean ± SD, *, $P < 0.05$ vs. control.

We performed an additional test using 100% of I_f conductance, equivalent to the injection of the total calculated synthetic I_f current. Injection of SDiF100 synthetic current also restored the control pacemaking rate (2.80 ± 0.28, not significant different from control), while injection of ML100 synthetic current produced a lower increment (2.36 ± 0.25, $P < 0.05$ significantly different from control).

Based on these results, we choose to adopt the SDiF model as the mathematical basis for shift calculations in the Iso/ACh experiments.

Rate-adaption of Dynamic Clamp for cell-specific experiments

Preliminary experiments with the ACh protocol showed in some cells a rapid hyperpolarization and an excessive rate reduction after the injection of the synthetic current ΔI_f. This caused the complete inhibition of pacemaking in some cases; we defined this cell behaviour "unstable" (**fig. 49**).

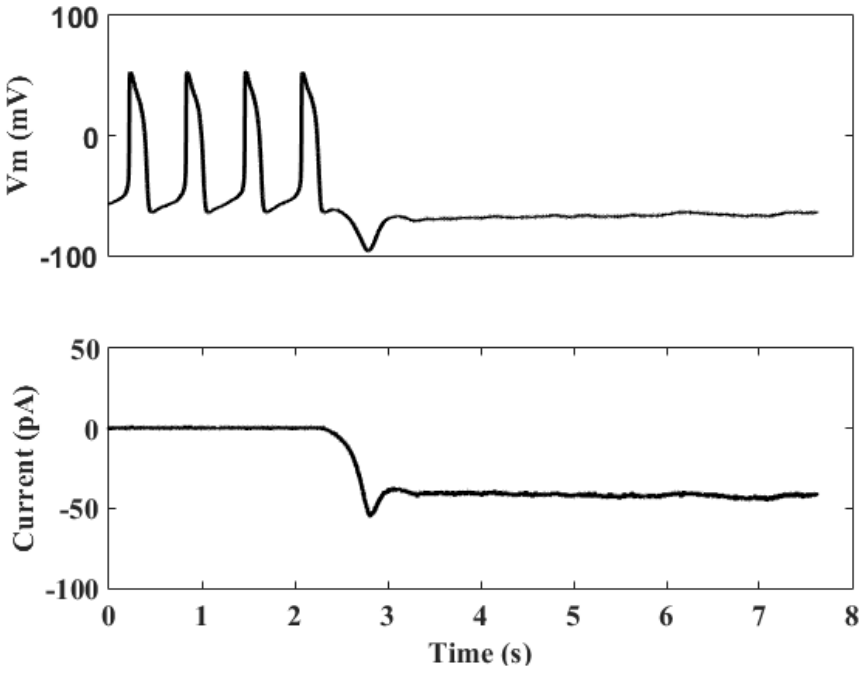

Figure 49. Negative shift induced by ACh protocol produced a complete block of spontaneous activity in "unstable" cells. Effect of synthetic negative shift on the potential (top) and current (bottom).

To better tune our mode we introduced an additional scaling factor which was computed based on evidence that it is possible (for a reasonable frequency range) to map the relation between maximum I_f conductance (gf) and the pacemaking frequency. The scaling factor was used to calculate the output synthetic current. At the beginning of each test the program measured control cycle length (CL) and return a proportional g-scale factor that was used to calculate the cell-specific conductance of the I_f current (**fig. 50**).

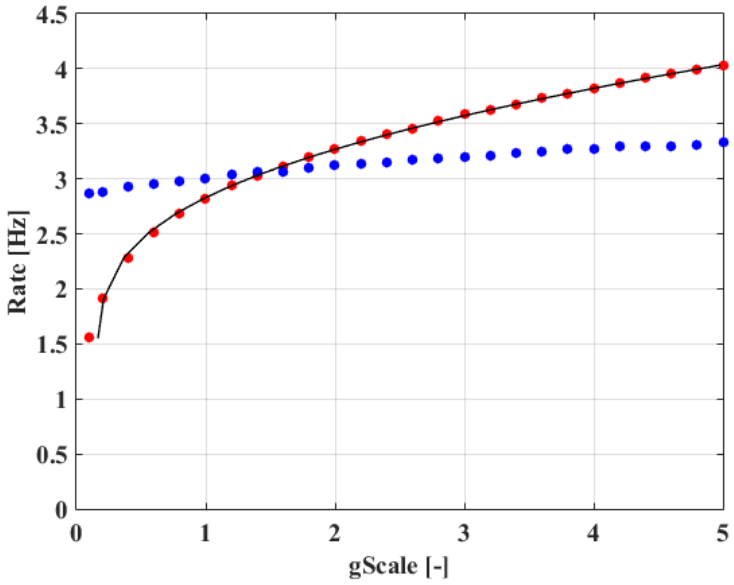

Figure 50. Effect of I_f conductance scaling on SDiF and ML model pacemaking rate. Behavior of the SDiF model (red points) was fitted with an empirical equation to obtain a scaling computation equation (black line). Behavior of the ML model is also reported (blue points)

Ivabradine results

The data obtained with the rate-adapted DC after perfusion of Ivabradine were fully consistent with the preliminary ones. The application of Iva 3 µM significantly reduced the pacemaking rate (**fig. 51, left**), which was completely restored by the injection of the SDiF66 synthetic current, while the injection of the ML66 current did not produce significant rate recovery.
We then analysed the slope of the early diastolic depolarization (EDD) and verified that it was restored by injecting the SDiF66 and SDiF100 current, whereas ML66 and ML100 did not elicit significant differences (**fig. 51, right**). No significant differences were also found among the MDPs of all groups.

Even though differences in the TOP values were statistically significant, it can be noticed from **table 5** that they are very small in amplitude (always less than 2 mV).

Group	Rate [Hz]	MDP (mV)	EDD (mV/ms)	TOP (mV)
Control	2.91 ± 0.37	-64.6 ± 2.4	0.0737 ± 0.0215	-45.1 ± 3.6
IVA	2.34 ± 0.37 ***	-64.0 ± 2.6	0.0418 ± 0.0127 ***	-45.9 ± 4.5
SDif66	2.76 ± 0.34	-63.7 ± 2.5	0.0706 ± 0.0103	-43.9 ± 4.0 **
SDif100	2.87 ± 0.36	-63.5 ± 2.3	0.0795 ± 0.0133	-44.0 ± 3.6 **
ML66	2.40 ± 0.34 ***	-64.1 ± 2.1	0.0464 ± 0.0122 ***	-45.6 ± 4.2
ML100	2.46 ± 0.35 ***	-64.0 ± 2.3	0.0478 ± 0.0125 ***	-45.5 ± 3.9

Table 5. Numeric results for the IVA experiment. ***, P < 0.001; **, P < 0.01.

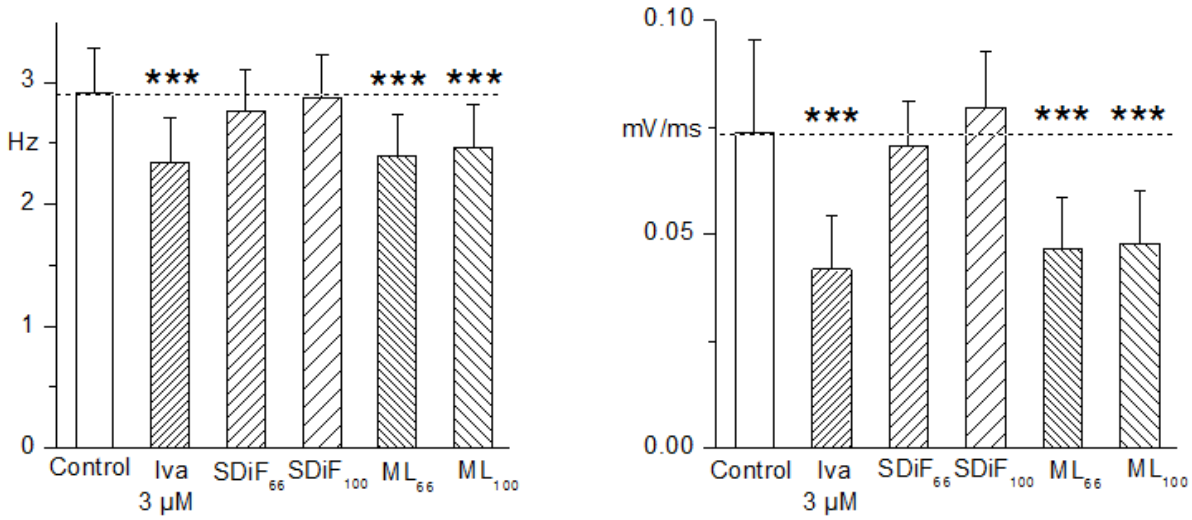

Figure 51. Effects of IVA protocol on pacemaking rate and EDD. Left, The reduction induced by IVA 3 µM was completely restored by injection of synthetic current using both SDiF66 and SDiF100 model. Whereas the ML66 and ML100 models were not able to restore the original rate. Right, the effect of DC models on EDD reflected the results on the rate. *** P < 0.001 vs. control; n = 7.

In **fig. 52** a representative time course of rate (left) and sample APs traces (right, top) are shown. The perfusion of Iva 3 µM caused a rate-reduction that was completely restored by SDiF66 but not by MF 66 synthetic current injection. The superimposition of the APs traces (black: control;

gray: Iva; green: SDiF66; blue: ML66) indicates the reduction of the steepness of EDD induced by Iva and the restore produced only by SDiF model.

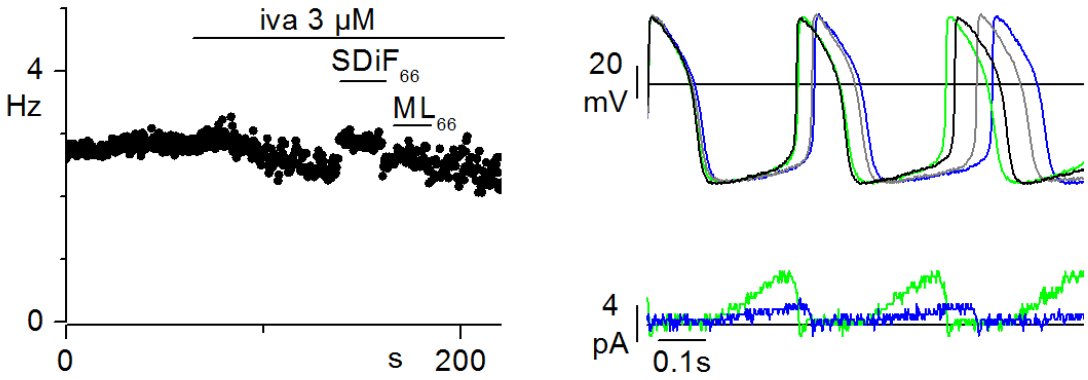

Figure 52. Example of IVA protocol on APs. Left, time course of the rate during different phases of the IVA experiment. Right upper, superimposed AP traces for control (black), ivabradine (gray), SDiF66 model (green), and ML66 model (blue). Right lower, corresponding current injection traces.

Isoprenaline results

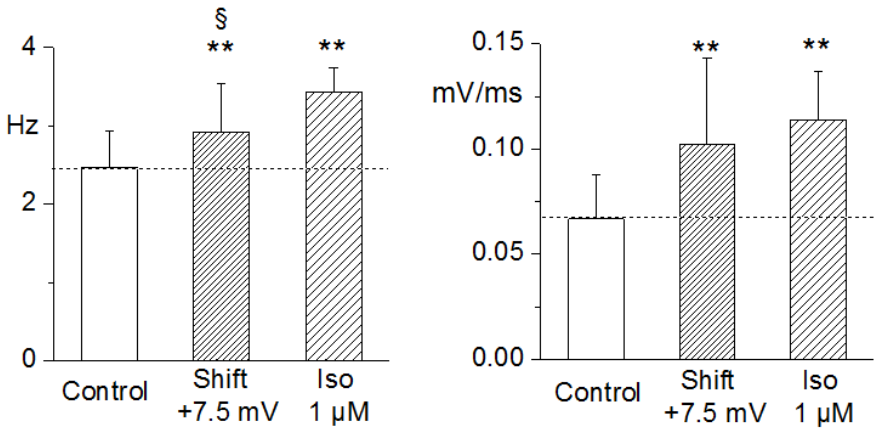

Figure 53. Effects of Iso protocol on pacemaking rate and EDD. Variations of pacemaking rate (left) and EDD (right) induced by injection of synthetic current (positive shift), and isoprenaline perfusion. ** $P < 0.01$ vs. control; § $P < 0.01$ vs. Iso; $n = 6$.

Group	Rate (Hz)	MDP (mV)	DD1 (mV/ms)	TOP (mV)
Control	2.46 ± 0.47	-64.8 ± 3.0	0.0666 ± 0.0209	-44.5 ± 5.2
Shift +7.5 mV	2.92 ± 0.62 ** §	-64.1 ± 3.3	0.102 ± 0.041 **	-42.7 ± 5.5
Iso 1 µM	3.43 ± 0.31 **	-63.9 ± 3.3	0.114 ± 0.023 **	-45.7 ± 5.3

Table 6. Numeric results for the Iso experiments. ** P < 0.01 vs. control; § P < 0.01 vs. Iso

We then proceeded to verify whether the SDiF model could reproduce the effect of isoprenaline stimulation of cell rate. In particular using the SDiF model we calculated the synthetic I_f current predicted by the model based on an isoprenaline-induced shift of the I_f current by +7.5 mV. This injection led to a significant increment of 18.7% of the pacemaking rate (P < 0.01 vs. control), **fig. 53**. This rate increase was compared with the real one obtained by perfusing the cell with Iso 1 µM and the acceleration of AP rate was 34.9% (P < 0.01 vs. control). The pacemaking rate during current injection was significantly different from control, but it was also significantly different from the value under real Iso drug (P < 0.01).

MDP was statistically different between two groups (P < 0.05) but the maximum difference is less than 1 mV. During the application of either SDiF synthetic current and real Iso, an increase in EDD was observed (P < 0.01), but no significant difference between the two conditions were found, **fig. 53**. During Iso perfusion, TOP was more negative than after synthetic current injection (P < 0.01).

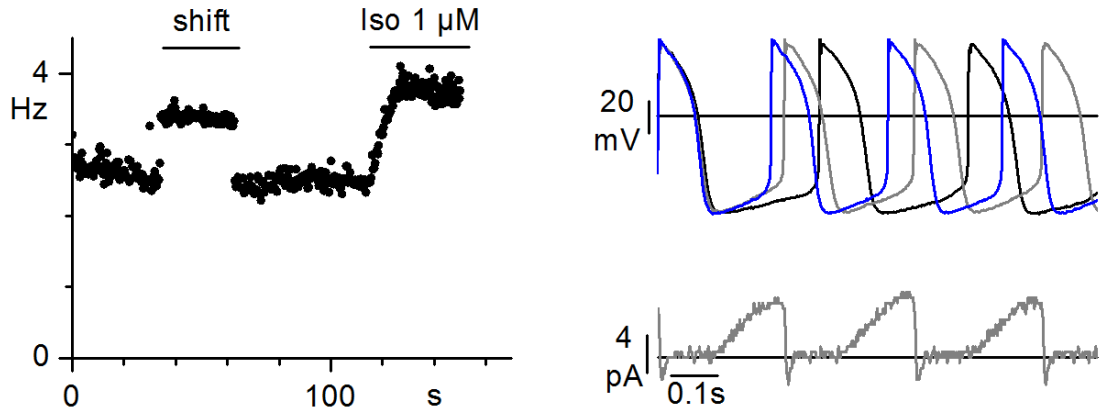

Figure 54. Example of Iso protocol on APs. Left, time course of the rate during different phases of the Iso experiment. Right upper, superimposed AP traces for control (black), shift +7.5 mV (gray), and isoprenaline (blue). Right lower, corresponding current injection traces.

Time course of rate (**fig. 54**) indicates a lower effect induced by synthetic current than real application of Iso. The AP traces superimposition allows to appreciate the increment of EDD steepness induced by both SDiF model current and Iso 1 µM.

Acetylcholine results

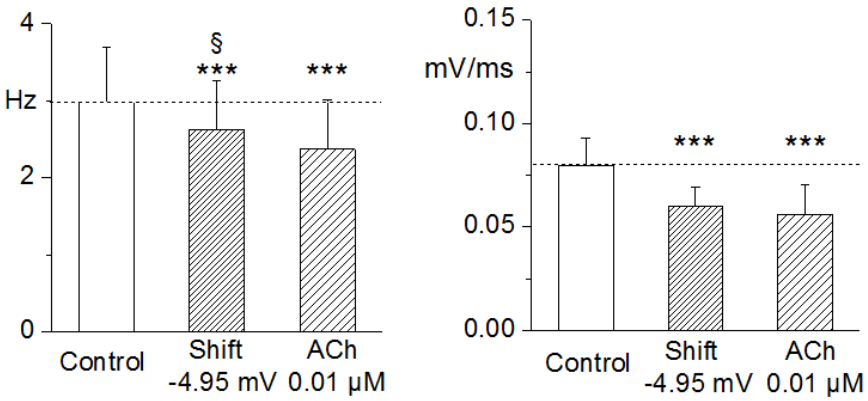

Figure 55. Effects of ACh protocol on pacemaking rate and EDD. Variations of pacemaking rate (left) and EDD (right) induced by injection of synthetic current (negative shift), and acetylcholine perfusion. *** P < 0.001 vs. control; § P < 0.05 vs. ACh; n = 6.

Group	Rate (Hz)	MDP (mV)	DD1 (mV/ms)	TOP (mV)
Control	2.98 ± 0.72	-62.6 ± 3.9	0.0795 ± 0.0135	-41.9 ± 2.6
Shift -4.95 mV	2.62 ± 0.64 *** §	-63.2 ± 3.7	0.0599 ± 0.0095 **	-43.0 ± 3.0
ACh	2.37 ± 0.64 ***	-62.7 ± 4.3	0.0560 ± 0.0141 **	-41.2 ± 3.7

Table 7. Numeric results for the ACh experiments. *** P < 0.001 vs. control; § P < 0.05 vs. Ach

Similar experiments as those described for Iso were also performed to study the effect of ACh modulation of rate mediated by modulation of the I_f current. The injection of the synthetic acetylcholine shift (-4.5 mV) simulated with the SDiF model led to a rate reduction of 12.1%, whereas the perfusion of real ACh produced a higher slowing effect (-20.2%) comparable with reported literature values (20.8 ± 3.2 %, Bucchi et al., 2007 a). The pacemaking rate during

current injection was significantly different both from control and from the value under real ACh drug ($P < 0.05$), **fig. 55**.

A reduction in EDD was observed between control value and SDiF synthetic current ($P < 0.001$). EDD also decreased when real ACh was applied ($P < 0.001$ vs. control) with no significant difference between the two conditions, **fig. 55**. No significant difference was found between groups in MDP and TOP.

Time course of the rate (**fig. 56**) indicates a lower effect induced by synthetic current than real application of ACh. The AP traces superimposition allows to appreciate the decrease of EDD steepness induced by both SDiF model current and ACh 0.01 µM.

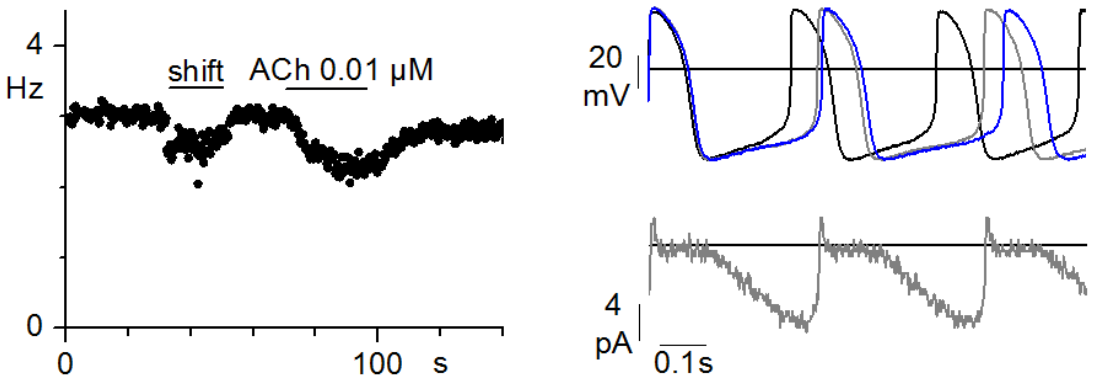

Figure 56. Example of ACh protocol on APs. Left, time course of the rate during different phases of the ACh experiment. Right upper, superimposed AP traces for control (black), shift -4.5 mV (gray), and acetylcholine (blue). Right lower, corresponding current injection traces.

6. DISCUSSION

During my Ph.D. I investigated the physiopathologic and pharmacologic role of the I_f current in the sinoatrial node region. I carried out three separate type of experiments: 1) pharmacological control of the current operated by a drug used in the traditional Chinese medicine, 2) analysis of the effect of a HCN4 channel mutation associated with IST, and 3) use of the dynamic-clamp approach to evaluate the quantitative contribution of the current.

My experiments confirm through independent and separate approaches that any alteration of the amount of the I_f current flowing during the diastolic depolarization leads to robust effect on automaticity of the SA node.
Although the results have been presented according to the chronological order of experiments during my Ph.D. here I prefer to discuss these data in a more logic order. I will start from the dynamic clamp experiments since they shed light on the physiological quantitative aspects of the current contribution to SA nide activity, and I will then discuss the patho-genetic finding and the pharmacological modulation.

Using an indirect approach based on mathematical models of SA node action potential, we studied the contribution of I_f current in the pacemaking. In the last years many models that describe the electrical behavior of SA node AP cells have been developed; among these models we chose to compare the models developed by Maltsev & Lakatta (2009) and by Severi-DiFrancesco (2012) with the dynamic-clamp approach. The ML model is based on the implementation of the interactions between intracellular calcium handling and membrane currents while the Severi-DiFrancesco formulation places a stronger focus on the role of the I_f current. So these two models attempt to describe the SA node automaticity although they place a different quantitative contribution to the I_f current. The SDiF model is associated with a higher contribution of I_f current during the diastolic depolarization, while the ML formulation leads to a smaller role of I_f in this phase. The experiments were therefore carried out with the specific aim to evaluate which of this model performs better since the dynamic-clamp approach allows to estimate amount of the I_f current flowing in a SAN cell as predicted by each of the two models. We then experimentally modified the real current by means of ivabradine and

substituted the delta current induced by this agent with synthetic currents calculated from the models. The synthetic delta currents were theoretically calculated from the models, but they were really injected into the cells to substitute for the currents variations induced by ivabradine. The synthetic current (SDiF or ML) that more properly compensate for ivabradine induced current reduction and therefore restores proper cell pacemaker rate (i.e the rate before agents were delivered) will therefore define which of the two models is more quantitative correct in identifying the amount of I_f flowing during diastole.

We used used ivabradine (3 μM) which should block about 66% of the physiological I_f current in rabbit sinoatrial node cells (Bucchi et al., 2002).

Results of the injection of synthetic currents show that the SDiF synthetic current is able to restore the original pacemaking rate of the cells, while the ML-based current not.

These data confirm the importance of the I_f current (and HCN channels) in SA node region, and validate the SDiF model thus suggesting that its quantitative formulation of the I_f current is appropriate.

Once the SDiF model was validated we moved to investigate the importance of I_f current in autonomic modulation by repeated the same protocol approach this time using isoprenaline as the mechanism causing I_f changes.

The injection of SDiF synthetic current miming the positive shift induced by isoprenaline 1 μM on I_f current, causes a +18.7% increase in pacemaking rate versus +39.4% effect observed during real isoprenaline administration. We interpreted this result considering that real isoprenaline affects other ionic current in addition to I_f, while our protocols only reproduce the effects on pacemaker current. This interpretation is confirmed by analysis of EDD (**fig. 53**), where no differences in the steepness are observed between real Iso and synthetic current injection, underlying that their effect on EDD is the same. This is in accordance with the work of Bucchi and colleagues (Bucchi et al., 2007 a) where it is demonstrated that the I_f current is responsible for pacemaking rate modulation in the EDD phase, while in late diastolic depolarization other mechanisms are involved.

Similar results were obtained during acetylcholine experiments, where the rate reduction induced by synthetic current is lower than the one produced by real drug (-12.1% vs. -20.2). No differences in EDD steepness were observed in either the conditions, confirming the main contribution of I_f to this phase (**fig. 55**).

Given the importance of the I_f current in the pacemaker process, it is important to study how mutations in HCN4 channel alter the I_f contribution in cardiac rate. Mutations on HCN channels

have long been associated with arrhythmogenic conditions; however, until today, all these mutations are of the loss-of-function type and are associated with bradycardia (Milanesi et al., 2015; Verkerk et al., 2015; DiFrancesco, 2015).
We found family members affected by inappropriate sinus tachycardia (IST), carrying the mutation R524Q. IST is a syndrome that causes unexpectedly fast sinus rate at rest, with minimal or no physical activity. The spectrum of symptoms of IST includes palpitations, weakness, fatigue, dizziness, or syncope (Olshansky et al., 2013).

IST is not defined by a specific heart rate, but patients generally have resting daytime sinus rates of more than 100 bpm and average 24-h heart rates of more than 90 bpm, that are not caused by physiologic demands or conditions known commonly to increase heart rate.

In IST no one therapy reduces heart rate and symptoms in complete and efficient manner; β-adrenergic blockers, even at high doses, generally are ineffective and tend to be associated with other symptoms. Other treatments (i.e. fludrocortisone, volume expansion, pressure stockings, phenobarbital, clonidine, psychiatric evaluation, and erythropoietin) have been suggested, but may be harmful and have not been proven (Still et al., 2002). Furthermore, patients resistant to conventional treatments respond successfully to ivabradine, a specific inhibitor of the I_f current (Cappato et al., 2012; Calo et al., 2010; Romeo et al., 2011; Zellerhoff et al., 2010; Femenia et al., 2012).

No specific channelopathy implicated in IST have been described before my study; indeed here I report the first evidence of a heterozygous gain-of-function mutation in the HCN4 channel associated with IST.

The position of the HCN4 mutation is crucial for the biophysical properties of the channel. Residue R524Q is located in the first α-helix (A') of the C-linker, a stretch of 81 residues connecting the cytoplasmic end of the S6 segment to the CNBD. This region acquired large importance since functional studies of mHCN2 channels have shown that C-linkers is involved in the cAMP-induced modulation (Zagotta et al., 2003; Craven et al., 2004; Craven et al., 2008). The mutation R524Q causes the substitution of the positively charged arginine with the polar, uncharged glutamine in the residue 524, and it is involved in the change of electrical charge distribution in the C-linker.

No differences in the intrinsic voltage-dependence of channel activation were observed between R524Q and wild-type channels. cAMP sensitivity was instead different: the dose-response curves for cAMP induced shift of the activation curves show that the half-maximal cAMP concentration decreased of about 4.6-fold (from 1.67 to 0.35 μM) in heterozygous wt-R524Q, and of more than 20-fold (from 1.67 to 0.08 μM) in homozygous R524Q mutant channels when compared to WT channels (1.67 μM).
Our data show an increment of cAMP sensitivity in the R524Q mutated channels, that results in a right shift of the activation curve, miming the effect of β-adrenergic stimulation.
In according to the results observed in HEK cells, newborn ventricular myocytes show a faster pacemaking rate when transfected with mutant rather than wild-type channels.

Our study represents the first evidence of a gain-of-function mutation in hHCN4 associated with IST, because it generates a condition where the pacemaker channel is in a permanent state of higher activation than normal channel, resulting in an increment of cardiac pacemaking. Our results allow to explain the faster intrinsic heart rate and the hypersensitivity to sympathetic stimulation, conditions tipical of IST. Finally, the data also explain the efficacy of the ivabradine treatment of IST condition observed during clinical practice.

The pharmacological research of agents able to reduce sinus heart rate has a strong interest for the treatment of ischemic heart disease, because myocardial ischemia represents one of the most common cause of death in the Western world and determines high morbidity, due to irreversible myocardial damage, produced by an imbalance between oxygen supply and demand.
The classical pharmacological approach to reduce heart rate is the use of β-blockers which are a class of agent able to antagonize the effect of adrenergic stimuli on β-receptors. Unfortunately, in addition to the desired bradycardic effects these agents also have several undesired side effects on the cardiovascular system and therefore in some cases are not tolerated by the patients. To overcome this limitation in the course of the years there has been an intense investigation aiming at identifying novel

Pharmacological agents able to specifically act only on SAN rate: these class of substances has been named “specific bradycardic agents” (Kobinger & Lillie, 1987). To date ivabradine is the sole specific bradycardic agent the has reached the clinic; ivabradine is a specific blocker of the I_f current and as such it modulates the steepness of the diastolic depolarization in SA node

myocytes, without altering action potential duration or causing negative inotropy (DiFrancesco & Borer, 2007).

Recently several compounds of TCM have acquired importance in the Western world for their therapeutic properties. For example, berberine (JKL1073A) and Wenxin Keli have important cardiovascular effects in the treatment of cardiac arrhythmias (Chiou et al., 1991; Bova et al., 1992; Chi et al., 1996; Burashnikov et al., 2012).

In this research project, we investigated TMYX drug, currently used in China for the treatment of cardiac disease, like cardiac regulator of both brady- and tachy-cardia. TMYX is a mixture of different substances amongst which liquorice. Liquorice derives from root extract of Glycyrrhiza glabra, a perennial herb cultivated in temperate and subtropical regions. Since ancient times, liquorice roots were used in traditional herbal medicine for the treatment of many disease (Armanini et al., 2002; Fiore et al., 2005). Only in the last 25 years the effects of Glycyrrhiza compounds have been scientifically investigated, confirming the knowledge acquired during history; for example liquorice constituents exhibit several biological and endocrine properties including anti-inflammatory (cortisol-like), antihepatotoxic, antibacterial, antiviral, and anticancer effects (Aly et al., 2005; Lee et al., 2009; Fiore et al., 2008; Hibasami et al., 2005); in addition they possess cardioprotective properties and modulate cardiac performance in Langendorff perfused rat heart, increasing heart rate (Parisella et al., 2012).

Our experiments show that TMYX acts as a dose-dependent rate-lowering agent in rabbit SA node cells. Based on the dose-response curve of the rate (**fig. 26**), I intend focus the discussion on the 2 mg/ml concentration because it produces a rate reduction similar to that caused by ivabradine 3 µM (23.6% vs. 24%, Bucchi et al., 2007 a), a bradycardic agent recently approved by European Evaluation Agency in the treatment of angina pectoris and heart failure (Borer et al., 2003; Swedberg et al., 2010).

At this concentration the prolongation of APD50, an important parameter to verify the safety of bradycardic agent (Thollon et al., 1994; Bois et al., 1996; Savelieva et al., 2006), is 6.5%, a value lower than ivabradine (8.9%, Thollon et al., 1994). At higher concentrations, for example 6 mg/ml, the prolongation of APD50 (+24.7%) combined with the strong reduction of the rate (-51.6%), produces a strongly arrhythmogenic substrate. Indeed it is known that ventricular tachyarrhythmia (torsades de pointes) occurs more frequently when the cardiac rate is slow and the duration of action potential is prolonged (Damiano & Rosen, 1984).

At first we demonstrated that percentage of bradycardic effect produced by TMYX is independent from cardiac rate and therefore no use-dependence is present (**fig. 30**).

Furthermore, the TMYX-dependent rate reduction is not influenced by autonomic modulators (isoprenaline and acetylcholine); this finding therefore suggests that TMYX and the neuro-modulators act with two different mechanisms.

The EDD reduction observed during current-clamp experiments suggests an effect of TMYX on I_f current. Interestingly, at the 2 mg/ml concentration (where the rate reduction is similar between TMYX and ivabradine) the blockade on the I_f current induced by TMYX results lower (20.9%) than ivabradine (~60%) (Bucchi et al., 2007 b).

The patch-clamp experiments on the I_f current show a dual effect induced by TMYX (**fig. 31**), a left shift of the activation curve and an enhancement of the current at the higher (not physiological) potential. In fact the activation curve and I/V function combined curve (that is the strady-state IV curve) suggests that at physiological potentials ≤ -80 mV, the contribution of the shift induced by TMYX is greater than the increment of the conductance, and leads to a reduction of current amplitude respect to the control condition.

Single cell electrophysiological data were then complemented by experiments on freely-moving mice implanted with an ECG transmitter.

Preliminary experiments surprisingly show an increment of heart rate after the i.p. injection of TMYX; however when TMYX was delivered during pharmacological blockade of only sympathetic or both sympathetic and parasympathetic autonomic system branches we observed a deep bradycardia.

These data thus confirm that when intrinsic heart rate is considered (i.e. during autonomic block) the pacemaking reduction observed is in agreement with data obtained *in-vitro*.

The increase in rate observed in intact animals is still unexplained. At first one could argue that increase of heart rate could be caused by the baroreflex, although this is possible, it remains obscure why in in-vitro experiments maximal adrenergic activation obtained by 10 μM isoprenaline in the presence of TMYX does not produce a net tachycardic action, although it partly reverses the bradycardic action of the drug.

7. BIBLIOGRAPHY

Accili EA, Proenza C, Baruscotti M, DiFrancesco D (2002)
From funny current to HCN channels: 20 years of excitation.
News Physiol Sci;17:32-7.

Altomare C, Bucchi A, Camatini E, Baruscotti M, Viscomi C, Moroni A, DiFrancesco D (2001)
Integrated allosteric model of voltage gating of HCN channels.
J Gen Physiol;117(6):519-32.

Altomare C, Terragni B, Brioschi C, Milanesi R, Pagliuca C, Viscomi C, Moroni A, Baruscotti M, DiFrancesco D (2003)
Heteromeric HCN1-HCN4 channels: a comparison with native pacemaker channels from the rabbit sinoatrial node.
J Physiol;549(Pt 2):347-59. Epub 2003 Apr 17.

Aly A, Al-Alousi L, Salem HA (2005)
Licorice: A possible anti-inflammatory and anti-ulcer drug
AAPS PharmSciTech. Volume 6, Issue 1, pp E74-E82

Anderson NH, Devlin AM, Graham D, Morton JJ, Hamilton CA, Reid JL, Schork NJ, Dominiczak AF (1993)
Telemetry for cardiovascular monitoring in a pharmalogical study: new approaches to data analysis.
Hypertension;33(1 Pt 2):248-55.

Anderson RG (1998).
The caveolae membrane system.
Annu. Rev. Biochem. 67: 199–225.

Anumonwo JM, Delmar M, Jalife J (1990)
Electrophysiology of single heart cells from the rabbit tricuspid valve.
J Physiol (Lond);425:145-167

Armanini D, Fiore C, Mattarello MJ, Bielenberg J, Palermo M (2002)
History of the endocrine effects of licorice.
Exp Clin Endocrinol Diabetes;110(6):257-61.

Arras M, Rettich A, Cinelli P, Kasermann HP, Burki K (2007)

Assessment of post-laparotomy pain in laboratory mice by telemetric recording of heart rate and heart rate variability.
BMC. Vet. Res. 3, 16

Barbuti A, Gravante B, Riolfo M, Milanesi R, Terragni B, DiFrancesco D (2004)
Localization of pacemaker channels in lipid rafts regulates channel kinetics.
Circ Res;94(10):1325-31. Epub 2004 Apr 8.

Barbuti A, Terragni B, Brioschi C, DiFrancesco D (2007)
Localization of f-channels to caveolae mediates specific β2-adrenergic receptor modulation of rate in sinoatrial myocytes.
J. Mol. Cell Cardiol. 42:71–78

Baruscotti M, Bucchi A, DiFrancesco D (2005)
Physiology and pharmacology of the cardiac pacemaker (‘‘funny’’) current.
Pharmacol Ther, 107:59-79

Baruscotti M, Bucchi A, Viscomi C, Mandelli G, Consalez G, Gnecchi-Rusconi T, Montano N, Casali KR, Micheloni S, Barbuti A, DiFrancesco D (2011)
Deep bradychardia and heart block caused by inducible cardiac-specific knockout of the pacemaker channel gene Hcn4.
Proc Natl Acad Sci U S A.;108(4):1705-10. doi: 10.1073/pnas.1010122108

Bensky D, Barolet R (1990)
Formulas and Strategies.

Bensky D. Gamble A. Kaptchuk TJ (1993)
Chinese herbal medicine: materia medica.

Bois P, Bescond J, Renaudon B, Lenfant J (1996)
Mode of action of bradycardic agent, S 16257, on ionic currents of rabbit sinoatrial node cells.
Br J Pharmacol, 118:1051-1057.

Borer JS, Fox K, Jaillon P, Lerebours G, ivabradine Investigators Group (2003)
Antianginal and antiischemic effects of ivabradine, an If inhibitor, in stable angina: a randomized, double-blind, multicentered, placebo-controlled trial.
Circulation, 107:817-823.

BoSmith RE, Briggs I, Sturgess NC (1993)

Inhibitory actions of ZENECA ZD7288 on whole-cell hyperpolarization activated inward current (If) in guinea-pig dissociated sinoatrial node cells.
Br J Pharmacol, 110:343-349

Bova S, Padrini R, Goldman WF, Berman DM, Cargnelli G (1992)
On the mechanism of vasodilating action of berberine: possible role of inositol lipid signaling system.
JPET vol. 261 no. 1318-323

Briggs I, Heapy CG (1992)
Actions of ICI D7288 on sino-atrial node cellular electrophysiology: action potentials.
Br J Pharmacol, 107:382P

Brodde OE, Leifert FJ, Krehl HJ (1982).
Coexistence of beta 1- and beta 2-adrenoceptors in the rabbit heart: quantitative analysis of the regional distribution by (-)-3H-dihydroalprenolol binding.
J. Cardiovasc. Pharmacol. 4: 34–43.

Brodde OE, Bruck H, Leineweber K, Seyfarth T (2001).
Presence, distribution and physiological function of adrenergic and muscarinic receptor subtypes in the human heart.
Basic Res. Cardiol. 96: 528–538

Brown HF, DiFrancesco D, Noble SJ (1979)
How does adrenaline accelerate the heart?
Nature; 280:235-236

Brown HF, DiFrancesco D (1980)
Voltage clamp investigations of membrane currents underlying pacemaker activity in rabbit sino-atrial node.
J Physiol (Lond); 308:331-351.

Bucchi A, Baruscotti M, DiFrancesco D (2002)
Current-dependent block of rabbit sino-atrial node If channels by ivabradine.
J Gen Physiol, 120:1-13

Bucchi A, Baruscotti M, Robinson RB, DiFrancesco D (2007) a
I(f)-dependent modulation of pacemaker rate mediated by cAMP in the presence of ryanodine on rabbit sinoatrial node cells.
J Mol Cell Cardiol.;35(8):905-13.

Bucchi A, Baruscotti M, Robinson RB, DiFrancesco C (2007) b
Modulation of rate by autonomic agonists in SAN cells involves changes in diastolic depolarization and the pacemaker current.
J Mol Cell Cardiol.;43(1):39-48.

Burashnikov A, Petroski A, Hu D, Barajas-Martinez H, Antzelevitch C (2012)
Atrial-selective inhibition of sodium-channel current by Wenxin Keli is effective in suppressing atrial fibrillation.
Heart Rhythm, Volume 9, Issue 1, Pages 125–131

Calo L, Rebecchi M, Sette A, Martino A, de Ruvo E, Sciarra L, De Luca L, Zuccaro LM, Giunta G, Ciccaglioni A, Lioy E, Fedele F. (2010)
Efficacy of ivabradine administration in patients affected by inappropriate sinus tachycardia.
Heart Rhythm 2010;7(9):1318-23

Cappato R, Castelvecchio S, Ricci C, Bianco E, Vitali-Serdoz L, Gnecchi-Ruscone T, Pittalis M, De Ambroggi L, Baruscotti M, Gaeta M, Furlanello F, DiFrancesco D, Lupo PP (2012)
Clinical efficacy of Ivabradine in patients with inappropriate sinus tachycardia
J Am Coll Cardiol. 2012;60(15):1323-1329

Cerbai E, Pino R, Sartiani L, Mugelli A (1999)
Influence of postnatal development on I(f) occurrence and properties in neonatal rat ventricular myocytes.
Cardiovasc Res;42:416-423

Cerbai E, Mugelli A (2006)
I(f) in non-pacemaker cells: Role and pharmacological implications.
Pharmacol Res;53:416-423

Chen YJ, Chen SA, Chang MS, Lin CI (2000)
Arrhythmogenic activity of cardiac muscle in pulmonary veins of the dog: Implication for the genesis of atrial fibrillation.
Cardiovasc Res;48:265-273.

Chen YJ, Chen SA, Chen YC, Yeh HI, Chan P, Chang MS, Lin CI (2001) a
Effects of rapid atrial pacing on the arrhythmogenic activity of single cardiomyocytes from pulmonary veins: Implication in initiation of atrial fibrillation.
Circulation;104:2849-2854.

Chen J, Mitcheson JS, Tristani-Firouzi M, Lin M, Sanguinetti MC (2001) b
The S4-S5 linker couples voltage sensing and activation of pacemaker channels.

Proc Natl Acad Sci U S A;98(20):11277-82. Epub 2001 Sep 11.

Chi JF, Chu SH, Lee CS, Chou NK, Su MJ (1996)
Mechanical and electrophysiological effects of 8-oxoberberine (JKL1073A) on atrial tissue.
British Journal of Pharmacology Volume 118, Issue 3, pages 503–512

Chiou WF, Yen MH, Chen CF (1991)
Mechanism of vasodilatory effect of berberine in rat mesenteric artery.
European Journal of Pharmacology, 204, pp. 35–40

Craven KB, Zagotta WN. (2004)
Salt bridges and gating in the COOH-terminal region of HCN2 and CNGA1 channels.
J Gen Physiol;124(6):663-77.

Craven KB, Olivier NB, Zagotta WN. (2008)
C-terminal movement during gating in cyclic nucleotide-modulated channels.
J Biol Chem 2008;283(21):14728-38

Damiano BP, Rosen MR. (1984)
Effects of pacing on triggered activity induced by early afterdepolarizations.
Circulation;69(5):1013-25.

Del Monte F, Kaumann AJ, Poole-Wilson PA, Wynne DG, Pepper J, Harding SE (1993).
Coexistence of functioning β1- and β2-adrenoceptors in single myocytes from human ventricle.
Circulation 88: 854–863.

Demir SS, Clark JW, Murphey CR, Giles WR (1994)
A mathematical model of a rabbit sinoatrial node cell.
American Journal of Physiology - Cell Physiology. Vol. 266 no. 3, C832-C852

Deurs B, Roepstorff K, Hommelgaard AM, Sandvig K (2003).
Caveolae: anchored, multifunctional platforms in the lipid ocean.
Trends Cell Biol. 13: 92–100

DiFrancesco D, Ojeda C (1980)
Properties of the current if in the sinoatrial node of the rabbit compared with those of the current iK2 in Purkinje fibres.
J Physiol (Lond); 308:353-367

DiFrancesco D (1981) a

A study of the ionic nature of the pace-maker current in calf Purkinje fibres.
J Physiol (Lond); 314:377-393

DiFrancesco D (1981) b
A new interpretation of the pace-maker current in calf Purkinje fibres.
J Physiol (Lond); 314:359-376

DiFrancesco D, Noble SG (1984)
A model of sino-atrial node electrical activity based on a modification of the DiFrancesco-Noble (1984) equations.
Proc R Soc Lond B Biol Sci. 1984 Sep 22;222(1228):295-304.

DiFrancesco D, Noble D (1985)
A model of cardiac electrical activity incorporating ionic pumps and concentration changes.
Philos Trans R Soc Lond B Biol Sci. 307(1133):353-98.

DiFrancesco D, Ferroni A, Mazzanti M and Tromba C (1986) a
Properties of the hyperpolarizing-activated current (if) in cells isolated from the rabbit sino-atrial node.
The Journal of Physiology Volume 377, Issue 1, pages 61–88

DiFrancesco D (1986) b
Characterization of single pacemaker channels in cardiac sino-atrial node cells.
Nature; 324:470-473

DiFrancesco D, Tortora P (1991).
Direct activation of cardiac pacemaker channels by intracellular cyclic AMP.
Nature 351: 145–147

DiFrancesco D. (1993)
Pacemaker mechanisms in cardiac tissue.
Annu Rev Physiol 55: 451-467

DiFrancesco D, Mangoni M (1994)
Modulation of single hyperpolarization-activated channels (if) by cAMP in the rabbit sino-atrial node
Journal of Physiology. 474.3

DiFrancesco D. (1999)
Dual allosteric modulation of pacemaker (f) channels by cAMP and voltage in rabbit SA node.
J Physiol.1;515 (Pt 2):367-76.

DiFrancesco & Camm (2004).
Heart rate lowering by specific and selective I(f) current inhibition with ivabradine: a new therapeutic perspective in cardiovascular disease.
Drugs;64(16):1757-65.

DiFrancesco D, Borer JS. (2007)
The funny current: cellular basis for the control of heart rate.
Drugs.;67 Suppl 2:15-24.

DiFrancesco (2015)
HCN4, Sinus Bradycardia And Atrial Fibrillation.
Arrhythmia & Electrophysiology Review

D'Souza A*, Bucchi A*, Johnsen AB*, Logantha SJRJ*, Monfredi O, Yanni J, Prehar S, Hart G, Cartwright E, Wisloff U, Dobryznski H, DiFrancesco D, Morris GM, Boyett MR (2014)
Exercise training reduces resting heart rate via downregulation of the funny channel HCN4
Nature Communications; DOI: 10.1038

Femenia F, Baranchuk A, Morillo CA. (2012)
Inappropriate sinus tachycardia: current therapeutic options.
Cardiol Rev 2012;20(1):8-14

Fiore C, Eisenhut M, Ragazzi E, Zanchin G, Armanini D. (2005)
A history of the therapeutic use of liquorice in Europe.
J Ethnopharmacol;99(3):317-24. Review.

Fiore C, Eisenhut M, Krausse R, Ragazzi E, Pellati D, Armanini D, Bielenberg J. (2008)
Antiviral effects of Glycyrrhiza species.
Phytotherapy Research. Volume 22, Issue 2, pages 141–148

Frace AM, Maruoka F, Noma A (1992)
External K+ increases Na+ conductance of the hyperpolarization-activated current in rabbit cardiac pacemaker cells.
Pflugers Arch; 421(2-3):97-9.

Fung FY, Linn YC. (2015)
Developing traditional Chinese medicine in the era of evidence-based medicine:current evidences and challenges.
Evid Based Complement Alternat Med.;2015:425037

Gargini C, Demontis GC, Bisti S, Cervetto L (1999)
Effects of blocking the hyperpolarization-activated current (I(h)) on the cat electroretinogram.
Vision Res, 39:1767-1774

Gasparini S, DiFrancesco D (1997)
Action of the hyperpolarizationactivated current (Ih) blocker ZD 7288 in hippocampal CA1 neurons.
Pflugers Arch, 435:99-106

Goaillard JM, Marder E (2006)
Dynamic clamp analyses of cardiac, endocrine, and neural function.
Physiology (Bethesda). Jun;21:197-207

Goethals M, Raes A, Van Bogaert PP (1993)
Use-dependent block of the pacemaker current If in rabbit sinoatrial node cells by zatebradine (UL-FS 49): on the mode of action of sinus node inhibitors.
Circulation, 88:2389-2401

Gravante B, Barbuti A, Milanesi R, Zappi I, Viscomi C, DiFrancesco D (2004)
Interaction of the pacemaker channel HCN1 with filamin A.
J Biol Chem;279(42):43847-53. Epub 2004 Jul 30.

Greenwood IA & Prestwich SA (2002)
Characteristics of hyperpolarization activated cation currents in portal vein smooth muscle cells.
Am J Physiol-Cell Ph;282:C744-C753.

Harris NC, Constanti A (1995)
Mechanism of block by ZD 7288 of the hyperpolarization-activated inward rectifying current in guinea pig substantia nigra neurons in vitro.
J Neurophysiol, 74:2366-2378.

Hibasami H, Iwasw H, Yoshioka K, Takahashi (2005)
Glycyrrhizin induces apoptosis in human stomach cancer KATO III and Human promyelotic leukemia HL-60 cells.
International Journal of Molecular Medicine. Volume 16 Issue 2, pages: 233-236

Hille, B (2000).
Ionic channels of excitable membranes.
Sinauer Associates, Inc., Sunderland, MA.

Ishii TM, Takano M, Ohmori H (2001)

Determinants of activation kinetics in mammalian hyperpolarization-activated cation channels.
J Physiol;537(Pt 1):93-100.

Joyner RW, Sugiura H, Tan RC (1991)
Unidirectional block between isolated rabbit ventricular cells coupled by a variable resistance.
Biophys J 1991;60:1038–45.

Jurevicius J, Fischmeister R (1996).
cAMP compartmentation is responsible for a local activation of cardiac $Ca2^+$ channels by beta-adrenergic agonists.
Proc. Natl. Acad. Sci. USA 93: 295–299.

Jurevicius J, Skeberdis VA, Fischmeister R (2003).
Role of cyclic nucleotide phosphodiesterase isoforms in cAMP compartmentation following β2-adrenergic stimulation of ICa,L in frog ventricular myocytes.
J. Physiol. 551: 239–252

Kobinger W, Lillie C. (1987)
Specific bradycardic agents--a novel pharmacological class?
Eur Heart J. Suppl L:7-15.

Krahn AD, Yee R, Klein GJ, Morillo C (1995)
Inappropriate sinus tachycardia: evaluation and therapy.
J Cardiovasc Electrophysiol;6: 1124–8

Kramer K, van Acker SA, Voss HP, Grimbergen JA, van der Vijgh WJ, Bast A (1993)
Use of telemetry to record electrocardiogram and heart rate in freely moving mice.
J. Pharmacol. Toxicol. Methods. 30 209-215

Kramer K & Kinter LB (2003)
Evaluation and applications of radiotelemetry in small laboratory animals.
Physiol. Genomics. 13, 197-205.

Lakatta EG, DiFrancesco (2009)
What keeps us ticking: a funny current, a calcium clock, or both?
Journal of Molecular and Cellular Cardiology Volume 47, Issue 2, Pages 157–170

Lao L, Xu L, Xu S (2012)
Traditional Chinese Medicine.
Integrative Pediatric Oncology, pp 125-135

Lee JR, Park SJ, Lee HS, Jee SY, Seo J, Know YK, Know TK, Kim SC (2009)
Hepatoprotective Activity of Licorice Water Extract against Cadmium-Induced Toxicity in Rats.
Evidence-Based Complementary and Alternative Medicine. Volume 6, Issue 2, Pages 195-201

Levy FO, Zhu X, Kaumann AJ, Birnbaumer L (1993).
Efficacy of β1-adrenergic receptors is lower than that of β2-adrenergic receptors.
Proc. Natl. Acad. Sci. USA 90: 10798–10802.

Li S, Okamoto T, Chun M, Sargiacomo M, Casanova JE, Hansen SH, Nishimoto I, Lisanti MP (1995)
Evidence for a regulated interaction between heterotrimeric G proteins and caveolin.
J. Biol. Chem. 270: 15693–15701,4646.

Liu YW, Guo JH, Zhang P, Li C (2009)
The effects of nardostachys chinensis beta 1 extract on the sodium current and transient outward potassium current of rat ventricular myocytes.
Chin J Cardiac Paceing Electrophysiol;23:533–5.

Ludwig A, Zong X., Hofmann F, Biel M (1999).
Structure and function of cardiac pacemaker channels.
Cell Physiol Biochem. 9(4-5):179-86.

Maltsev VA, Lakatta EG (2009)
Synergism of coupled subsarcolemmal Ca^{2+} clocks and sarcolemmal voltage clocks confers robust and flexible pacemaker function in a novel pacemaker cell model
America Journal of Physiology. Vol. 296 no. 3, H594-H615

Mannikko R, Elinder F, Larsson HP (2002)
Voltage-sensing mechanism is conserved among ion channels gated by opposite voltages.
Nature 419, 837-841

Marrouche NF, Beheiry S, Tomassoni G (2002)
Three-dimensional nonfluoroscopic mapping and ablation of inappropriate sinus tachycardia. Procedural strategies and long-term outcome.
J Am Coll Cardiol; 39:1046 –54

Marshall PW, Rouse W, Briggs I, Hargreaves RB, Mills SD, McLoughlin BJ (1993)

ICI D7288, a novel sinoatrial node modulator.
J Cardiovasc Pharmacol, 21:902-906

Mattes A, Lemmer B (1991)
Effects of amlodipine on circadian rhythms in blood pressure, heart rate, and motility: a telemetric study in rats.
Chronobiol Int;8(6):526-38.

Matulef K, Flynn GE, Zagotta WN (1999)
Molecular rearrangements in the ligand-binding domain of cyclic nucleotide-gated channels.
Neuron;24(2):443-52.

McCormick DA, Pape HC (1990)
Noradrenergic and serotonergic modulation of a hyperpolarization-activated cation current in thalamic relay neurones.
J Physiol;431:319-42.

Milanesi R, Baruscotti M, Gnecchi-Ruscone T, DiFrancesco D (2006)
Familial sinus bradycardia associated with a mutation in the cardiac pacemaker channel.
N Engl J Med 2006;**354**(2):151-7.

Milanesi R, Bucchi A, Baruscotti M (2015)
The genetic basis for inherited forms of sinoatrial dysfunction and atrioventricular node dysfunction.
J Interv Card Electrophysiol

Moosmang S, Stieber J, Zong X, Biel M, Hofmann F, Ludwig A (2001)
Cellular expression and functional characterization of four hyperpolarization-activated pacemaker channels in cardiac and neuronal tissues.
Eur J Biochem;268(6):1646-52.

Moroni A, Barbuti A, Altomare C, Viscomi C, Morgan J, Baruscotti M, DiFrancesco D (2000)
Kinetic and ionic properties of the human HCN2 pacemaker channel.
Pflugers Arch;439(5):618-26.

Moroni A, Gorza L, Beltrame M, Gravante B, Vaccari T, Bianchi ME, Altomare C, Longhi R, Heurteaux C, Vitadello M, Malgaroli A, DiFrancesco D (2001)
Hyperpolarization-activated cyclic nucleotide-gated channel 1 is a molecular determinant of the cardiac pacemaker current I(f).
J Biol Chem.;276(31):29233-41. Epub 2001 Apr 27.

Noble D, DiFrancesco D, Denyer (1989)
Ionic Mechanisms in Normal and Abnormal Cardiac Pacemaker Activity.
Neuronal and Cellular Oscillators, pp. 59-85

Olshansky MD, Renee M, Sullivan MD (2013)
Inappropriate Sinus Tachycardia
Brian Journal of the American College of Cardiology Vol. 61, No. 8

Ono K, Ito H (1995)
Role of rapidly activating delayed rectifier K+ current in sinoatrial node pacemaker activity.
American Journal of Physiology - Heart and Circulatory Physiology Vol. 269 no. 2, H453-462

Pape HC (1996)
Queer current and pacemaker: the Hyperpolarization- Activated Cation Current in Neurons.
Annu Rev. Phyiol. 58:29%327

Parisella ML, Angelone T, Gattuso A, Cerra MC, Pellegrino D (2012)
Glycyrrhizin and glycyrrhetinic acid directly modulate rat cardiac performance.
J Nutr Biochem;23(1):69-75.

Parton RG (2003)
Caveolae–from ultrastructure to molecular mechanisms.
Nat. Rev. Mol. Cell Biol. 4: 162–167.

Perez-Lugones A, McMahon JT, Ratliff NB, Saliba WI, Schweikert RA, Marrouche NF, Saad EB, Navia JL, McCarthy PM, Tchou P, Gillinov AM, Natale A (2003)
Evidence of specialized conduction cells in human pulmonary veins of patients with atrial fibrillation.
J Cardiovasc Electrophysiol;14:803-809

Prinz AA, Abbott LF, Marder E (2004)
The dynamic clamp comes of age.
Neurosciences 2004;27(4):2218-224.

Qu J, Barbuti A, Protas L, Santoro B, Cohen IS, Robinson RB (2001)
HCN2 overexpression in newborn and adult ventricular myocytes: distinct effects on gating and excitability.
Circ Res;**89**(1):E8-14.

Qu J, Altomare C, Bucchi A, DiFrancesco D, Robinson RB (2002)
Functional comparison of HCN isoforms expressed in ventricular and HEK 293 cells.
Pflugers Arch;444(5):597-601. Epub 2002 Jun 12.

Rich TC, Fagan KA, Nakata H, Schaack J, Cooper DM, Karpen JW (2000).
Cyclic nucleotide-gated channels colocalize with adenylyl cyclase in regions of restricted cAMP diffusion.
J. Gen. Physiol. 116: 147–161.

Rich TC, Tse TE, Rohan JG, Schaack J, Karpen JW (2001).
In vivo assessment of local phosphodiesterase activity using tailored cyclic nucleotide-gated channels as cAMP sensors.
J. Gen. Physiol. 118: 63–78.

Robinson RB, Yu H, Chang F, Cohen IS (1997)
Developmental change in the voltage-dependence of the pacemaker current, if, in rat ventricle cells.
Pflug Arch Eur J Phy;433:533-535.

Rodefeld MD, Beau SL, Schuessler RB, Boineau JP, Saffitz JE (1996)
β-adrenergic and muscarinic cholinergic receptor densities in the human sinoatrial node: identification of a high β2-adrenergic receptor density.
J. Cardiovasc. Electrophysiol. 7: 1039–1049.

Romeo E, Grimaldi N, Sarubbi B, D'Alto M, Santarpia G, Scognamiglio G, Russo MG, Calabro R. (2011)
A pediatric case of cardiomyopathy induced by inappropriate sinus tachycardia: efficacy of ivabradine.
Pediatr Cardiol;32(6):842-5.

Rubenstein JC, Freher M, Kadish A, Goldberger JJ (2010)
Diurnal heart rate patterns in inappropriate sinus tachycardia.
Pacing Clin Electrophysiol; 33:911–9

Rybin VO, Xu X, Lisanti MP, Steinberg SF (2000)
Differential targeting of betaadrenergic receptor subtypes and adenylyl cyclase to cardiomyocyte caveolae. A mechanism to functionally regulate the cAMP signaling pathway.
J. Biol. Chem. 275: 41447–41457.

Santoro B, Tibbs GR (1999)
The HCN gene family: molecular basis of the hyperpolarization-activated pacemaker channels.
Ann N Y Acad Sci;868:741-64. Review.

Satoh H, Hashimoto K (1986)
Electrophysiological study of alinidine in voltage clamped rabbit sino-atrial node cells.
Eur J Pharmacol, 121:211-219.

Satoh TO, Yamada M (2002)
Multiple inhibitory effects of zatebradine (UL-FS 49) on the electrophysiological properties of retinal rod photoreceptors.
Pflugers Arch, 443:532-540.

Savelieva I, Camm AJ. (2006)
Novel If current inhibitor ivabradine: safety considerations.
Adv Cardiol;43:79-96. Review.

Schmitz-Spanke S, Granetzny A, Stoffels B, Pomblum VJ, Gams E, Schipke JD (2004)
Effects of a bradycardic agent on postischemic cardiac recovery in rabbits.
J Physiol Pharmacol, 55:705-712

Scott S (1979)
Stimulation simulation of young yet cultured beating hearts
PhD Thesis, State Univeristy of New York at Buffalo.

Seifert R, Scholten A, Gauss R, Minchevat A, Lichter P, Kaupp UB (1999)
Molecular characterization of a slowly gating human hyperpolarization-activated channel predominantly expressed in thalamus, heart, and testis.
PNAS vol. 96 no. 169391-9396

Severi S, Fantini M, Charawi LA, DiFrancesco D (2012)
An updated computational model of rabbit sinoatrial action potential to investigate the mechanisms of heart rate modulation
The Journal of Physiology. Volume 590, Issue 18, 4483-4499

Sgoifo A, Stilli D, Medici D, Gallo P, Aimi B, Musso E (1996)
Electrode positioning for reliable telemetry ECG recordings during social stress in unrestrained rats.
Physiol Behav;60(6):1397-401.

Sharp AA, O'Neil MB, Abbott LF, Marder E (1993) a
The dynamic clamp: artificial conductances in biological neurons.
Trends Neurosci. 16, 389–394

Sharp AA, O'Neil MB, Abbott LF, Marder E (1993) b
Dynamic clamp: computer-generated conductances in real neurons.
J. Neurophysiol. 69, 992–995

Shi W, Wymore R, Yu H, Wu J, Wymore RT, Pan Z, Robinson RB, Dixon JE, McKinnon D, Cohen IS (1999)

Distribution and prevalence of hyperpolarization-activated cation channel (HCN) mRNA expression in cardiac tissues.
Circ Res;85(1):e1-6.

Snyders DJ, Van Bogaert PP (1987)
Alinidine modifies the pacemaker current in sheep Purkinje fibers.
Pflugers Arch, 410:83-91.

Steinberg SF, Brunton LL (2001).
Compartmentation of G protein-coupled signaling pathways in cardiac myocytes.
Annu. Rev. Pharmacol. Toxicol. 4: 7–7.

Steinberg SF (2004)
β2-Adrenergic receptor signaling complexes in cardiomyocyte caveolae/lipid rafts.
J. Mol. Cell Cardiol. 37: 407–415

Still AM, Huikuri HV, Airaksines KEJ, Koistinen MJ, Kettunen R, Hartikainen J, Mitrani RD, Castellanos A, Myerburg RJ, Raatikainen PJP (2002).
Impaired Negative Chronotropic Response to Adenosine in Patients with Inappropriate Sinus Tachycardia.
Journal of cardiovascular electrophysiology, Volume 13, No. 6

Swedberg K, Komajda M, Böhm M, Borer JS, Ford I, Dubost-Brama A, Lerebours G, Tavazzi L; SHIFT Investigators. Collaborators (784) (2010)
Ivabradine and outcomes in chronic heart failure (SHIFT): a randomised placebo-controlled study.
Lancet. 2010 Sep 11;376(9744):875-85. doi: 10.1016/S0140-6736(10)61198-1

Tang QZ (2004)
Effect of Nardostachys chinensis Batal extract on sodium and L-type calcium channels of rabbit ventricular myocytes.
Chin J Cardiol;32:267–70.

Tang QZ (2008)
The effect of NcBe from Buchangwenxin on potassium channels in single rabbit ventricular myocytes.
Chin Physician Tribune;9:56–7.

Tardif JC, Ford I, Tendera M, Bourassa MG, Fox K (2005)
Efficacy of ivabradine, a new selective If inhibitor, compared with atenolol in patients with chronic stable angina.
Eur Heart J, 26:2529-2536

Thollon C, Cambarrat C, Vian J, Prost J-F, Peglion JL, Vilaine JP (1994)
Electrophysiological effects of S 16257 a novel sino-atrial node modulator, on rabbit and guinea-pig cardiac preparations: comparison with UL-FS 49.
Br J Pharmacol, 112:37-42.

Ulens C, Tytgat J (2001)
Functional heteromerization of HCN1 and HCN2 pacemaker channels.
J Biol Chem;276(9):6069-72. Epub 2000 Dec 27.

Ulens C, Siegelbaum SA (2003)
Regulation of Hyperpolarization-Activated HCN Channels by cAMP through a Gating Switch in Binding Domain Symmetry.
Neuron, Volume 40, Issue 5, Pages 959–970

Vaca L, Stieber J, Zong X, Ludwig A, Hofmann F, Biel M (2000)
Mutations in the S4 domain of a pacemaker channel alter its voltage dependence.
FEBS Lett;479(1-2):35-40.

Van Bogaert PP, Goethals M (1987)
Pharmacological influence of specific bradycardic agents on the pacemaker current of sheep cardiac Purkinje fibres. A comparison between three different molecules.
Eur Heart J, 8:35-42.

Van Bogaert PP, Pittoors F (2003)
Use-dependent blockade of cardiac pacemaker current (If) by cilobradine and zatebradine.
Eur J Pharmacol, 478:161-171

Van Ginneken AC, Giles W (1991)
Voltage clamp measurements of the hyperpolarization-activated inward current I(f) in single cells from rabbit sino-atrial node.
jphysiol.1991.sp018459

Varnum MD, Black KD, Zagotta WN (1995)
Molecular mechanism for ligand discrimination of cyclic nucleotide-gated channels.
Neuron;15(3):619-25.

Verkerk AO, Wilders R. (2014)
Pacemaker activity of the human sinoatrial node: effects of HCN4 mutations on the hyperpolarization-activated current.
Europace 2014;**16**(3):384-95

Verkerk AO, Wilders R (2015)
Pacemaker activity of the human sinoatrial node: an update on the effects of mutations in HCN4 on the hyperpolarization-activated current.
Int J Mol Sci; **16**(2):3071-94

Vilaine JP (2006)
The discovery of the selective If current inhibitor ivabradine. A new therapeutic approach to ischemic heart disease.
Pharmacol Res, 53:424-434

Viscomi C, Altomare C, Bucchi A, Camatine E, Baruscotti M, Moroni A, DiFrancesco D (2001)
C Terminus-mediated Control of Voltage and cAMP Gating of Hyperpolarization-activated Cyclic Nucleotide-gated Channels.
The American Society for Biochemistry and Molecular Biology, Inc.

Wainger BJ, DeGennaro M, Santoro B, Siegelbaum SA, Tibbs GR (2001)
Molecular mechanism of cAMP modulation of HCN pacemaker channels.
Nature;411(6839):805-10.

Wang J, Chen S, Siegelbaum SA (2001)
Regulation of hyperpolarization-activated HCN channel gating and cAMP modulation due to interactions of COOH terminus and core transmembrane regions.
J Gen Physiol;118(3):237-50.

Weber I, Steitz T (1987)
Structure of a complex of catabolite gene activator protein and cyclic AMP refined at 2.5 Å resolution.
Journal of Molecular Biology, Volume 198, Issue 2, Pages 311-326

Verkerk AO, Wilders R. (2014)
Pacemaker activity of the human sinoatrial node: effects of HCN4 mutations on the hyperpolarization-activated current.
Europace. Mar;16(3):384-95. doi: 10.1093/europace/eut348.

Wilders R (2006)
Dynamic clamp: a powerful tool in cardiac electrophysiology
J Physiol. 576:349-59

Wit AL, Fenoglio JJ Jr,Wagner BM, Bassett AL (1973)

Electrophysiological properties of cardiac muscle in the anterior mitral valve leaflet and the adjacent atrium in the dog. Possible implications for the genesis of atrial dysrhythmias.
Circ Res;32:731-745.

Wood JM, Schnell CR, Cumin F, Menard J, Webb RL (2005)
Aliskiren, a novel, orally effective renin inhibitor, lowers blood pressure in marmosets and spontaneously hypertensive rats.
J Hypertens;23(2):417-26.

Xue T, Marbán E, Li RA (2002)
Dominant-negative suppression of HCN1- and HCN2-encoded pacemaker currents by an engineered HCN1 construct: insights into structure-function relationships and multimerization.
Circ Res;90(12):1267-73.

Yusuf & Camm (2003)
Sinus tachyarrhythmias and the specific bradycardic agents: a marriage made in heaven?
J Cardiovasc Pharmacol Ther;8(2):89-105.

Zaccolo M, Pozzan T (2002)
Discrete microdomains with high concentration of cAMP in stimulated rat neonatal cardiac myocytes. Science 295: 1711–1715.

Zagotta WN, Olivier NB, Black KD, Young EC, Olson R, Gouaux (2003)
Structural basis for modulation and agonist specificity of HCN pacemaker channels.
Nature;425(6954):200-5.

Zaza A, Robinson RB, DiFrancesco (1996)
Basal responses of the L-type Ca^{2+} and hyperpolarization-activated currents to autonomic agonists in the rabbit sino-atrial node
The Journal of Physiology. Volume 491, Issue 2, pages 347-355

Zellerhoff S, Hinterseer M, Felix Krull B, Schulze-Bahr E, Fabritz L, Breithardt G, Kirchhof P, Kaab S. (2010)
Ivabradine in patients with inappropriate sinus tachycardia.
Naunyn Schmiedebergs Arch Pharmacol;382(5-6):483-6.

Zong X, Stieber J, Ludwig A, Hofmann F, Biel M (2000)
A Single Histidine Residue Determines the pH Sensitivity of the Pacemaker Channel HCN2.
The American Society for Biochemistry and Molecular Biology, Inc.